STUDY OF THE TANDEM SOLAR CELL

Fong Chun Hui

**A project report submitted in partial fulfilment of the
requirements for the award of the degree of
Bachelor (Hons.) of Physics**

**Faculty of Engineering and Science
Universiti Tunku Abdul Rahman**

September 2011

DECLARATION

I hereby declare that this project report is based on my original work except for citations and quotations which have been duly acknowledged. I also declare that it has not been previously and concurrently submitted for any other degree or award at UTAR or other institutions.

Signature :

Name   :   Fong Chun Hui

ID No.   :   08UEB06974

Date   :   September 9th 2011

APPROVAL FOR SUBMISSION

I certify that this project report entitled **"STUDY OF THE TANDEM SOLAR CELL"** was prepared by **Fong Chun Hui** has met the required standard for submission in partial fulfilment of the requirements for the award of Bachelor of Science (Hons.) Physics at Universiti Tunku Abdul Rahman.

Approved by,

Signature :

Supervisor : Dr. Lew Kim Luong

Date   : September 9th 2011

PROJECT TITLE IN CAPITAL LETTER
TITLE TO BE THE SAME AS FRONT COVER

ABSTRACT

Tandem cells can achieve a very high efficiency by distribute different parts of the solar spectrum onto individual cells of corresponding band-gap energies. Theoretically, an efficiency of 85% is achievable. This thesis examines the performances of Cold Mirror and Prism tandem cell work under the sun and also solar simulator. The analyses of the drawback factors have listed out and discussed, thus the improvement can be effectively done to increase the efficiency. α-Si and Poly-Si are used as a multi-junction solar cell to absorbed different spectrum in order to produce higher power. The Cold Mirror tandem cell has successfully increase the efficiency to 15.76%, while Prism tandem cell has fail to achieved higher efficiency, giving only 9.31% efficiency under the AM 1.5 condition. The analyses for the both cases are studied, and improvements are suggested to tackle the lost efficiency.

TABLE OF CONTENTS

LIST OF TABLES

LIST OF FIGURES

LIST OF SYMBOLS / ABBREVIATIONS

V	voltage, V
I	ampere, A
eV	electron volt
T	temperature, K
q	charge, As
I_o	reverse saturation current, A
R_s	series resistance, Ω
I_l	light generated current, A
P	power, W
FF	fill factor
η	efficiency, %
θ_c	critical angle, ˚
n	refractive index of prism
n'	refractive index of air
V_{oc}	open circuit voltage
m	diode ideality factor
k	Boltzmann constant, J/K
A	area, m^2
i	intensity, W/m^2

LIST OF APPENDICES

CHAPTER 1

INTRODUCTION

1.1   Background

Energy is fundamental to the quality of our lives, all activities are impossible with absence of energy. There are various ways in converting energy to usable forms, mostly burning fossils fuel (coal, natural gas and etc.) to generate energy, but the emission of green house gasses leads to environmental pollution. Secondly, the fossils fuels will soon depleted in near future. In order for sustainable development, renewable energy technologies are introduced as an alternative solution to tackle the problem between environmental issues and development. These technologies offer the promise of clean, abundant energy gathered from self-renewing resource such as sun, wind, tidal, and plants. Recently, the research and development in renewable energy has been greatly emphasised among government and research institute, especially after the Fukushima Nuclear leak disaster.

Sun is a fundamental energy source for all life forms. The energy that radiates from sun onto earth is far more enough for all sorts of utilisation. Since the sun will radiates energy for another 7.8 billion years and it is free, solar cell technology has great potential in a long run development.

Although we do not pay for the sun light, but to converting into useable forms, it requires knowledge and resource to realize the technology. Photovoltaic energy source is being increasingly recognized as cost effective generation source in small isolated power system.

Photovoltaic (PV) device collect energy from the sun and convert solar radiation energy into electrical energy. When sunlight falls on a PV cell, the photons of the absorbed sunlight dislodge the electrons from the atoms of the cell. The free electron then move through the cell, creating and filling in holes in the cell. It is the movement of electrons and holes that generates electricity. This physical process known as photovoltaic effect. Although photovoltaic effect was observed in 1839 by the French scientist Alexandre-Edmond Becquerel, it was not fully comprehensible until the development of quantum theory of light and solid state physics in early to middle 1900s. Since its first commercial use in powering orbital satellites of the US space programs in 1950s, PV has made significant progress.

One single PV cell produces up to 2 watts of power, too small even for powering pocket calculators or wristwatches. To increase power output, many PV cells are connected together to form modules, which are further assembled into larger units called arrays. This modular nature of PV enables designers to build PV systems with various power output for different types of applications.

A complete PV system consists of PV modules, but also the "balance of system" or BOS – the support structure, wiring, storage, conversion devices, etc. i.e. everything else in a PV system except the PV modules. The major types of PV system are available in the market today is, flat plate and concentrators. As the most prevalent type of PV systems, flat plate systems build the PV modules on a rigid and flat surface to capture sunlight. Concentrator systems use lenses to concentrate sunlight on the PV cells and increase the cell power output. Comparing the two systems, flat plat systems are typically less complicated but employ a large number of cells while the concentrator systems use smaller areas of cells but require more sophisticated and expensive tracking systems.

1.2   Aims and Objectives

The aim of this project is to design a small scale solar cell which gives higher efficiency than the conventional individual PV cell. Due to the limited budget provided by institute, this project has to be carried in low cost with simple set-up.

After taking all of the possible factors into consideration, Dichroic Beam Splitter Tandem Cell and Prism Tandem Cell are proposed in achieving higher rate of efficiency.

The overall objectives are
- Design a higher efficiency solar cell technology.
- Realize the technology and examine the efficiency experimentally.
- Compare the efficiency between individual PV cell and tandem cell technology.

CHAPTER 2

LITERATURE REVIEW

2.1   The Beam Splitting Concept

Photothermal processes convert solar energy to heat with an efficiency that is relatively constant over the solar spectrum, depending only on the optical properties of the window and/or coating of the thermal receiver employed. Photovoltaic conversion, on the other hand, is highly wavelength-dependent and most efficient when converting photons of energies close to the PV cell band-gap energy. Photons below the band-gap energy pass through the active area of the cell without being absorbed, and are ultimately dissipated as heat in other parts of the cell. Photons of energy larger than the band-gap can only be partly utilized, and the remainder of their energy is also dissipated as heat. Because of these factors, an optimal method of using solar cells is to direct onto them only the part of the solar spectrum for which high conversion efficiency can be achieved, and to recover the radiation outside this range by diverting it to a second receiver, i.e., thermal, chemical, or a different PV band-gap receiver. This is the underlying concept of PV/thermal solar hybrid systems, where the incident beam is split into PV and thermal spectral components as illustrated in Fig.2.1.
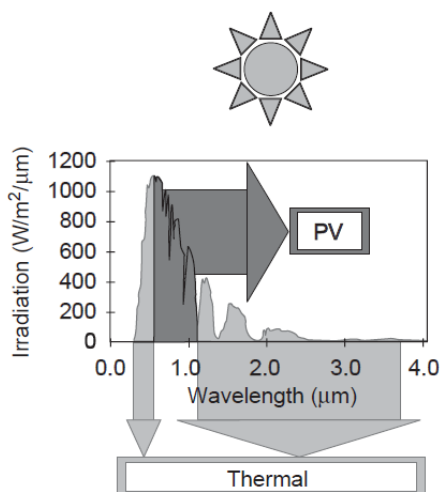
Figure 2.1: Splitting the solar spectrum into components for PV and thermal energy conversion.

Several filtering techniques for PV cells have been described in the literature; the main categories include all-dielectric and metal-dielectric multilayer filters [1–3], heat reflectors [4,5], refraction or prism spectrum splitting [6–8], holographic filters [9–11], fluorescent methods [12–14], and liquid absorption filters [3,15,16]. In PV-only systems, filtering techniques can be carried out using either the tandem-cell approach in which two or more solar cells of different semiconductor materials are mechanically or monolithically stacked in series and arranged in order of decreasing energy band-gap [17–19], or the spectrum splitting approach in which an optical filter separates the light into spectral components directed onto individual cells of different band-gap energies [20–22].

The PV cells can alternatively combine with a thermal solar collector in a so-called PV/T system, where one part of the spectrum is filtered out by the PV cells for electricity production and the residual is transmitted to a heat transfer fluid for thermal applications [23–25]. A similar method has been used for thermoelectric devices to extract waste heat by cooling and thus maintain a high temperature gradient across the device, which results in improved conversion efficiency [24, 26]. The electric conversion efficiency for PV/T and thermoelectric receivers is constrained by the increase in temperature of the cooling medium, which is in direct thermal contact with solar conversion device, and will not be further discussed here.

The first attempts to use spectral beam splitters as a means of increasing the efficiency of solar energy conversion may be traced back to the invention of the TPV converter in the early 1960s. In the TPV concept, a high-temperature energy source heats up a ''black body'' cavity, which re-emits radiation at a lower temperature. PV cells immersed in the cavity will absorb the emitted photons of higher energies and produce electricity. The longer wavelengths that cannot be utilized by the cells are reflected back to the radiator by a spectrally selective filter, allowing the energy to be recycled as heat. However, efficient recycling of unused long wavelength radiation becomes a critical issue if high conversion efficiencies are to be achieved. Various semiconductor materials have been considered for TPV conversion; the most suitable materials appear to be those of low band-gap values which provide a better spectral match with the lower temperature thermal radiation sources contemplated for use in these systems.

The energy crises that struck in the 1970s brought new requirements for fuel economy, and while fossil-fuel powered TPV development came to a virtual halt, solar TPV research was given a boost [27–30]. The reader is referred to Nelson [31] for a further reading on the historical development of TPV technology.According to White et al. [32], the TPV converter was first presented by Pierre Aigrain during a lecture series as a visiting professor at the Massachusetts Institute of Technology, Massachusetts, in 1960/1961. Wedlock [33] demonstrated improvements in the TPV conversion efficiency by band-limiting the radiation incident on the PV cells to the region of maximum collection efficiency near the energy gap. He suggested a coaxial arrangement with a central radiator and photovoltaic cells placed along the outer walls, as shown in Fig.2.2. A thin-film optical filter placed between the radiator and the PV cells allowed residual reflection to be utilized as heat.
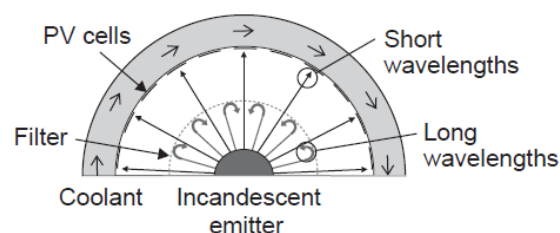
Figure 2.2: Early coaxial TPV design with optical filtering [33].

A series of variations on the TPV concept followed, investigating the possibilities of using spectral selectivity to increase conversion efficiency. Werth [34] and Kittl and Guazzoni [35] suggested using a more advanced multilayer interference coating with germanium cells, whereas Bracewell and Swanson [36] and Swanson [29] investigated silicon cells with a silver plate heat reflector, placed at the back of the cells.

The solar TPV system proposed by Swanson is illustrated in Fig.2.3. Concentrated sunlight from a primary parabolic mirror was incident on a secondary compound parabolic concentrator (CPC), which increased the solar flux to about 20,000 suns to allow cavity temperatures as high as 2000–2400 K. The PV converter, consisting of silicon p –i–n cells, received concentrated radiation at a level of 300–500 suns. The cells were kept below 70 ˚C by active cooling and incorporated back-silvered surfaces for reflection of IR radiation back to the emitter.
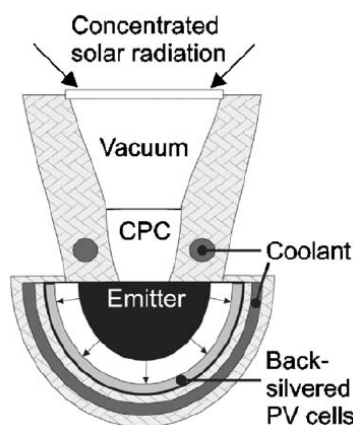
Figure 2.3: A solar TPV design proposed by Swanson [29].

System modelling had predicted TPV cell conversion efficiencies of up to 40–50% under these conditions, laboratory tests achieved a maximum of 26% for a radiator operating at 2300 K. The complete system was however not built, and the overall solar TPV conversion efficiency is thus not known. Swanson pointed out that although operation at such high temperatures allows a larger percentage of photons to fall within the useful PV range, yet rapid oxidation may shorten TPV converter life markedly.

A different solar TPV configuration suggested by Horne [30] involved a Cassegrainian system in which a paraboloidal primary reflector and a hyperboloidal secondary reflector directed solar radiation in through a window of a black body cavity. Cassegrainian reflector, is designed for reflecting telescope [66], attributed to Laurent Cassegrain, published in the 1672, Journal des scavans [67]. As illustrated in Fig.2.4, the cavity consisted of a paraboloidal ceiling which provided more uniform illumination of the emitted light and redirected the light towards PV cells attached to a flat wall at the back.
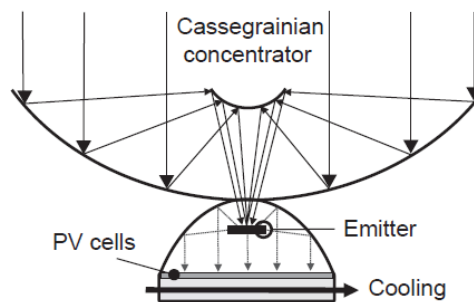
Figure 2.4: Cassegrainian solar TPV system presented by Horne [30].

The requirements on mirror optics and alignment in a Cassegrainian system are in general quite stringent in order to have the focal point appear below the primary mirror, such as shown in Fig.2.4. The system will suffer from increased Fresnel losses as the beam is reflected twice, and then passed through a window to enter the high temperature cavity. This particular design also requires an additional reflective surface within the cavity to redirect the emitted light, which adds to the optical losses, while uniformity may still be an issue as the emitter view factor of the center cells is different from that of the peripheral cells.

Oglesby and Crackel [37] proposed a spectral converter close to the TPV configuration, but rather than tailoring the incident radiation for PV conversion, the idea was to shift the spectrum to UV frequencies within the range 105–400 nm and transport it through light guides for utilization in a chemical dissociation cell. The light would pass through a small window to a high-pass dielectric filter, before being collimated and coupled to the optical light guide. There are several potential problems with this approach. A small window in the cavity wall would transmit only a fraction of the radiation field within the cavity, implying that very high

temperatures and radiation densities are required if a substantial amount of radiation is to pass through to the light guide. The cavity walls would need to withstand high temperatures while providing high reflection of both UV and heat radiation. In practice it would be difficult to find suitable materials for the optical management system, i.e., lenses, dielectric filter materials, and fibre-optic guides, operating at high temperatures and being highly transparent in the UV. Special UV-grade synthetic fused silica is transparent only down to about 200nm and available at a relative high cost. A major challenge is to collimate and couple light efficiently into the light guide. It is questionable whether there would be any gain in cost or performance over a solar concentrator producing electricity for dissociation by more traditional means.

2.2   Photovoltaic Spectrum Splitting System

Very high conversion efficiencies can be achieved by directing different parts of the solar spectrum onto PV cells with matching energy absorption bands. In theory, efficiencies in the range of 85% are possible [38, 39]. This may be realized either by stacking the cells on top of each other in an optical and electrical series connection, commonly called a cascade, tandem, or multijunction cell, or placed next to each other in a parallel connection. The tandem cell is illustrated in Fig.2.5A. Sunlight is incident on the largest band-gap cell where short-wavelength photons excite electrons to a higher potential. Light not absorbed by the upper cell is transmitted to the second cell of a smaller band-gap value, where longer wavelengths will excite electrons to a potential which lower than in the first cell. In theory, any number of different cells may be stacked on top of each other to fully utilize the incident solar spectrum.

(A) Tandem or cascading system.

(B) Separate beam splitting filter.

(A)   (B)
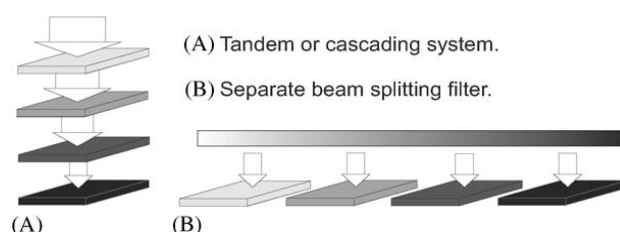
Figure 2.5: Two schemes for PV spectrum splitting.

In monolithic tandem cells, tunnel junctions provide series connections which allow the voltages of the stacked cells to be added. Alternatively, a metal grid structure may be used to interconnect the cells for a high voltage output. A larger voltage and smaller current means smaller resistance losses at high concentrations. Another benefit of the tandem cell is that only a single load and power-conditioning circuit is required, and there is no need for separate optical filters. However, tandem systems face difficulties with current and lattice matching, as well as cooling issues since the top cell is normally cooled via the connection to the bottom heat-sinked cell. Fig.2.5B shows the alternative solution where the cells are placed in parallel; in this case, light is separated into spectral components by a beam splitting filter and is directed onto individual cells of corresponding band-gap energies. In this way, each cell can be separately designed and manufactured on unique, optimized substrates without concern for substrate transparency or lattice mismatch. There are no constraints on the currents flowing through each of the cells; hence, the spectrum splitting approach has a slightly higher theoretical efficiency than that of the cascading approach, assuming ideal beam splitting optics. The increase in efficiency is so small, though, that this may not be the determining factor [40].

Furthermore, there is several loss factors associated with the introduction of realistic dielectric beam splitting filters, e.g., sloped transition edges between reflective and transmissive regions which cause mixing of wavelengths at the different PV cells, Fresnel optical losses, angular sensitivity, and misalignment issues. Of the two spectrums splitting approaches mentioned, the tandem cell is by far the most commonly widespread technology today, mainly due to the cost-related advantages arising from mainstream semiconductor production techniques and from avoiding the cost of advanced discrete optical components. The multi-layered solar cell approach was first mentioned by Jackson [41], who calculated the case of a 3-layer PV tandem cell capable of 69% energy utilization. However, at that time only one-sun illumination was considered and the added complexity could not be economically justified. The development of the multi-gap concept did not get much attention until the mid-1970s, when higher efficiencies and power densities were demonstrated in concentrating solar cell systems [18, 19, 40, 42–44].

Experience gained from concentrator PV and TPV research stimulated the development of both cascading and spectrum splitting PV receivers, which effectively spanned the solar spectrum. Several studies followed on the optimization of multiple PV cell systems, their fundamental efficiency limits, and possible implementations, see for instance [20, 38, 45]. A review of the PV tandem cell development is beyond the scope of this paper. Instead, an overview is given of some of the systems that have proposed to use spectrum splitting techniques to operate separate PV receivers in parallel.

2.3   Transmissive and Reflective Filtering Methods

Cape et al. [46] and Masden and Backus [21] studied a two-cell system in which the concentrated incident solar spectrum was split between GaAs and Si cells by a dielectric multilayer dichroic mirror. Predicted theoretical efficiencies were around the 30%, and a similar practical device reported by Vander Plas et al. [47] measured efficiencies of 27% at 113 suns concentration and 26% at 489 suns concentration, using Si and AlGaAs cells. Moon et al. [48] considered the same system of Si and AlGaAs cells in combination with a computer-optimized dielectric multilayer filter, fabricated on a polished, fused silica substrate and mounted at 22 ˚ to the incident beam. The filter and cells were tested experimentally, giving a total efficiency of 28.5% at 165 suns and AM1.23 spectrum, which represented a marked improvement in performance compared to the single PV receiver systems. For an ideal filter this corresponded to 31% efficiency for the two cells combined. Allowing for losses in the concentrator optics and filter, the system efficiency was estimated to 25%.

The first demonstration of this spectrum splitting system at PV module level was presented by Borden et al. [49, 50]. The modules were equipped with point-focusing, curved-groove, facet Fresnel lenses with transmittance of about 80% and a geometric concentration ratio of 477 suns. A dichroic mirror mounted below the lens would transmit light to the high-band-gap AlGaAs cell (10% optical loss) and reflect light to the low-band-gap Si cell (5% optical loss). Although the spectral

performance of the dichroic mirror was lower than expected due to a fabrication error, the best module measured a solar-to-electric conversion efficiency of 20.5% at AM2 spectrum, not including the thermal recovery from the AlGaAs -cells operating at around 100˚C. If compared to the best GaAs and Si modules at the time, measured at 17% and 12% efficiency, respectively, the spectrum splitting module represented a 20% (GaAs) and 70% (Si) improvement. However, after lens transmission and beam splitting, the radiation arriving at each of the PV cells was reduced to an energy concentration ratio well below 200 suns. This was not sufficient for economic operation of the system. The two main factors that were found to contribute to excessive cost were the filter and the long focal length design, which had been chosen to minimize the effect of non-uniformities across the PV cells but also meant that more materials were needed and a tracking system was required.

Spectrum splitting PV systems were also considered an attractive solution for power generation in space. Onffroy et al. [22] discussed a high-efficiency, concentrating multi-solar-cell system for orbital power generation, using several dichroic mirrors in series to divide the solar spectrum into the desired spectral bands. A two-stage optical concentration system consisting of a Cassegrainian and a CPC, both assumed to a have a reflection loss of 10%, was chosen to meet the design specifications of 1000 suns under AM0 spectrum for each of the PV cells. Ideal efficiencies were calculated for optimum band-gap materials, ranging from 32% for 1 cell to 53% for 4 cell systems. Non-ideal efficiency calculations using realistic system design parameters were also performed; for the four potential solar cell materials Ge, Si, GaAs and GaP efficiencies up to about 33% were predicted.

Onffroy et al. concluded that the 4-cell system would not be cost-effective, since the assumed 10% transmission loss of each dichroic mirror reduced the overall potential increase in efficiency to a point where the associated system cost was too large. The most cost-effective configuration consisted of a single dichroic beam splitter with GaAs and Si solar cell arrays, generating 100kW of power at an efficiency of about 28%, and a radiator which removed excess heat to keep both of the solar cell arrays at an operating temperature of 300 K. The main cost was found to be that of the primary mirror and the radiator, whereas the solar cells costs were almost negligible.

In a spectrum splitting configuration considered by Ellion [51], the solar cells were mounted in a non-coplanar arrangement so that the beam would be directed serially from one cell to the next by reflection from a silver surface at the back of the cell, each cell extracting energy from the incident light beam and ideally passing onto the next solar cell the portion of the beam not converted to electricity. A practical arrangement of four different band-gap cells was proposed, expected to obtain solar-to-electric conversion efficiencies of up to about 50%. Fig.2.6A illustrates a hollow triangular mounting structure with cells mounted on adjacent sides, the cells having their active interfaces lying at an angle to each other to avoid total internal reflection. The cells facing the sun are transparent to the portion of the light not utilized by the cells, whereas the remaining cells inside the cavity have back-silvered coatings to reflect non-absorbed light. Fig.2.6B is in the shape of a parallelogram with at least one solar cell mounted on each side. The hollow core of the support structures allows heat to be radiated away from the solar cells or, alternatively, a coolant to be passed down the center of the structure.
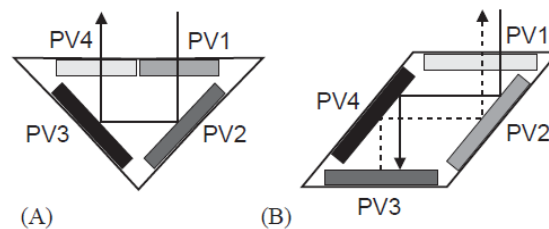
Figure 2.6: PV cascade splitting in a non-coplanar configuration [51].

Ellion has not specified whether the receiver is intended for a linear or point focus concentrator design, but the use of four different band-gap cells suggests that a point focus will be needed to justify the cost of materials. Apart from high tracking accuracy, high-quality optics would be required in order to produce an intense collimated beam that impinges normally onto the first, high-band-gap PV cell surface, which ensures that the solar rays follow the intended path within the receiver. Scattering and defocusing of the collimated light could become a problem if the PV surfaces are not smooth or the cells contain defects. The connection of metal leads and efficient cooling of the cells under high flux intensity, in particular of the selectively transparent front cells, represents a technical challenge that has not been further discussed by the author.

2.4   Refractive and Absorptive Filtering Methods

A prism will refract and disperse incident white light into a rainbow of colours. As illustrated in Fig.2.7, a PV receiver assembly may use refractive elements to direct spectrally dispersed light onto PV cells of matching band-gap energies (Spring, [52]; Dettling, [53]). A collimated incident beam is required in order to prevent overlap of spectral bands on the different PV cell materials.
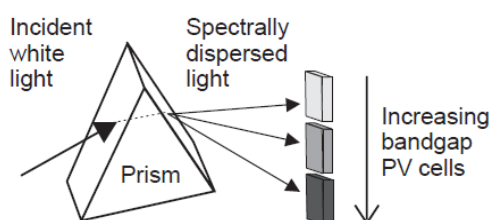
Figure 2.7: Prism spectrum splitting.

A practical prism arrangement may take the shape of a sawtooth Fresnel lens, as discussed in some recent studies where a line-focus of spectrally separated beams is incident on horizontally aligned sub-arrays of associated PV cells [8, 54]. Penn [8] estimates achievable conversion efficiencies of 45–60% for such a line-focus concentrator system operating at 100–500 suns and incorporating 5–6 different single band-gap cells. This system achieves high concentration by combining a first lens or mirror, which provides a relatively high linear concentration along a first north-south aligned axis, with a second, orthogonal lens that tracks the daily motion of the sun along an east–west direction. The second lens splits the beam spectrally and performs a small degree of concentration to increase the overall effective concentration.

2.5   Tracking Linear Beam Splitter

Figure 8 shows a tracking linear Fresnel lens is focusing light through a cylindrical plano-concave lens and onto a linear PV array which is thermally fixed to a copper substrate containing cooling channels [55]. A spectrally selective heat-mirror positioned between the plano-concave lens and the PV receiver splits part of the

beam off to an evacuated tube receiver, placed out of the path of the incident rays. Reflective wing secondary concentrators are provided at the aperture of both the PV and evacuated tube receivers for improved light collection. The optical losses could be substantial in this design, hence attention should be given to whether the concentration achieved will be sufficient for the efficient operation of both PV and thermal receivers.
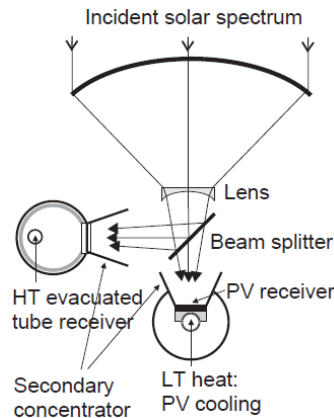
Figure 2.8: Total solar co-generation system proposed by Soule [55].

2.6   Dish Receiver System

Several Cassegrainian cogeneration systems of the same basic design as shown in Fig.2.9 have been suggested in the literature [56–59]. Common for these systems is the use of a reflective paraboloidal mirror producing a highly concentrated beam, and a Cassegrainian or Gregorian lens, positioned in front of or behind the focal point, respectively, that splits the beam by transmission and reflection of selected wavelength components.
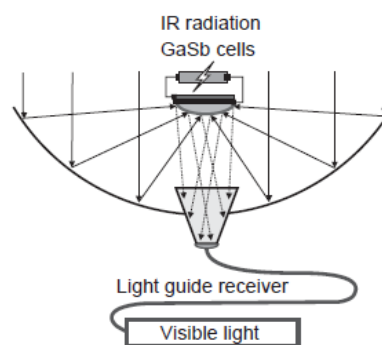
Figure 2.9: Cassegrainian hybrid PV and lighting system [56, 60–64].

In the system proposed by Lasich et al. [59], visible light is transmitted to a PV receiver placed in the focal region of the dish, while infrared energy is reflected into a light guide and redirected to a second thermal, chemical, or low-bandgap PV receiver. The system was successfully demonstrated in an experimental set -up comprising a 1.5m diameter paraboloidal dish reflector , a 10-cell silicon PV module operating at 30˚C, and a thermal receiver operating at 1100˚C. The PV array produced 187W at 282 suns, equivalent to a module efficiency of 18.4%, while the thermal receiver simultaneously produced 135W of high-grade heat, equivalent to 13.4% efficiency, giving an overall cogeneration efficiency of 31.8%.produced 187W at 282 suns, equivalent to a module efficiency of 18.4%, while the thermal receiver simultaneously produced 135W of high-grade heat, equivalent to 13.4% efficiency, giving an overall cogeneration efficiency of 31.8%.

Yogev et al. [65] proposed a triple-foci Cassegrainian concentrator for satellite applications, as shown in Fig.2.10. The incident spectrum is split into three parts by a Cassegrainian hyperboloidal mirror, coated with a long pass filter, and a dichroic beam splitter for the simultaneous operation of a solar pumped laser, a PV receiver, and a thermal receiver.
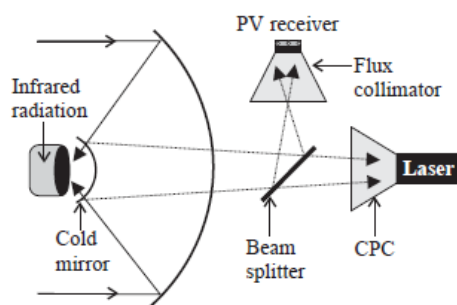
Figure 2.10: Triple-foci beam splitting system for PV, laser and thermal receiver [65].

Whether a triple-foci system would be the most cost-effective way of providing the energy required for space applications, compared to a simpler single-focus or double-foci system, remains a question. It is clear that high quality of tracking and optics would be required to get a sufficiently high concentration of solar flux for the operation of three receivers. Using a beam splitter in series with a cold mirror adds another interface of optical losses, and cooling of all the components without cluttering the optical path may prove to be a difficult task.

CHAPTER 3

Methodology Part 1: Theories and Implementation Plan

3.1   Principle of Photovoltaic

Photovoltaic are made of semiconductor materials, part of the PV cell in use today are Silicon-based. Silicon has four valence electrons which paired with each other four neighbouring atoms as shown in Fig.3.1(Photovoltaic fundamentals)
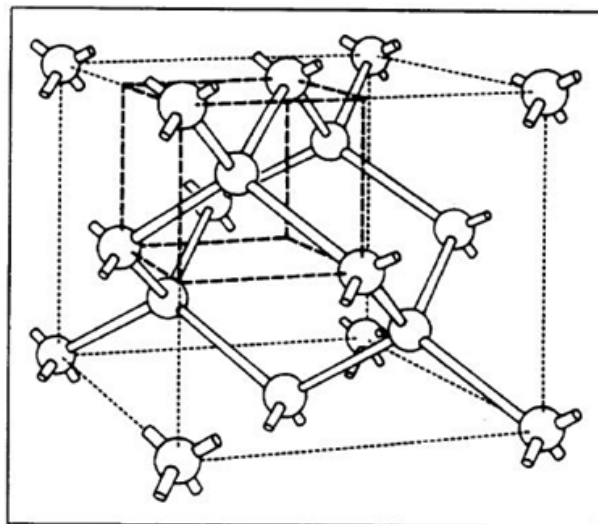
Figure 3.1: Silicon atom shares its four valence electrons with four neighbouring atoms.

The electron valence is bonded with certain amount of energy. It requires additional energy to overcome the bonded energy level. When sufficient energy (photon) is supplied, the electron absorbed the energy and breaks free from the bond, become free drifting electron (Fig.3.2) and then collected in external load.
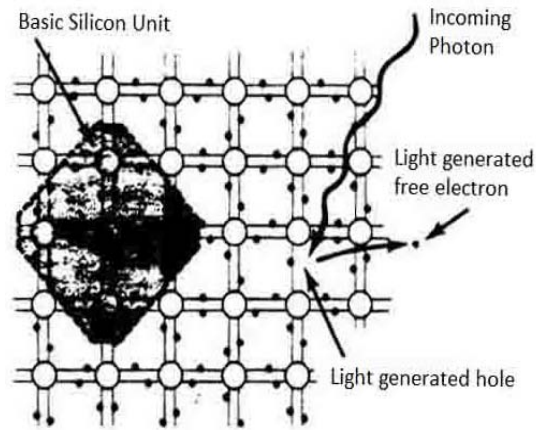
Figure 3.2: Electron breaks free from the bond and collected in external load.

Quantum mechanics states that energy can be described in quantized form. An energy level diagram (Fig.3.3) shows electron in valence band is localized and has low energy, while electron in conduction band is a delocalized free drifting electron. By supplying sufficient energy to an electron in valence band, the electron will be excited to the conduction band.
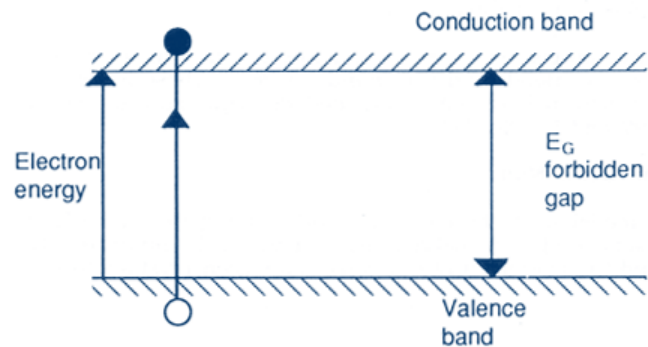
Figure 3.3: Energy Diagram

3.2   Power Loss

The photon will be absorbed only if the energy exceeded the band gap energy. Hence, low efficiency is limited due to the inability of converting broad range of photons in solar spectrum. Photon energy below the bandgap energy is lost and appears as heat. Heat will further decrease the conversion in efficiency, like all others semiconductor, unnecessary heat increase resistivity and decrease conductivity. For the case of incident photon energy exceeds band gap energy, absorption takes only the amount of band gap energy from photon to produce electron-hole pair, the remaining energy will also lost as heat, which is undesired.
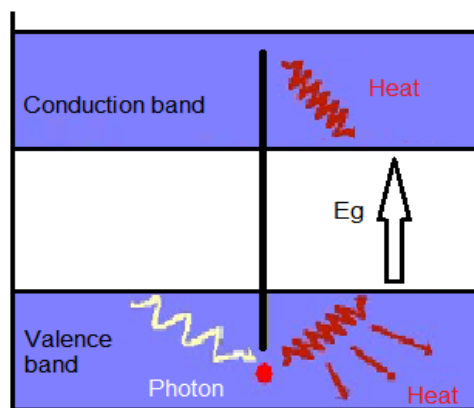
Figure 3.4: Energy losses to heat
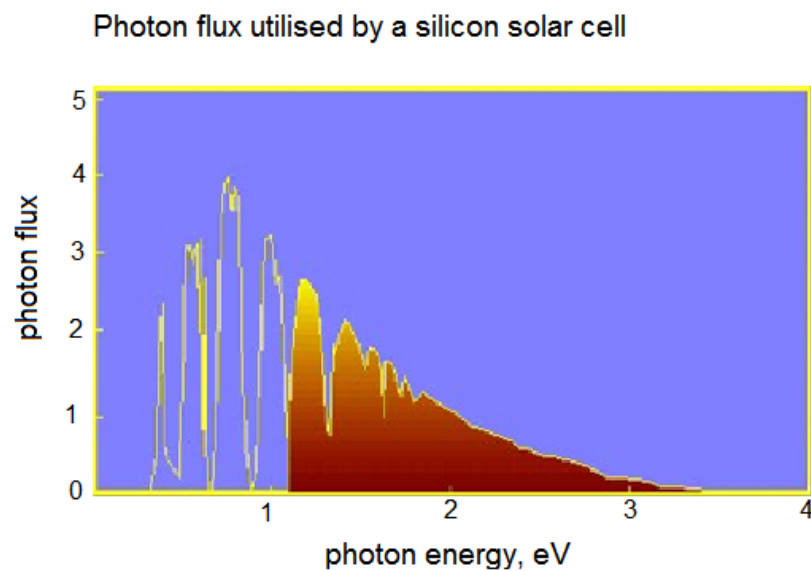
Graph 1: Energy absorbed inefficiently

Graph 1 shows the absorbing range of Silicon cell. The band gap of Silicon is 1.1 eV. The yellow shaded area indicates the absorbing range. The energy which below 1.1 eV is left to unabsorbed, therefore we consider as power loss.

Overall Power Loss can be categories as:

1. Fundamental loss

2. Recombination

3. Series Resistance

Temperature, irradiance and light reflection also takes effect on the efficiency.

3.2.1   Fundamental Loss
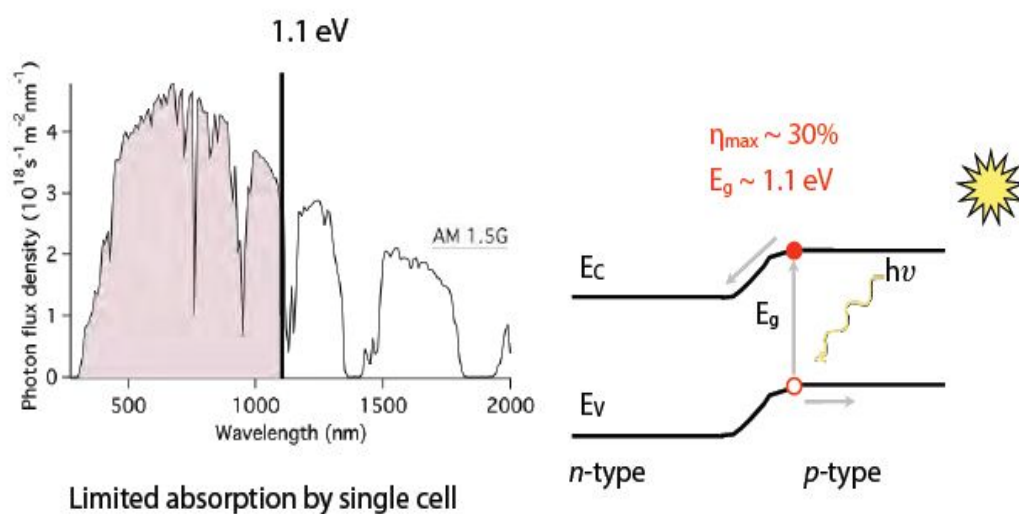
Figure 3.5: Fundamental Loss

Fundamental loss is the losses due to limited absorption. Different material has different value of band gap, efficient lost due to inability to convert broad range of energy from solar spectrum to electricity.

Take Silicon as example, 1.1 eV in bandgap, 1127 nm in wavelength, it can only absorbed the wavelength before 1127 nm, hence the efficiency is approximate 30 percent. Fig.3.5 gives a simple illustration.

3.2.2 Recombination
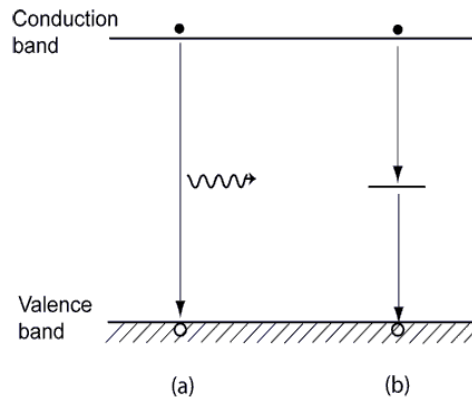
Figure 3.6: Two type of Recombination

There are two types of recombination, which is Surface (direct, Fig.3.6a) recombination and Defect energy level (indirect, Fig.3.6b) recombination. Surface recombination is recombination of electron-hole pair spontaneously, this can be avoided by shorten the depletion region length. The second recombination, defect energy level, is cause by the impurities or lattice defects. Both create a R-G centre which act as a stepping stone recombining electron-hole pairs. Recombination reduces the efficiency as the total amount of collected free drifting electron in conducting band reduced.

3.2.3 Series Resistance

Series Resistance on Silicon
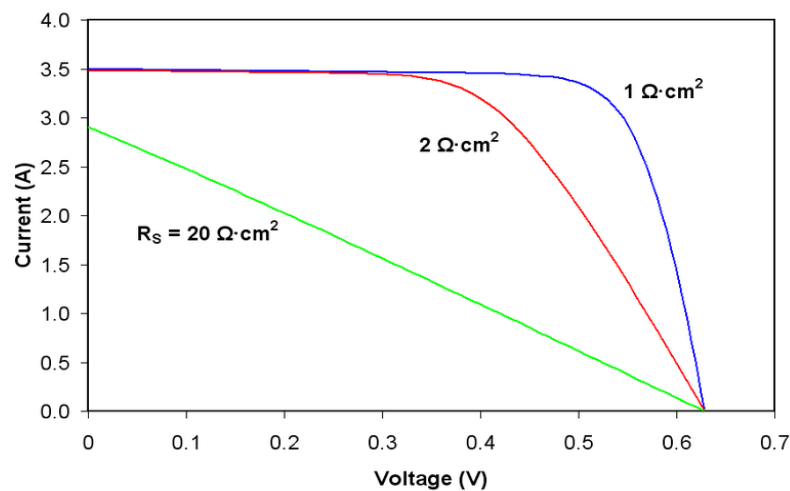
Graph 2: Series Resistance Graph

Series resistance in photovoltaic has three causes: firstly the movement of current through emitter and base, secondly the contact resistance between the metal contact and the silicon, and finally the resistance of the top and the rear metal contacts. The main impact is that reduce in fill factor. Fill factor is a measure of the maximum power output over circuit output, which indicates the ratio of the circuit performance to the optimum condition, $FF = I_M V_M / I_{SC} V_{OC}$. It is advantageous to have FF as close as unity as possible to achieve optimum output efficiency, typically FF values are in the range between 70%-85%.

From the formula, $I = I_l - I_o [\exp (qV+IR_s) / nkT]$, where I_l is light generated current, I_0 is reverse saturation current, R_s Series resistance play as a factor that affect the external current I, ultimately affected the overall efficiency.

3.2.4   Temperature
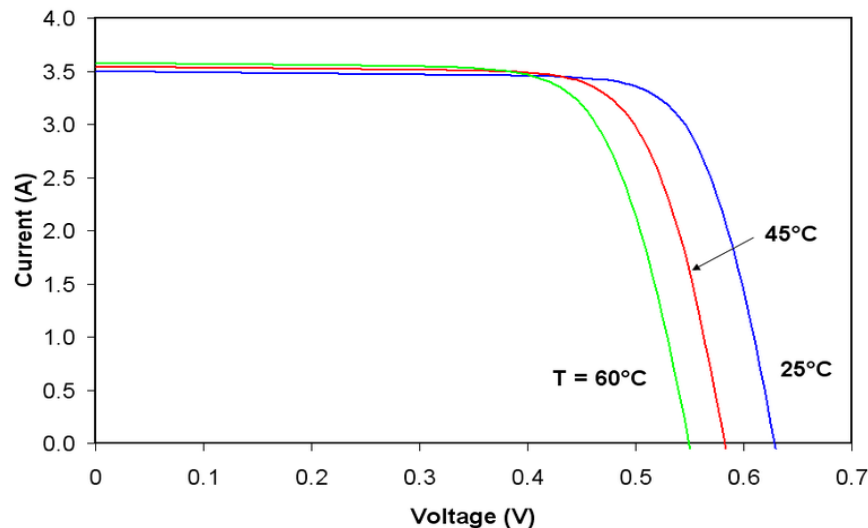
Graph 3: Temperature Graph

The graph indicates that the relationship between temperature and power obtained. Increase in temperature gives lesser power, means lower efficiency.

3.2.5   Irradiance

IV Curves at various levels of irradiance at
Air Mass 1.5 and 25° C Cell Temperature
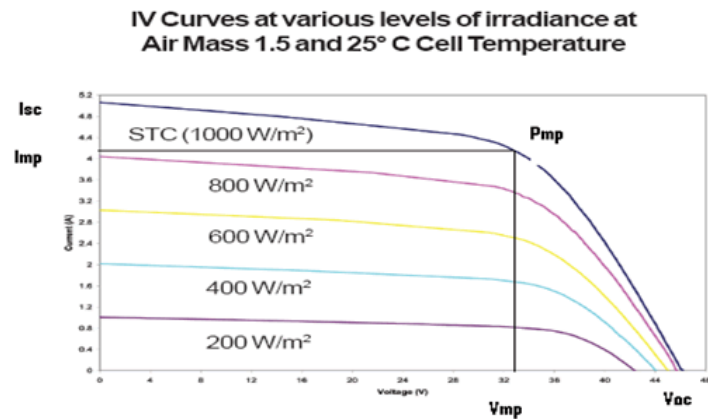
Graph 4: Irradiance Graph

The graph 4 shows the relationships of solar irradiance with the IV power output curve. Under Standard Test Condition (STC), 1.5 Air Mass, 25℃ cell temperature, 1 sun, achieve the highest power output. As the irradiance going down, the area under IV graph decrease as well, dropping in power output. This indicates total output power strongly depends on the solar irradiance.

3.2.6   Light Reflection

Reflected light means lesser light being absorbed. Two ways to reduce reflected light, one is by using ARC (Antireflection Coating), by covering a thin layer of dielectric material on the photovoltaic surface to minimize the light reflection. The second method is using the pyramidal texture surface so that higher chance of reflected light is being absorbed. Figure below illustrated the picture to reduce reflection.
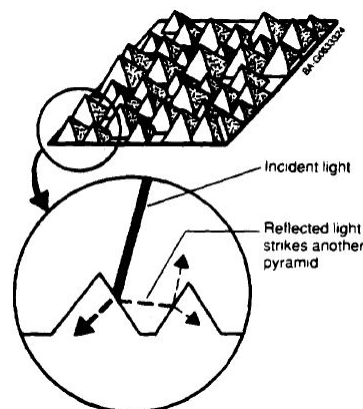
Figure 3.7: ARC, Anti Reflection Coating

3.2.7   Overall
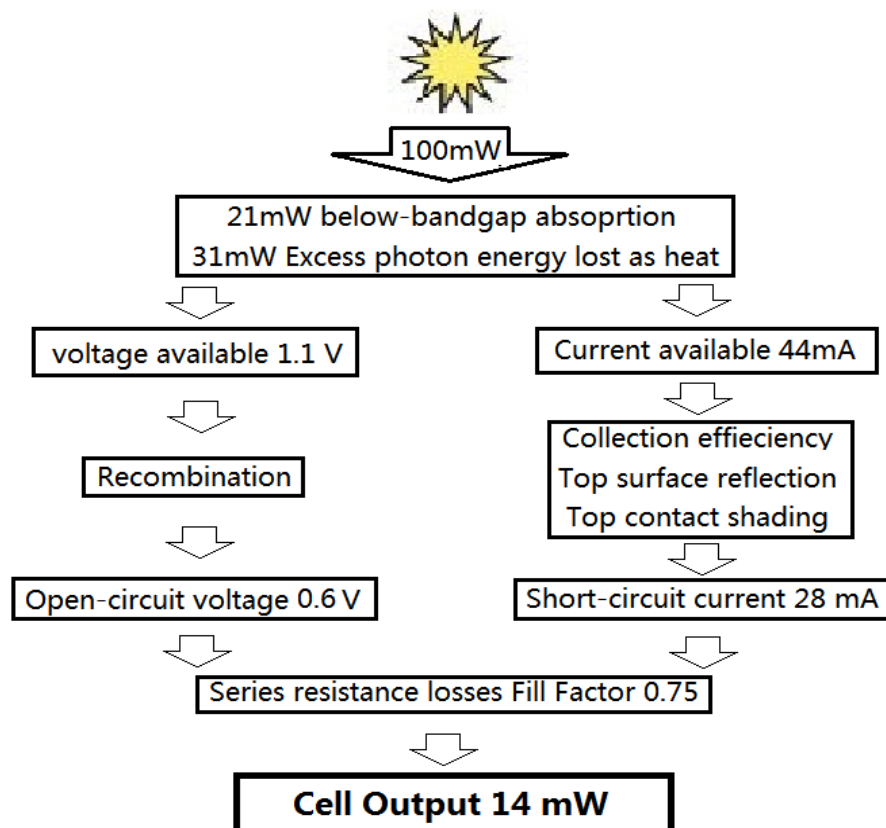
Figure 3.8: Overall outlined in efficiency of Silicon Semiconductor

An overall picture of the factors impact on efficiency in Silicon PV has outlined. Given a 100mW radiation source, taking all the factors into account, the final output is 14mW, 14 percent of efficiency. Obviously, the fundamental loss responsible for the biggest loss, 52mW of power lost, accounted for 52 percent. Thus fundamental loss is the most potential part to grab in retrieving the lost efficiency.

3.3   Improvement in retrieving lost efficiency

Due to the limited absorption by single cell photovoltaic, improvement can be done by adding up more cells to give a wider absorbing range. By using multi-junction cell, each of the different cell has characteristic bandgap energy, absorbing different part in the spectrum, giving higher conversion efficiency.

Single junction solar cell

1.1 eV

η_max ~ 30%
E_g ~ 1.1 eV

AM 1.5G

Photon flux density (10^{18} s^{-1} m^{-2} nm^{-1})

Wavelength (nm)

Limited absorption by single cell

E_c
E_g
hv
E_v

n-type   p-type
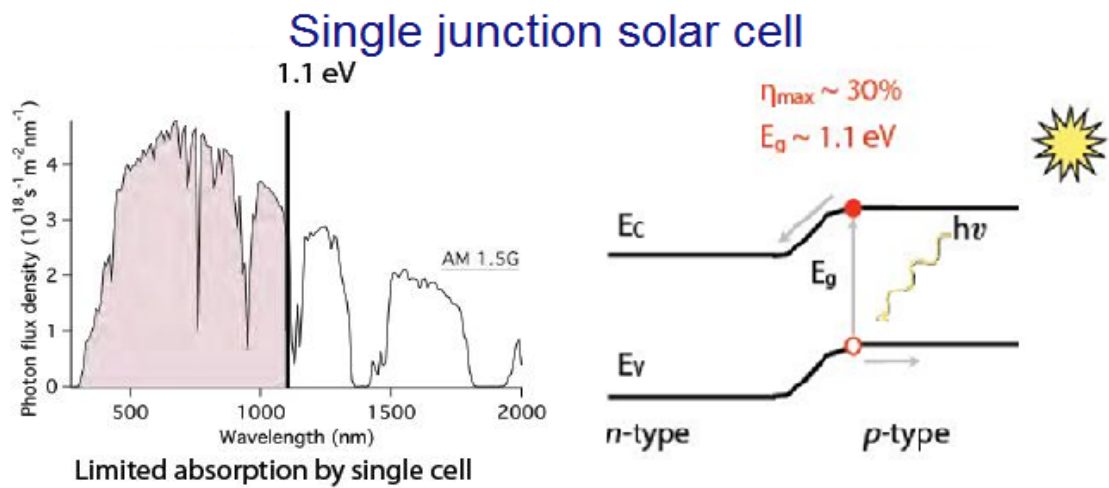
Figure 3.9: Single Junction cell

Double junction solar cell

1.6 eV   0.9 eV

Photon flux density (a. u.)

Wavelength (nm)

top cell
bottom cell

η_max = 45%
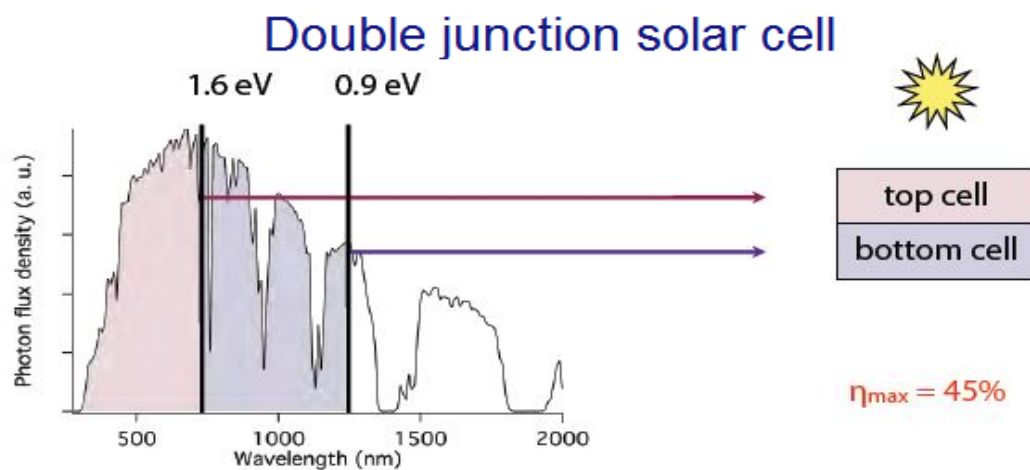
Figure 3.10: Double Junction cell

Triple junction solar cell

1.8 eV   1.2 eV   0.7 eV

Photon flux density (a. u.)

Wavelength [nm]

top
middle
bottom

η_max = 50%
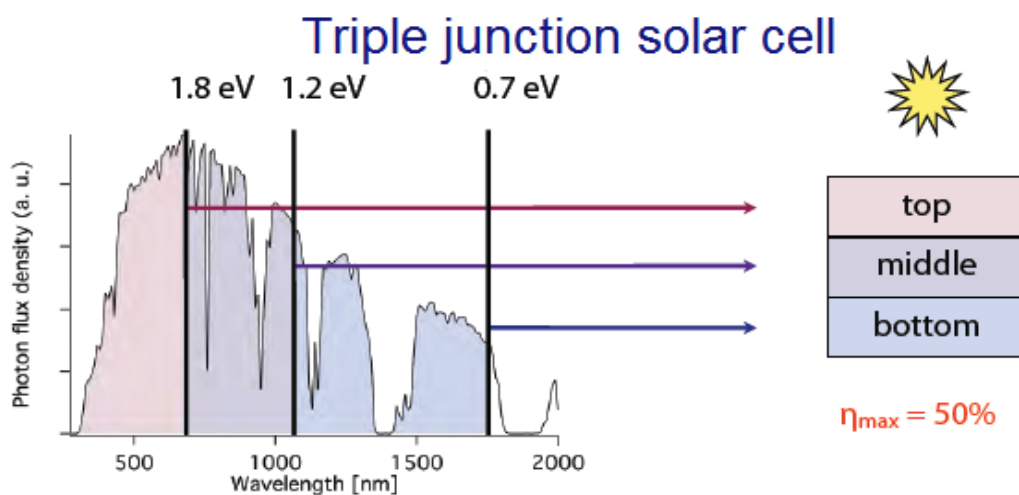
Figure 3.11: Triple Junction cell

3.4   Tandem Cell

High conversion efficiency can be achieved by directing different parts of the solar spectrum onto different PV cells with matching energy absorption bands. Theoretically in the range of 85% are possible. Basically, there are two types of tandem cell, which are Cascading tandem cell and Splitting tandem cell.
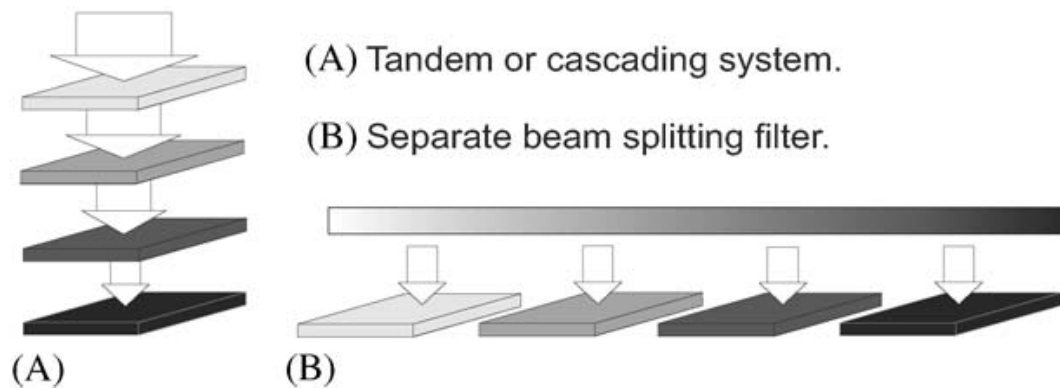
Figure 3.12: Cascading and Beam Splitting System

3.4.1   Cascading Tandem Cell

Cascading system is built by stacking the cells on top of each other in an optical and electrical series connection. Sunlight is incident on the largest band-gap cell where short-wavelength photons excite electrons to a higher potential. Light not absorbed by the upper cell is transmitted to the second cell of a smaller band-gap value, where longer wavelengths will excite electrons to a potential lower than in the first cell. In theory, any number of different cells may be stacked on top of each other to fully utilize the incident solar.

There are two kind of cascade tandem cell:
- Monolithic tandem cell
- Mechanically stacked tandem cell

3.4.1.1 Monolithic Tandem Cell

In monolithic tandem cells, tunnel junctions provide series connections which allow the voltages of the stacked cells to be added. Alternatively, a metal grid structure may be used to interconnect the cells for a high voltage output. A larger voltage and smaller current means smaller resistance losses at high concentrations. Another benefit of the tandem cell is that only a single load and power-conditioning circuit is required, and there is no need for separate optical filters. However, cascading tandem is built using many layers of epitaxial deposited film, it faces difficulties with lattice matching, challenging in choosing material to optimizing highest efficiency. Producing this is time consuming, costly, and they are mainly made of rare earth. Cooling issues is also another problem to deal with since different material has different in expansion rate. In different temperature, different rate of expansion might damaged the cell and reduce the conversion efficiency. Cooling system must provide in order to keep temperature stabilized. Although monolithic tandem cell gives a high efficiency, but it do not consider cost effective.
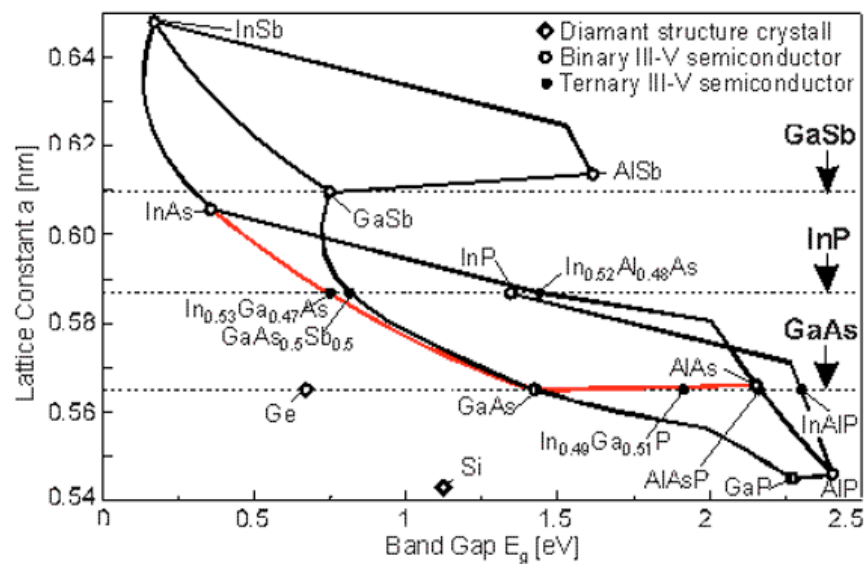
Graph 4: Lattice Matching Graph

3.4.1.2 Mechanically Stacked Tandem Cell

Mechanically stacked tandem cell is technically easier in producing compare to monolithic tandem cell. Different junction of cell is mechanically supported and stacked together, by this the crystal lattice matching problem are solved. Drawback is, this technology required a mechanically support to hold different cell separately, and the gap in between affect the efficiency.
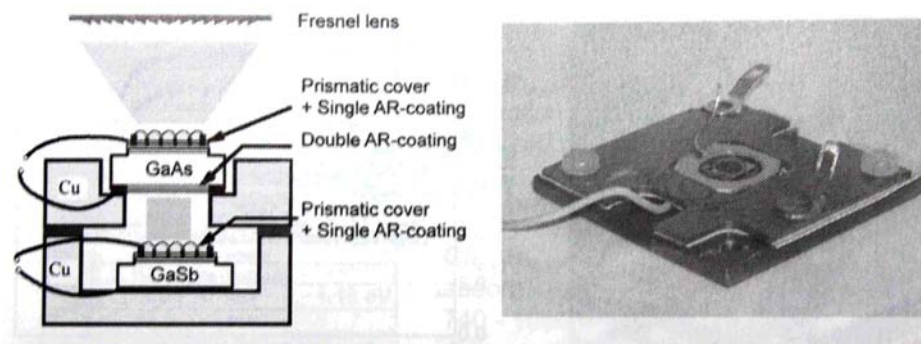
Figure 3.13: Mechanically Stacked Tandem Cell

3.4.2 Splitting Tandem Cell

Splitting tandem cell replace a different degree dispersing splitter to split the radiation spectrum directed onto different individual cells of corresponding wavelength or bandgap. This technically solves the stacking problem and each cell can be separately designed and manufactured on unique, optimized substrates without concern for substrate transparency or lattice mismatch. There are no constraints on the currents flowing through each of the cells; hence, the spectrum splitting approach has a slightly higher theoretical efficiency than that of the cascading approach, assuming ideal beam splitting optics.

Furthermore, there are several losses factors associated with the introduction of realistic dielectric beam splitting filters, e.g., sloped transition edges between reflective and transmissive regions which cause mixing of wavelengths at the different PV cells, Fresnel optical losses, angular sensitivity, and misalignment issues.

The tandem cell is by far the most commonly widespread technology today, mainly due to the cost-related advantages arising from mainstream semiconductor production techniques and from avoiding the cost of advanced discrete optical components.

There is also two kind of splitting tandem cell technology
- Prism tandem cell (figure 3.14)
- Dichroic Beam Splitter tandem cell (figure 3.15)
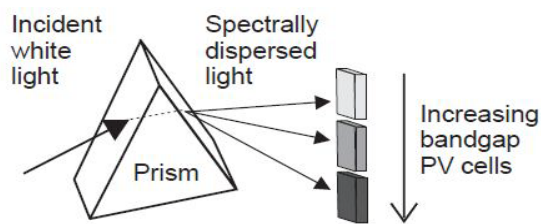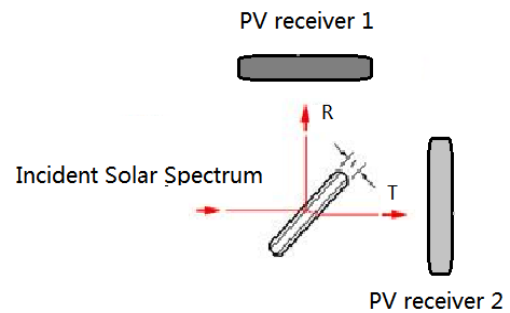
Figure 3.14: Prism   Figure 3.15: Dichroic Beam Splitter

3.4.2.1   Prism Tandem Cell

Prism split light into different wavelength targeted onto different PV cell. If the cells are placed in series, the splitting rays interface in spreading angle, causing reflection. The gap between cells contribute undesired loss, especially under concentrating system, a small percentage loss can be enormously huge.

3.4.2.2   Dichroic Beam Splitter Tandem Cell

This technology avoids the spreading ray by using beam splitter plate which splits incoming ray into two according by a specific wavelength. The beam splitter plate allowed a certain range of wavelength to be transmitted, and reflected the wavelength which fall out of the transmitted range. The transmitted ray passes straight onto one of the photovoltaic, and the reflected ray go for another cell. By adding more splitter plate in series and correct sequences, three or more split spectrum can be acquired.

3.5   Material of Photovoltaic

Different materials have different bandgap, thus absorbing different wavelength of light energy. Tandem cell is designed to absorb different wavelength to increase conversion efficiency. To achieve optimum efficiency, materials have to choose carefully to absorb wider solar spectrum.

3.5.1   Crystalline Material

3.5.1.1 Single-crystal Silicon

Single-crystal silicon cells are the most common in the PV industry. The main technique for producing single-crystal silicon is the Czochralski (CZ) method. High-purity polycrystalline is the melted in a quartz crucible. A single-crystal silicon seed is dipped into this molten mass of polycrystalline. As the seed is pulled slowly from the melt, a single-crystal ingot is formed. The ingots are then sawed into thin wafers about 200-400 micrometers thick. The thin wafers are then polished, doped, coated, interconnected and assembled into modules and arrays.

Single-crystal silicon has a uniform molecular structure. Compare to non-crystalline materials, its high uniformity results in higher energy conversion efficiency. The conversion efficiency for single-silicon commercial modules ranges between 15-20 percent. Other then energy efficient, single-silicon modules are highly reliable for outdoor power applications.

About half of the manufacturing cost comes from wafering, a time consuming and costly batch process in which ingots are cut into thin wafers with a thickness no less than 200 micrometers thick. If the wafers are too thin, the entire wafer will break in wafering and subsequent processing. Due to this thickness requirement, a PV cell requires a significant amount of raw silicon and half of this expensive material is lost as sawdust in wafering.

3.5.1.2 Polycrystalline Silicon

Consisting of small grains of single-crystal silicon, polycrystalline PV cells are less energy efficient than single-crystalline silicon PV cells. Its bandgap energy is 1.1 eV. The grain boundaries in polycrystalline silicon hinder the flow of electrons and reduce the power output of the cell. The energy conversion efficiency for a commercial module made of polycrystalline silicon ranges between 10 to 14 percent.

A common approach to produce polycrystalline silicon PV cells is to slice thin wafers from blocks of cast polycrystalline silicon. Another more advanced approach is the "ribbon growth" method in which silicon is grown directly as thin ribbons or sheets with the approach thickness for making PV cells. Since no sawing is needed, the manufacturing cost is lower. The most commercially developed ribbon growth approach is EFG (edge-defined film-fed growth).

Compared to single-crystalline silicon, polycrystalline silicon material is stronger and can be cut into one-third the thickness of single-crystal material. It also has slightly lower wafer cost and less strict growth requirements. However, their lower manufacturing cost is offset by the lower cell efficiency.

3.5.1.3 Gallium Arsenide

A compound made of gallium (Ga) and arsenic (As), GaAs has a crystal structure similar to that of silicon, with direct bandgap energy 1.43 eV. An advantage of GaAs is that it has high level of light absorptivity. To absorb the same amount of sunlight, GaAs requires only a layer of few micrometers thick while crystalline silicon requires a wafer of about 200-300 micrometers thick.[3] Also, GaAs has a much higher energy conversion efficiency than crystal silicon, reaching about 25 to 30%. Its high resistance to heat makes it an ideal choice for concentrator systems in which cell temperatures are high. GaAs is also popular in space applications where strong resistance radiation damage and high cell efficiency are required.

The biggest drawback of GaAs PV cells is the high cost of the single-crystal substrate that GaAs is grown on. Therefore it is most often used in concentrator systems where only a small area of GaAs cells is needed.

3.5.2   Thin Film Material

In a thin-film PV cell, a thin semiconductor layer of PV materials is deposited on low-cost supporting layer such as glass, metal or plastic foil. Since thin-film materials have higher light absorptivity than crystalline materials, the deposited layer of PV materials is extremely thin, from a few micrometers to even less than a micrometer (a single amorphous cell can be as thin as 0.3 micrometers). Thinner layers of material yield significant cost saving.Also, the deposition techniques in which PV materials are sprayed directly onto glass or metal substrate are cheaper. So the manufacturing process is faster, using up less energy and mass production is made easier than the ingot-growth approach of crystalline silicon.

However, thin film PV cells suffer from poor cell conversion efficiency due to non-singlecrystal structure, requiring larger array areas and increasing area-related costs such as mountings.

Materials used for thin film PV modules are as follows:

3.5.2.1   Amorphous Silicon (a-Si)

Used mostly in consumer electronic products which require lower power output and cost of production, amorphous silicon has been the dominant thin-film PV material since it was first discovered in 1974.

Amorphous silicon is a non-crystalline form of silicon i.e. its silicon atoms are disordered in structure, with direct bandgap 1.75 eV. A significant advantage of a-Si is its high light absorptivity, about 40 times higher than that of single-crystal silicon. Therefore only a thin layer of a-Si is sufficient for making PV cells (about 1 micrometer thick as compared to 200 or more micrometers thick for crystalline silicon cells). Also, a-Si can be deposited on various low-cost substrates, including

steel, glass and plastic, and the manufacturing process requires lower temperatures and thus less energy. So the total material costs and manufacturing costs are lower per unit area as compared to those of crystalline silicon cells.

Despite the promising economic advantages, a-Si still has two major roadblocks to overcome. One is the low cell energy conversion efficiency, ranging between 5-9%, and the other is the outdoor reliability problem in which the efficiency degrades within few months of exposure to sunlight, losing about 10-15%.

3.5.2.2   Cadmium Telluride (CdTe)

As a polycrystalline semiconductor compound made of cadmium and tellurium, CdTe has a high light absorptivity level -- only about a micrometer thick can absorb 90% of the solar spectrum. Another advantage is that it is relatively easy and cheap to manufacture by processes such as high-rate evaporation, spraying or screen printing. The conversion efficiency for a CdTe commercial module is about 7%, similar to that of a-Si.

The instability of cell and module performance is one of the major drawbacks of using CdTe for PV cells. Another disadvantage is that cadmium is a toxic substance. Although very little cadmium is used in CdTe modules, extra precautions have to be taken in manufacturing process.

3.5.2.3   Copper Indium Diselenide (CuInSe2, or CIS)

A polycrystalline semiconductor compound of copper, indium and selnium, CIS has been one of the major research areas in the thin film industry. The reason for it to receive so much attention is that CIS has the highest "research" energy conversion efficiency of 17.7% in 1996 is not only the best among all the existing thin film materials, but also came close to the 18% research efficiency of the polycrystalline

silicon PV cells. (A prototype CIS power module has a conversion efficiency of 10 %.) Being able to deliver such high energy conversion efficiency without suffering from the outdoor degradation problem, CIS has demonstrated that thin film PV cells are a viable and competitive choice for the solar industry in the future.

CIS is also one of the most light-absorbent semiconductors -- 0.5 micrometers can absorb 90% of the solar spectrum. CIS is an efficient but complex material. Its complexity makes it difficult to manufacture. Also, safety issues might be another concern in the manufacturing process as it involves hydrogen selenide, an extremely toxic gas. So far, CIS is not commercially available.

Table 3.1: Description on Different PV semiconductor Materials

Material	Thickness	Efficiency	Features
Monocrystalline Si solar cells	0.3 mm	15- 18 %	Lengthy production procedure, wafer sawing necessary. Best researched solar cell material - highest power/area ratio.
Polycrystalline Si solar cells	0.3 mm	13- 15 %	Wafer sawing necessary. Most important production procedure at least for the next ten years.
Polycrystalline transparent Si solar cells	0.3 mm	10 %	Lower efficiency than monocrystalline solar cells. Attractive solar cells for different BIPV applications.
EFG	0.28 mm	14 %	Limited use of this production procedure Very fast crystal growth, no wafer sawing

Polycrystalline ribbon Si solar cells	0.3 mm	12 %	Limited use of this production procedure, no wafer sawing necessary. Decrease in production costs expected in future.
Apex (polycrystaline Si) solar cells	0.03 to 0.1 mm + ceramic substrate	9.5 %	Production procedure used only by one producer, no wafer sawing, production in form of band possible. Significant decrease in production costs expected in future.
Monocrystaline dendritic web Si solar cells	0.13 mm incl contacts	13 %	Limited use of this production procedure, no wafer sawing, production in form of band possible.
Amorphous silicon	0.0001 mm + 1 to 3 mm substrate	5 - 8 %	Lower efficiency, shorter life span. No sawing necessary, possible production in the form of band.
Cadmium Telluride (CdTe)	0.008 mm + 3 mm glass substrate	6 - 9 % (module)	Poisonous raw materials, significant decrease in production costs expected in future.
Copper-Indium-Diselenide (CIS)	0.003 mm + 3 mm glass substrate	7.5-9.5% (module)	Limited Indium supply in nature. Significant decrease in production costs possible in future.
Hybrid silicon (HIT) solar cell	0.02 mm	18 %	Limited use of this production procedure, higher efficiency, better temperature coefficient and lower thickness.

3.6   Conclusion on selecting Materials and Technology

Due to low cost restriction, the materials of the PV cells will be

- **Amorphous Silicon (a-Si)**   - 1.75 eV
- **Poly Silicon (Poly-Si)**   - 1.1 eV

For wavelength splitting technology, **Dichroic Beam Splitter Plate** and **Prism** meet the requirement both in produce higher efficiency and low cost production. To determine the characteristic of the splitting wavelength according to the PV cells:

$E = hc / \lambda$

$\lambda = hc / E$

α-Si $= 1.7$ eV, $\lambda = 729$ nm

Poly-Si $= 1.1$ eV, $\lambda = 1127.3$ nm

Functioning Bandwidth for α-Si: **0 nm < x < 730 nm**

Functioning Bandwidth for Poly-Si: **730 nm < x < 1130 nm**

The stopping wavelength must be around **730 nm** in order to separate incoming ray.
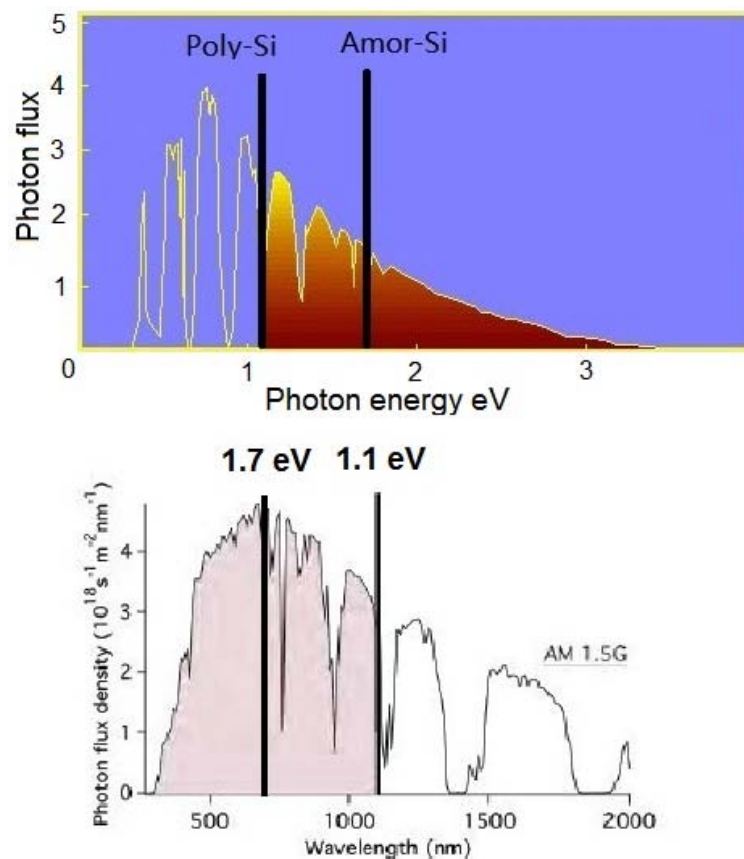
Graph 5

CHAPTER 4

Methodology Part 2: Implementation

4.1   Hardware Configuration

Tandem cell technology is designed for Concentrated Photovoltaic (CPV) purpose, hence both experiment have to be done in a confined box to direct the sun radiation and distribute the spectrum into PV cells accordingly.

4.2   Prism Tandem Cell

Below is the parameter of prism and PV cells.

Prism   - 50mm x 50mm   (Width x Length)

Amorphous PV   - 44.7mm x 53mm (Width x Length) (data sheet in Appendix*)

Poly-Silicon PV   - 60mm x 12.5mm (Width x Length) (data sheet in Appendix*)

To split the spectrum accordingly to α-Si and Poly-Si PV cell, the first step is to find out the diffraction characteristic of the prism. The characteristic of the prism can be obtained either by theoretically and experimentally.

4.2.1   Mathematical Method for Prism Diffraction Angle

Light diffracts into different wavelength with different diffraction angle in prism. Due to the fact that different wavelength in the prism will have different velocity,

thus the index of refraction will also be different (n = c/v, where c the light speed). It can be said that the index of the prism is depend on speed of wavelength. In general, the index of refraction n is greater for shorter wavelength thus greater the diffraction angle is. But to get a specific relationship between wavelength with diffraction angle is pretty tedious, as it involves a lot of theoretical in optics and mathematical solutions in geometrical optics. To safe time, an empirical solution is introduced. By knowing the material of the particular prism, Sellmeier equation is able to tell the relationship between wavelength and diffraction index precisely [69].

$$n^2(\lambda) = 1 + \frac{B_1\lambda^2}{\lambda^2 - C_1} + \frac{B_2\lambda^2}{\lambda^2 - C_2} + \frac{B_3\lambda^2}{\lambda^2 - C_3}$$

(4.1)

where n is the refractive index, λ is the wavelength, and $B_{1,2,3}$ and $C_{1,2,3}$ are experimentally determined Sellmieir coefficient according to its material[100]. The refractive index is obtained by inserting the coefficient into the equation, follow by the Snell's equation we can then know the refractive angle for different wavelength. With the limited fund available, it is unable to provide the project with a quality prism. A cheap prism without data sheet comes along is the only option. Hence without knowing the material, it is unable to determine the diffraction angle. This method has to be allocated. But in this method will still be introduced in the improvement and recommendation section.

4.2.2   Experimental Method for Prism Diffraction Angle

Diffraction angle can be determined through experiment. A light source is passing through a single slit and incident on prism. The light is then diffracted into beams of colour spectrum. Measure the angle difference between red and violet colour, by extending the length of the spectrum colour from the two edges of the prism until it fit the parameter of α-Si PV. The exact position of the Poly-Si PV is, unfortunely, unable to determine since the spreading wavelength is invisible. Since the shorter wavelength is followed by longer wavelength, by placing Poly-Si next to α-Si, the longer wavelength spectrum will eventually fell on it.

Notice that the angle of incident light on prism must be within the total internal reflection angle. Secondly, different incident angle on the prism yield different diffraction angle, hence incident angle must consistent when determining the position of PV cells. Generally, the incident angle on prism determines the whole parameter of the diffracted spectrum and PV cells position.

The configuration of the PV cells and prism are shown as below:
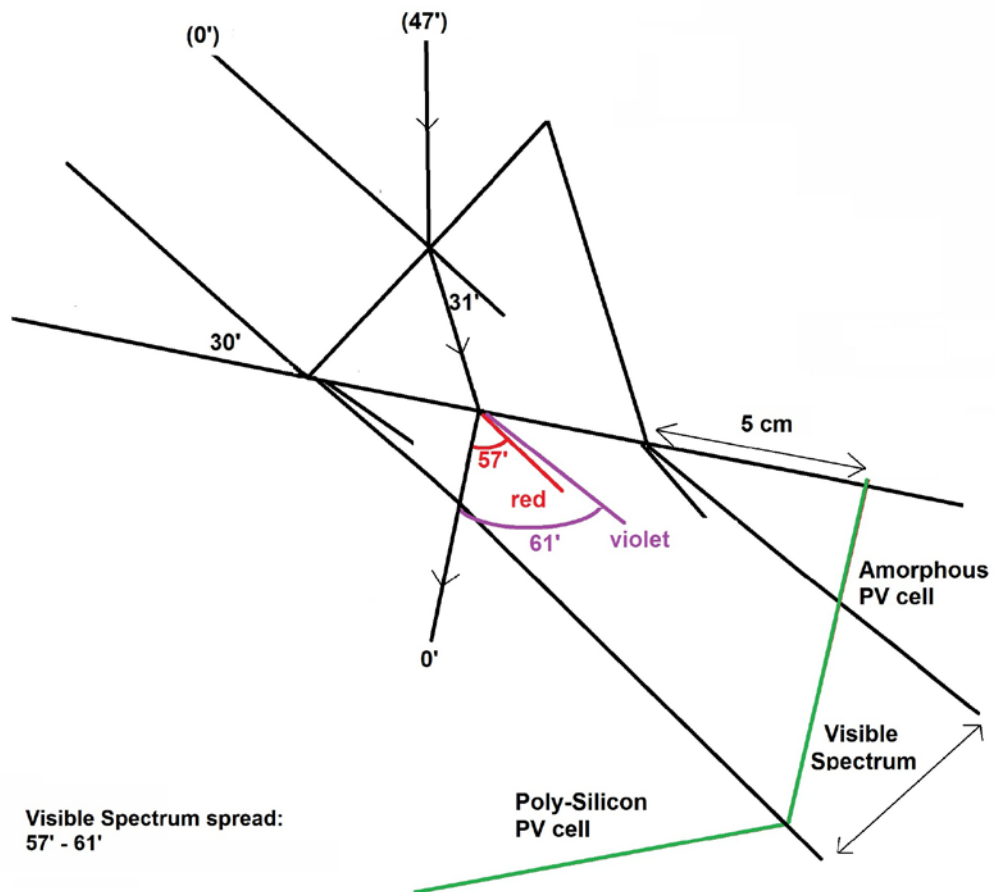
Figure 4.1: As smaller wavelength refract at higher angle, α-Si has to place as above to capture 0-730nm. Poly-Si is placed next to α-Si to capture wavelength after 700nm.

4.2.3   Flexibility to Reduce Error in Hardware Set-up

To reduce the possible affection caused by set-up, for example the diffracted spectrum may not fully incident on the PV cell, some improvement and flexibility

can be design on hardware configuration. Hence unnecessary lost is able to be retrieve by doing some minor adjustment.

1. The frame of the Poly-Si is thick, and this gives a large gap in between PV. The gap can be removed by stacking the α-Si on the edge of Poly-Si PV frame. To give Poly-Si a larger effective area absorbing a wider diffracted spectrum, a tilt-able PV rack is designed to hold this two PV cell (If the Poly-Silicon is lie flat as α-Si, it will lost part of the long diffracted wavelength spectrum as in Fig.4.2). The Fig.4.3 shows the hardware design.
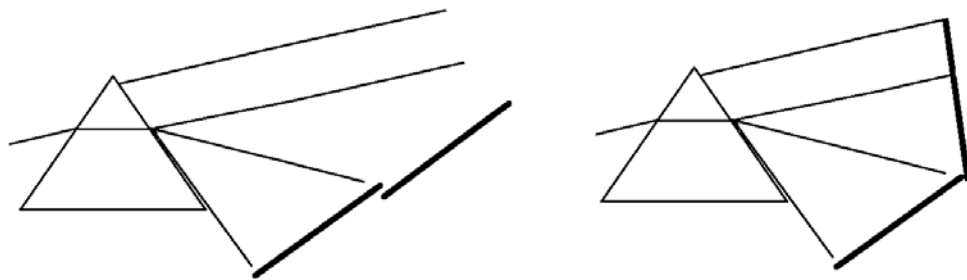
Figure 4.2: The PV cell has to be tilt-able to capture wider diffracted spectrum.
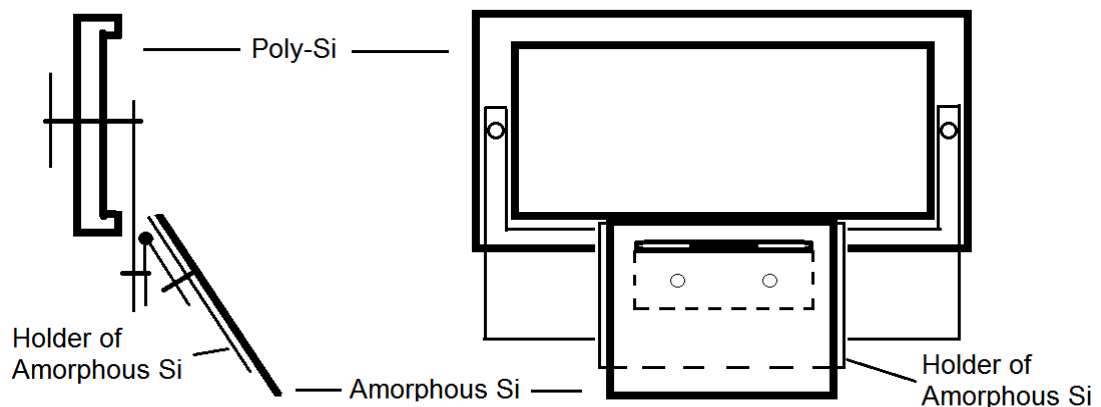
Figure 4.3: α-Si is attached to Poly-Si to eliminate the gap in between, and is tilt-able.

2. The holder of the PV rack can be lift up and lower down to allow the flexibility in adjustment. This lead to an opening hole for the holder to move up and downward, hence extra structure is designed to keep the box confined.
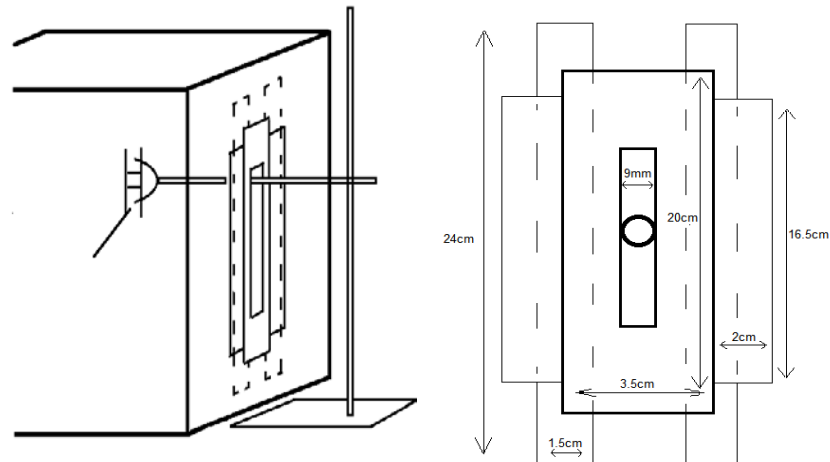
Figure 4.4: (Left) Configuration of the PV rack holder.

Figure 4.5: (Right) The design to adjusting the height of holder while keep box in confined.

3. To make the prism tilt-able in adjusting the incident angle, a prism holder is designed with a handle that link outside the box. A 360° protractor is attached to the handle as an indicator of the incident angle.
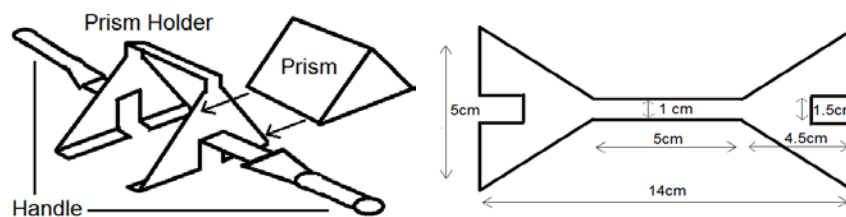
Figure 4.6:: (Left) Prism Holder. Figure 4.7: (Right) Parameter of Prism Holder.

4. The area of the opening hole to expose from sunlight is 10cm². A channel is built in order to block the diffusive sunlight, and only direct sunlight is directed towards prism. The internal of confine box is in black in colour, this is to absorb and reduce the reflected sunlight inside the confine box (part of sunlight will undergo internal reflected within prism, other than that, PV cell rack, prism holder and handle will also reflect light).

5. Due to the stand of the PV rack holder is outside of the confine box, platform is necessary to hold both together when directing toward sun.
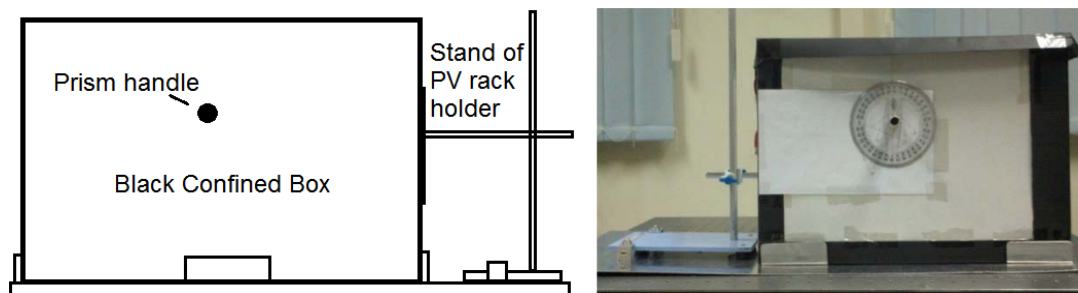
Figure 4.8: The overall view from side with platform.
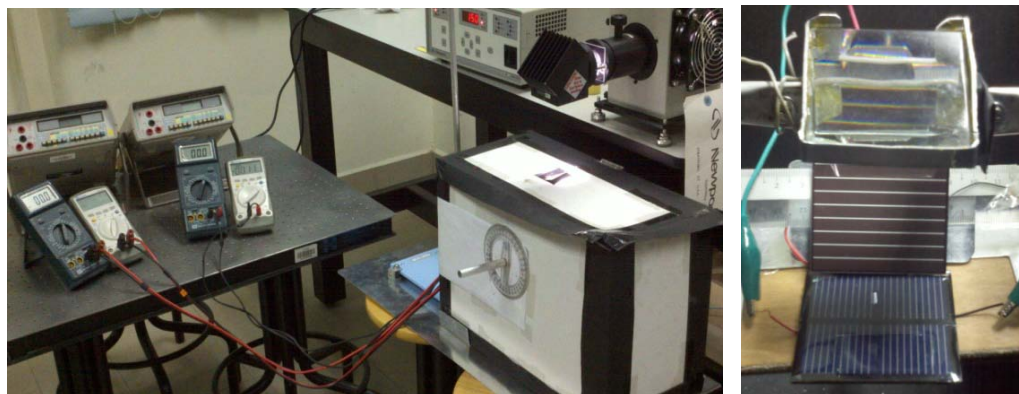
Figure 4.9: Set-up of Prism tandem cell in dark room.
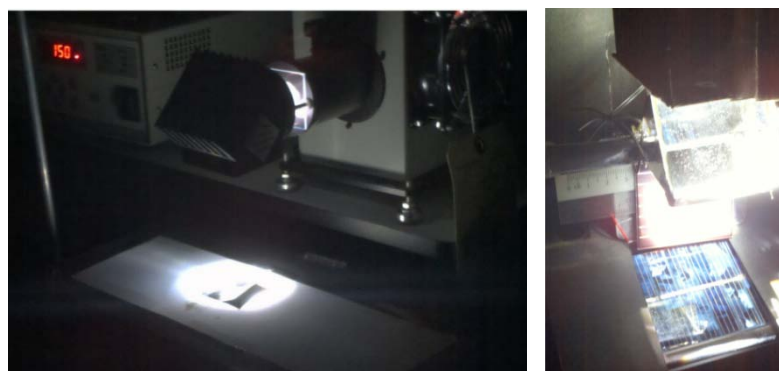
Figure 4.10: Experiment carries in dark room, expose to Solar Simulator.
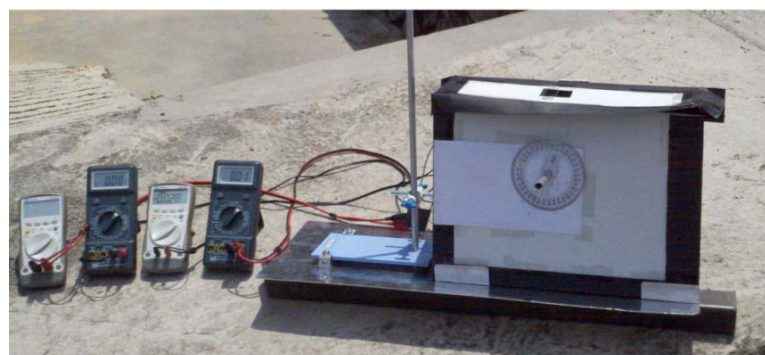
Figure 4.11: Experiment carries at outdoor, expose to the sun.

4.3   Dichroic Beam Splitter Tandem Cell

This technology require the beam splitter plate band-pass the 0nm – 730nm wavelength to α-Si and reflect 730nm – 1130nm wavelength to Poly-Si. This particular beam splitter plate has to tailor made and all of the supplier available in market accept order only for mass production, hence it is too expensive to purchase a piece of dichroic beam splitter just for this research. Alternatively, dichroic beam splitter can be replaced by cold mirror.

4.3.1   Cold Mirror

The purpose of a mirror is to reflect image. For wavelength which fall outside the visible range wavelength is invisible and hence unnecessary. Cold mirror is designed to filter off invisible wavelength since those wavelengths carry energy and might heat up device, mirroring a relatively colder image. Cold mirror reflect the visible wavelength and band-pass all the invisible wavelength. It reflects 400nm to 700nm visible wavelength, while transmits 0nm to 400nm and 700nm to infinity invisible wavelength. Cold mirror contributes 2 major drawbacks in term of efficiency. First drawback is, the 0nm to 400nm wavelength supposingly reflects toward α-Si but not transmits toward Poly-Si. Although range of this wavelength able to generate power in Poly-Si, yet it gives a relatively lower power compare to α-Si and thus decreasing the overall efficiency. Secondly, wavelength from 0nm-400nm which falls on Poly-Si generates more heat, thus further decrease the efficiency. And lastly the operating wavelength range for α-Si has shortened from 730nm to 700nm. It is a small range yet from the aspect of power intensity, this range is the peak intensity in the sun spectrum. This contributes an amount of lost efficiency which is significant. The lost in efficiency will be tremendously serious especially in concentrated system.

Despite all drawbacks mentioned in above, cold mirror stands an advantage. It is cost-effective compare to dichroic beam splitter as dichroic requires high initial capital investment. However this advantage will be less significant with a higher concentrated device. As the limited fund is unaffordable, it is the only option for the non or pre-concentrated research purpose. Below (Graph 6) is the data sheet provided by the Edmund optics supplier.
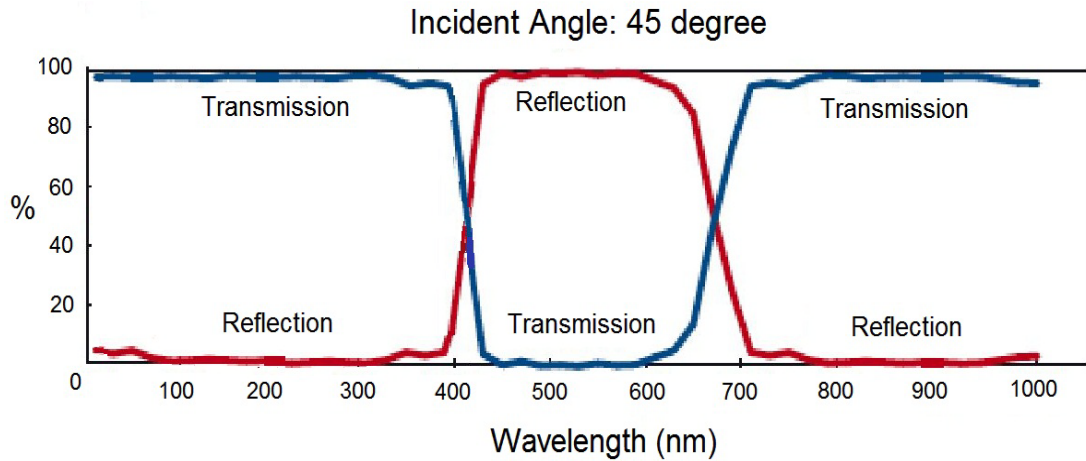
Graph 6: Cold mirror reflect from 400nm to 700nm (Appendix I)

4.3.2   Cold Mirror Holder
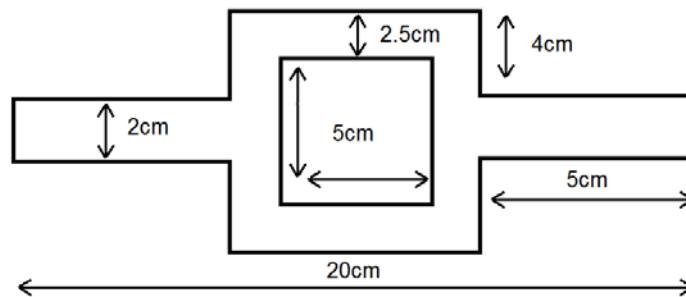
Figure 4.12: Cold mirror holder.

A holder is designed without clamps on mirror to eliminate obstacle blocking the incident radiation, framing the cold mirror in place to give an optimum splitting result. But in another word, it is trading off its firmness to performance. As the holder undergoes thermal expand under sunlight, cold mirror could possibly fell off. To increase the firmness, the cold mirror must precisely fit into the holder, and using superglue to further stabilise it.

4.3.3 Confine box of Cold mirror Tandem Cell
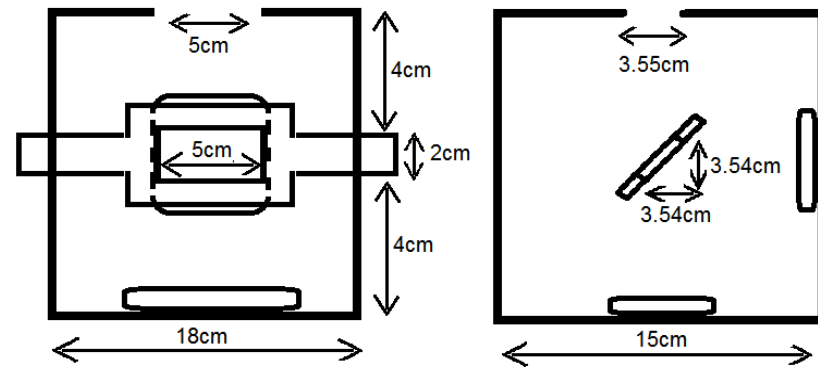
Figure 4.13: (Left) Front view of the box. Figure 4.14: (Right) Side view of the box.

Figure 4.15: Cold mirror tandem cell.
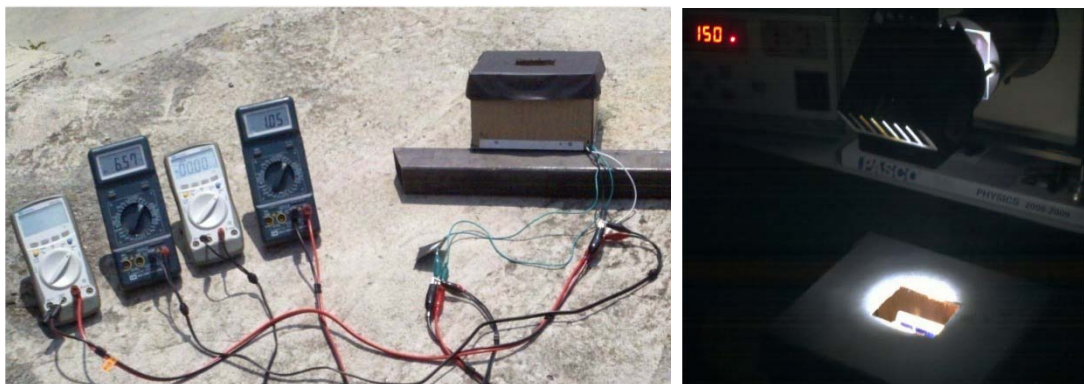
Figure 4.16: (Left) Cold mirror tandem cell exposed under sun.

Figure 4.17: (Right) Cold mirror tandem cell exposed under solar simulator.

CHAPTER 5

RESULTS AND DISCUSSIONS

5.1   Results under the Sun

Table 5.1: α-Si with Big Poly-Si

	α-Si			*Big Poly-Si*		
	V (V)	**I (mA)**	**Power (mW)**	**V (V)**	**I (mA)**	**Power (mW)**
Prism	6.5	8.70	56.6	1.7	5.80	9.86
Cold Mirror	6.7	17.1	115	3	11.0	33.0

Table 5.2: α-Si with Small Poly-Si:

	α-Si			*Small Poly-Si*		
	V (V)	**I (mA)**	**Power (mW)**	**V (V)**	**I (mA)**	**Power (mW)**
Prism	6.5	8.90	57.9	1	41.5	41.5
Cold Mirror	6.7	17.3	116.1	1.09	171.0	186.0

To obtain FF (Fill Factor),

$$FF = \frac{I_{mpp} \cdot V_{mpp}}{I_{sc} \cdot V_{oc}} \approx \left| \frac{v_{oc} - \ln(v_{oc} + 0.72)}{v_{oc} + 1} \right|$$

(5.1)

and ,

$$\left| v_{oc} = V_{oc} \frac{q}{m \cdot k \cdot T} \right|$$

(5.2)

Where,   m = 1 (diode ideality factor)

 k = 1.38 x 10^{-23} J/K (Boltzmann constant)

T = 298K (Temperature)

q = 1.6 x 10^{-19} As (charge of electron)

V_{oc} = open circuit voltage

*The full calculation for efficiency are provided in Appendix A

**Data sheet for α-Si and Poly-Si is provided in Appendix G and Appendix H.

Table 5.3: Prism

	FF for α-Si	*FF for Poly-Si*	*Total Power (mW)*	*Efficiency η*
α-Si with Big Poly-Si	0.974	0.923	64.23	*6.4%*
α-Si with Small Poly-Si	0.974	0.923	93.1	*9.31%*

Table 5.4: Cold Mirror

	FF for α-Si	*FF for Poly-Si*	*Total Power (mW)*	*Efficiency η*
α-Si with Big Poly-Si	**0.975**	0.951	143.508	*8.11%*
α-Si with Small Poly-Si	**0.975**	0.891	278.92	*15.76%*

Table 5.5: List of Efficiency by Different Technology

	α-Si + Big Poly-Si	**α-Si + Small Poly-Si**
Prism	6.4%	9.31%
Cold Mirror	8.11%	15.76%

5.1.1 Analysis on the efficiency

To analyse the lost efficiency, PV is directly exposed under the sunlight to compare with the results of prism and cold mirror.

Table 5.6: PV Fully Exposed under the Sun

α-Si			Big Poly-Si			Small Poly-Si		
V (V)	I (mA)	Power (mW)	V (V)	I (mA)	Power (mW)	V (V)	I (mA)	Power (mW)
6.7	31.6	212.0	4.02	136.1	547.3	1.1	399.73	439.7

Table 5.7: PV under Tandem Cell Technology

	α-Si			Big Poly-Si			Small Poly-Si		
	V (V)	I (mA)	Power (mW)	V (V)	I (mA)	Power (mW)	V (V)	I (mA)	Power (mW)
Prism	6.5	8.90	57.9	1.7	5.80	9.86	1.0	41.5	41.5
Cold Mirror	6.7	17.3	116.1	3.0	11.0	33.0	1.1	171.0	186.0

Table 5.8: Percentage Power Difference between tandem PV and Exposed PV

	$\Delta\%_{\alpha}$	$\Delta\%_{big\ poly}$	$\Delta\%_{small\ poly}$
Prism	28.81%	1.80%	14.76%
Cold Mirror	54.76%	6.03%	42.30%

Analysis:

1. α-Si in Prism Technology

Percentage power difference of α-Si between under exposed and under prism is 28.81%

Factors:

    a. The transmission rate of the prism is very low. An experiment (Appendix B) conducted in dark room is done to examine the transmission rate of the prism.

4 set of results is produced to give an average results. The first peak near $100°$ is the light intensity diffracted by prism. The average peak transmission rate is 37.15%. The rest of the intensity appears in graph is the result of internal reflection before diffracted out from prism.
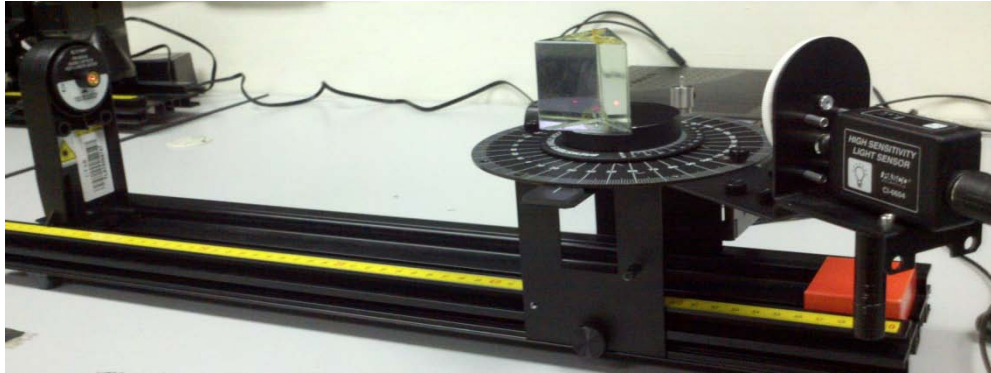
Figure 5.1: A red laser and a light sensor are located at two ends. The prism is placed in between laser and sensor. By rotating the sensor around prism, the transmission rate is obtained from computer.
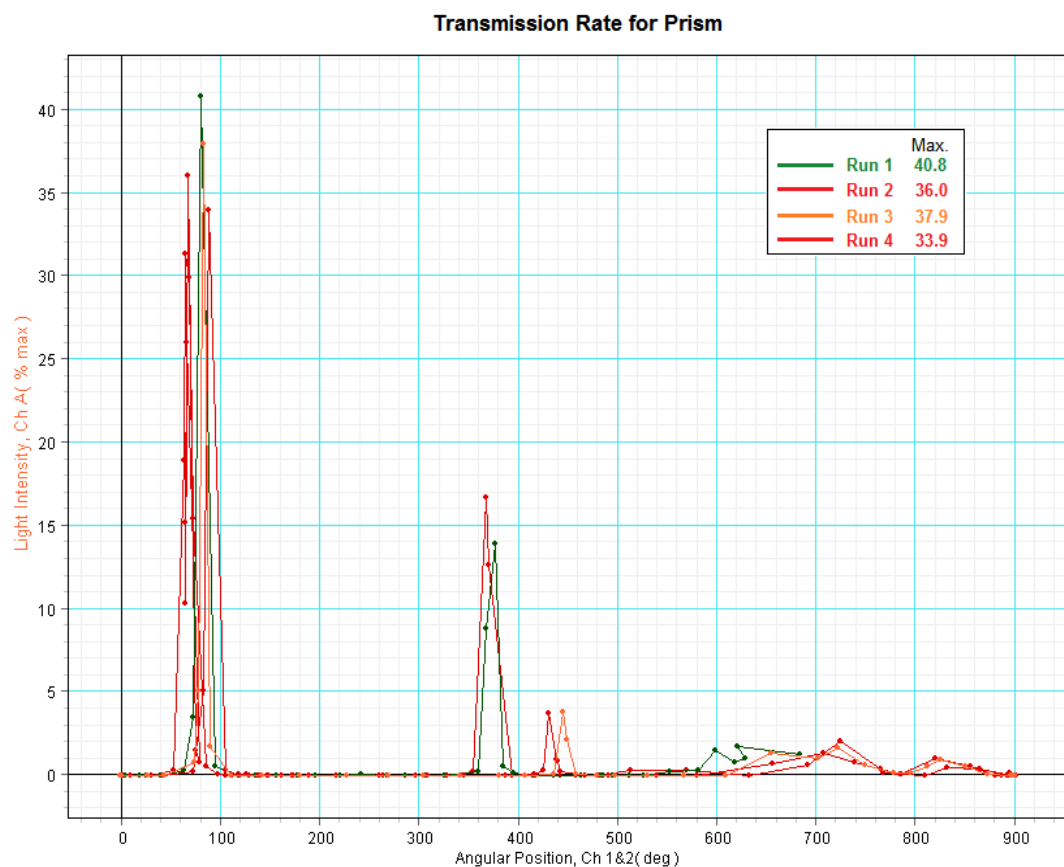
Graph 7: Results of the transmission rate of prism

b. Inaccurate in targeting toward sun gives shadow and reduce the light incident area on PV cell, eventually lead to a lost in efficiency. It is impossible to targeting toward sun precisely without the sun tracking system. Although the flexible design retrieve a lot of losses, but some losses are still unavoidable.

c. The prism holder blocked part of the sun light that diffracted toward PV. Although it did not significantly reduce the incident diffracted light on PV, yet it still gives a little impact on the efficiency.

d. After the lost in incident area of diffracted light, internal resistance arises in PV due to the incapability to provide current in shaded area. Inside the PV, a number of cells, called array, are either connected by series or parallel to form up a PV cell. Experiment to examine and reduce the internal resistance effect for both α-Si and Poly-Si is provided in Appendix F.

2. Poly-Si in Prism Technology

Percentage power difference between under exposed and under prism are 1.8% (big poly-Si) and 14.76% (small poly-Si).

Factors:

a. The prism used in this project, in fact, is for education purposes like demonstrating the rainbow effect. Therefore the transmission rate for invisible spectrum through prism is estimated to be lower than the visible red 670nm laser light.

b. Since there is no data sheet provided for prism, the material is then unknown, therefore it is unable to determine the parameter of diffracted light in different wavelength. Even though the experiment able to determine the diffraction angle of the visible spectrum, but the invisible spectrum is left unknown. By placing Poly-Si PV next to α-Si could only capture the spectrum followed by the short wavelength 730nm, but it does not tell to what extent the poly-Si PV able to capture. The big poly-Si has a large size, when the cell area is shaded or no incident spectrum fell on it, it operates as

an open circuit with high resistance. This reduces plenty amount of power when the cells are connected in series. To reduce the drawback effect, a smaller poly-Si PV is then replaced, and proved to be producing a higher rate of power.

c. Part of the spectrum miss dropped onto another PV cell. This is unavoidable since the surface of prism is wide which diffract all spectrum and limited in PV cell size and position. This drawback decreases significant with the help of flexible design introduce onto the PV cells. The lost in efficiency is relatively small, but it is worth to be noticed. The spectrum miss fall on Poly-Si is acceptable as poly-Si has a wider converting energy range, but in another way, miss fall on α-Si can be treat as total lost
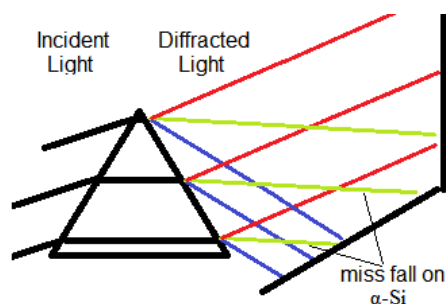
Figure 5.2: Green spectrum missed fall onto α-Si instead of Poly-Si

3. α-Si in Cold Mirror

Percentage power difference of α-Si between under exposed and under cold mirror is 57.76%

Factors:

a. The reflection rate for visible spectrum of the cold mirror is very efficient. An experiment (Appendix C) similar in examining prism has carried out. The results give an average of 92.9% reflection rate (graph 8) and 3.15% of transmission rate (graph 9). The 4% which do not accounted in both reflection and transmission rate are the destructive interference in thin film, which add up with 3.15% transmission rate to give a total 7.1% lost.
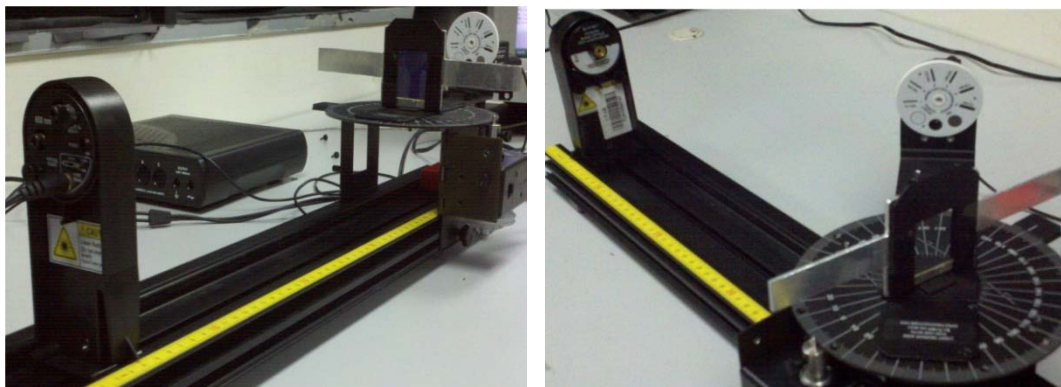
Figure 5.3: (left) Examine transmission rate. (Right) Examine reflection rate.
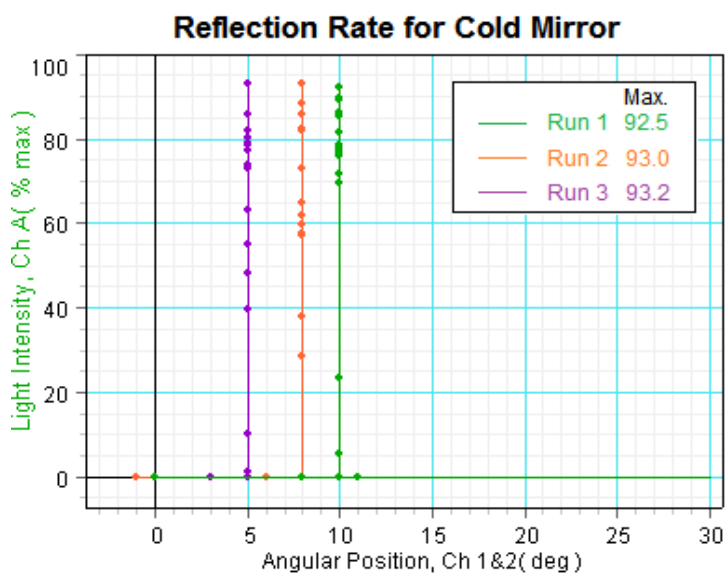
Graph 8: Reflection rate for Cold Mirror
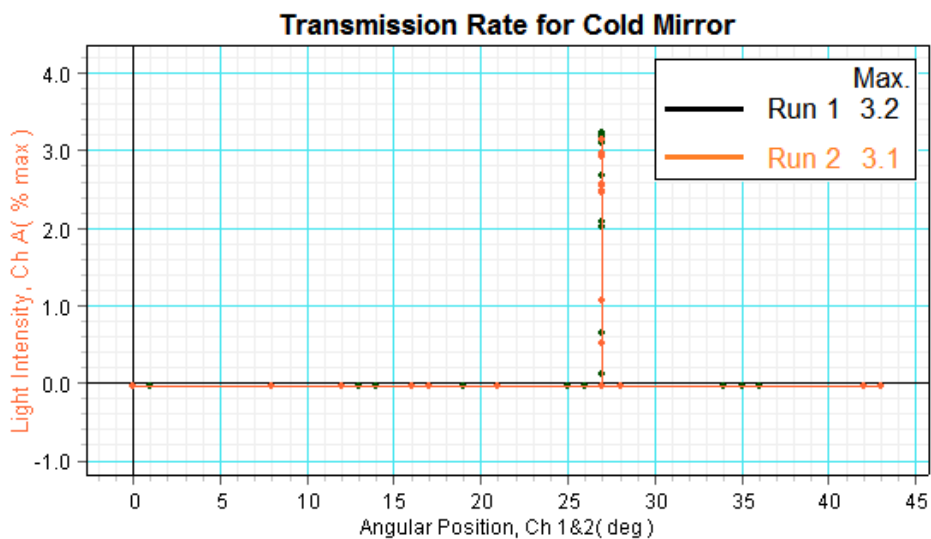
Graph 9: Transmission rate for Cold Mirror
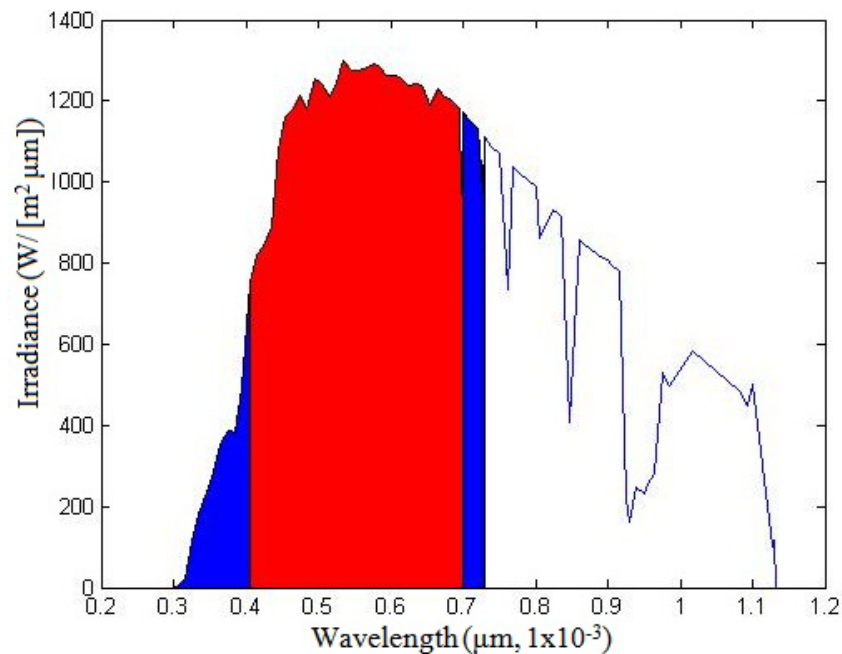
Graph 10: Absorbing range for α-Si is 290nm – 730nm (blue + red colour area).
Absorbing range for α-Si under cold mirror is 400nm – 700nm (red colour area).

b. The spectrum of sun radiation start from 290nm instead of 0nm under condition AM 1.5, hence the working range for an α-Si is 290nm – 730nm. Yet cold mirror only reflect 400nm - 700nm wavelength towards α-Si, this means that α-Si has lost the absorbing spectrum of 290nm – 400nm, and 700nm – 730nm. The lost due to the spectrum distribution is 15.05%. The calculation of the lost efficiency and the graph is plotted using MatLab (programming is listed in Appendix D), and the data for the graph is collected from Alan L. Fahrenbruch and Richard H. Bube (1983), Fundamentals of Solar Cells [68].

c. The area of light incident is smaller than the area of α-Si, giving internal resistance, therefore lowering down efficiency. The mirror is tilted 45° degree respect to incident light to give a right angle reflection toward α-Si. The mirror is 5cm x 5cm square in dimension, after tilted to 45°, the incident area become 5cm x 3.54cm(23.7cm^2 area), while the effective area of α-Si is 5.3cm x 4.47cm(17.7cm^2 area). Hence the shaded area, where internal resistance takes effect in, is 7 cm^2, 24.54% of the total α-Si area. To reduce this resistance effect, a method is introduced in Appendix F.

d. Percentage of lost efficiency for each factor:

15.08% lost as spectrum distribution for the spectrum from 290-400nm and 700-1130nm. 84.92% left.

84.92% undergoes cold mirror of 92.9% reflection rate, 79.9 left%.

From the cold mirror data sheet, the transmission rate does not change to reflection rate sharply at 400nm and 700nm. In fact, transmission rate change gradually to reflection rate from 400nm to 440nm, that means half of the 400-440nm spectrum transmitted to poly-Si. This happen as well in the spectrum of 600-700nm, reflection rate gradually change to transmission rate. Within 600-700nm spectrum, half of the radiation transmitted towards poly-Si. Due to 600-700nm is the peak intensity, and 400-440nm is around peak region, huge amount of spectrum is directed towards poly-Si. Roughly a 20% of power has losses to poly-Si, hence from 79.9% reduces to 59.9%. Hence the overall spectrum distribution is 59.9%.

The percentage goes down to final results of 54.76%, hence the internal resistance is around 5.14%.

Table 5.9: Factors of losses in α-Si

	Losses (α-Si)
Cold Mirror Spectrum Distribution	**15.08%**
Overall Spectrum Distribution	**40.18%**
Internal Resistance	**5.14%**
Reflection Rate of Cold Mirror	**7.1%**
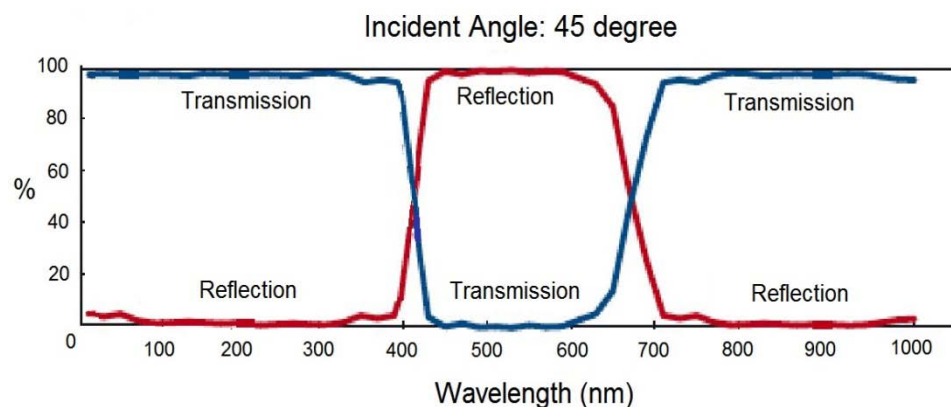
Graph 6: Cold mirror reflect from 400nm to 700nm (Appendix I)

4. Poly-Si in Cold Mirror

Percentage power difference between under exposed and under cold mirror are 6.03% (big poly-Si) and 66.17% (small poly-Si).

Factors:

a. Transmission rate for 0-400nm and 700-∞nm wavelength is around 92.9% (Appendix I). The 7% losses is an acceptable loss.
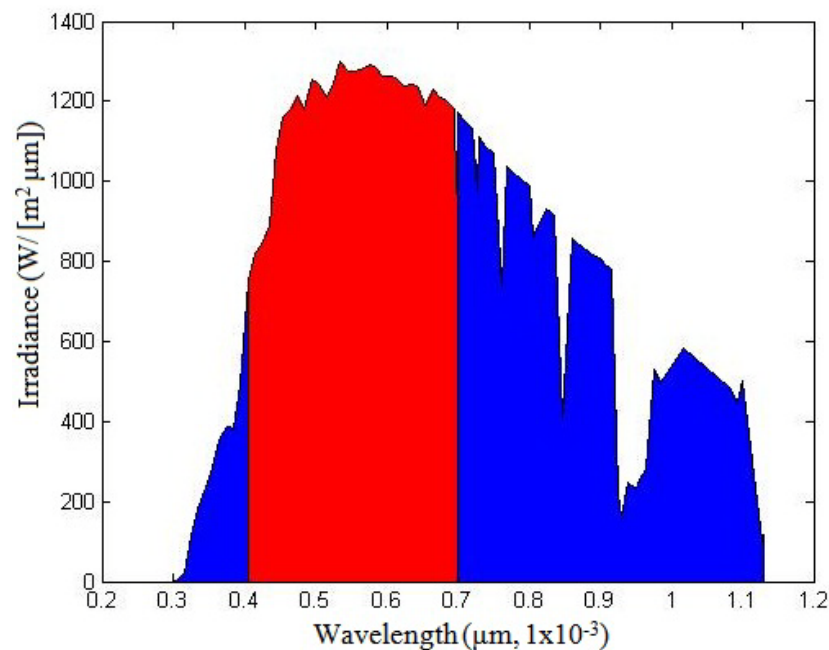
Graph 11: Absorbing range for Poly-Si is 290nm - 1130nm (Blue + red region).
Absorbing range for Poly-Si under cold mirror is 290nm - 400nm and
700nm - 1130nm (blue region).

b. Poly-Si lost the spectrum from 400-700nm due to the cold mirror reflected to α-Si, hence only converts energy from spectrum 290nm - 400nm and 700nm - 1130nm wavelength. The lost due to the reflected spectrum takes 52.3%, therefore only 47.6% of spectrum falls on Poly-Si. The data [69] and MatLab programming is provided in Appendix E. Noted the percentage obtained in lost efficiency is a rough estimation. As the reflection and transmission rate of cold mirror is not directly stop at 400nm and 700nm, it takes a range of spectrum before reaching the rate of 92.9% transmission and reflection rate.

c. For the big size poly-Si, the large shaded area gives results to high internal resistance and hence largely reduced in power production. While for the small poly-Si, the shaded area is relatively small and hence it gives a higher power. Secondly, due to the small poly-Si has a smaller area, this gives an advantage in avoiding series resistances due the connection within the PV array (refer Appendix F). The effective area of big and small poly-Si relatively is 75cm^2 (6cm x 12.5cm) and 36cm^2 (6cm x 6cm), while incident light area under the sun is 17.7cm^2. Hence the percentage area without incident light for big and small poly-Si is 76.4% and 50.8%.

d. Percentage of lost efficiency for each factor:

52.30% lost as spectrum distribution by cold mirror, 47.70% left.

47.70% undergoes cold mirror of 92.9% transmission rate, 44.31% left.

For small poly-Si, the transmission rate does not change to reflection rate sharply at 400nm and 700nm. From the data sheet, the transmission rate change gradually to reflection rate from 400nm to 440nm, that means half of the 400-440nm spectrum transmitted to poly-Si. This happen as well in the spectrum of 600-700nm, reflection rate gradually change to transmission rate. Within 600-700nm spectrum, half of the radiation transmitted towards poly-Si. Due to 600-700nm is the peak intensity, and 400-440nm is around peak region, huge amount of spectrum is directed towards poly-Si. Roughly a 20% of power has added to 44.31% (percentage that transmitted for spectrum 290-400nm and 400-1130nm) on poly-Si, give a overall spectrum distribution of 64.31%. The percentage reduce to final results of 42.30%, hence internal resistance is about 22.01%.

For big poly-Si case, 64.31% reduces to the final results of 6.03%, thus lost due to internal resistance is expected around 58.28%.

Table 5.10: Factors of losses in poly-Si

	Losses (Big Poly-Si)	Losses (Small Poly-Si)
Cold Mirror Spectrum Distribution	52.30%	52.30%
Overall Spectrum Distribution	35.69%	35.69%
Internal Resistance	58.28%	22.01%
Transmission Rate of Cold Mirror	7%	7%

5.2   Results under Solar Simulator

Table 5.11: α-Si with Big Poly-Si

	α-Si			*Big Poly-Si*		
	V (V)	**I (mA)**	**Power (mW)**	**V (V)**	**I (mA)**	**Power (mW)**
Prism	6.5	3.17	20.6	1.7	1.20	2.04
Cold Mirror	6.7	5.50	36.9	3	2.40	7.20

Table 5.12: α-Si with Small Poly-Si

	α-Si			*Small Poly-Si*		
	V (V)	**I (mA)**	**Power (mW)**	**V (V)**	**I (mA)**	**Power (mW)**
Prism	6.5	3.58	23.3	0.91	16.6	15.1
Cold Mirror	6.69	5.69	38.1	1.09	70.1	76.4

(Procedure to obtained the FF and efficiency is available in Appendix A)

Table 5.13: Prism

	FF for α-Si	*FF for Poly-Si*	*Total Power (mW)*	*Efficiency η*
α-Si with Big Poly-Si	0.974	0.923	21.95	*0.014%*
α-Si with Small Poly-Si	0.974	0.874	45.38	*0.023%*

Table 5.14: Cold Mirror

	FF for α-Si	*FF for Poly-Si*	*Total Power (mW)*	*Efficiency η*
α-Si with Big Poly-Si	0.975	0.951	42.83	*0.016%*
α-Si with Small Poly-Si	0.975	0.891	98.9	*0.038%*

Table 5.15: List of Efficiency by Different Technology

	α-Si + Big Poly-Si	**α-Si + Small Poly-Si**
Prism	0.014%	0.023%
Cold Mirror	0.016%	0.038%

5.2.1   Analysis on the efficiency

Table 5.16: PV fully exposed to Solar Simulator

α			Big Poly-Si			Small Poly-Si		
V (V)	I (mA)	Power (mW)	V (V)	I (mA)	Power (mW)	V (V)	I (mA)	Power (mW)
6.64	9.84	65.3	3.4	32.8	112.01	1.15	91.2	105.04

Table 5.17: PV under Tandem Cell Technology

	α-Si			Big Poly-Si			Small Poly-Si		
	V (V)	I (mA)	Power (mW)	V (V)	I (mA)	Power (mW)	V (V)	I (mA)	Power (mW)
Prism	6.5	1.27	8.28	1.7	1.20	2.04	0.9	16.6	14.9
Cold Mirror	6.7	5.50	36.9	3	2.70	8.10	1.1	29.0	31.9

Table 5.18: Percentage Power Difference between tandem PV and Exposed PV

	$\Delta\%_\alpha$	$\Delta\%_{big\ poly}$	$\Delta\%_{small\ poly}$
Prism	22.68%	1.82%	14.22%
Cold Mirror	56.43%	7.23%	30.38%

Analysis:

1. **α-Si in Prism Technology**

Percentage power difference of α-Si between under exposed and under prism is 12.68%
Factors:

   a. The transmission rate for prism is 37.15. 62.85% is lost to internal reflection.

   b. The area of light from solar simulator is too small thus unable to fully incident on the PV cell. The shaded part of the PV hence unable to produce power. The radius of the light from solar simulator is 1.75cm, yet even the smallest PV has an area of 4.4cmx5.3cm. The internal resistance is expected

to be pretty big. Furthermore, the solar simulator beam has an abnormal circular edge.

c. The value shown in the screen indicates the power of the spectrum is 150W. The power density of the spectrum is 15.59W/cm^2, much higher than AM 1.5, which is 0.1W/cm^2. In another word, solar simulator beam gives a concentrated of 156 suns (156 times concentrated under AM 1.5 sun light). Yet the power obtained from the PV is very low.

2. Poly-Si in Prism Technology

Percentage power difference between under exposed and under prism are 1.82% (big poly-Si) and 14.22% (small poly-Si).

Factors:

a. The cheap prism gives a very low transmission rate in visible wavelength, and is estimated to be even lower in invisible spectrum.

b. The area of light from solar simulator is small, causing part of the PV cell unable to produce power.

c. The power supplied to the light from solar simulator may not be the value shown in the screen. The exact power of the solar simulator beam could be much lesser than that value.

d. The internal resistance arises due to shaded region (refer to Appendix F).

e. Part of the spectrum miss dropped onto another PV cell. Refer the explanation in factors of poly-Si in prism technology under sun.

3. α-Si in Cold Mirror

Percentage power difference of α-Si between under exposed and under cold mirror is 56.43%.

Factors:

a. The reflection and transmission rate in visible spectrum of the cold mirror is 92.9% (graph 8) and 3.15% (graph 9) respectively. The lost is 7.1%.

b. The spectrum distribution of spectrum within 290-400nm and 700-1130nm gives a total loss of 15.08%. A rough estimation is shown in Appendix D.

c. The area of light incident is smaller than the area of α-Si, giving internal resistance, therefore lowering down efficiency. The mirror is tilted 45° degree respect to incident light to give a right angle reflection toward α-Si. The incident light area for solar simulator is 9.6cm^2, while the effective area of α-Si is 5.3cm x 4.47cm (17.7cm^2 area). Hence the shaded area, where internal resistance takes effect in, is 8.1cm^2, 45.76% of the total α-Si area. To reduce this resistance effect, a method is introduced in Appendix F.

d. Percentage of lost efficiency for each factor:

15.08% lost as spectrum distribution for the spectrum from 290-400nm and 700-1130nm. 84.92% left.

20% transmitted to poly-Si, the overall spectrum distribution is 64.92%.

64.92% reduces to the final results of 57.76%, hence lost due to internal resistance is expected around 7.16%.

Table 5.19: Factors of losses in efficiency

	Losses
Cold Mirror Spectrum Distribution	**15.08%**
Overall Cold Mirror Spectrum Distribution	**35.08%**
Internal Resistance	**7.16%**
Reflection Rate of Cold Mirror	**7.1%**

4. Poly-Si in Cold Mirror

Percentage power difference between under exposed and under cold mirror are 7.23% (big poly-Si) and 30.38% (small poly-Si).

Factors:

a. Transmission rate for 0-400nm and 700-1130nm wavelength is 92.9% (Appendix I). The loss to reflection rate is 7.1%.

b. Poly-Si lost the spectrum from 400-700nm due to the cold mirror reflected to α-Si, hence converts energy from spectrum 290-400nm and 700-1130nm wavelength. The reflected spectrum takes 52.3%, therefore only 47.6% of spectrum falls on Poly-Si. Rough estimation is provided in Appendix E.

c. For the big size poly-Si, the large shaded area gives results to high internal resistance. While for the small poly-Si, the shaded area is relatively small and gives higher power. The effective area of big and small poly-Si relatively is $75cm^2$ (6cm x 12.5cm) and $36cm^2$ (6cm x 6cm), while incident light area for solar simulator is $9.6cm^2$. Hence the percentage area without incident light for big and small poly-Si is 87.2% and 73.33%.

d. Percentage of lost efficiency for each factor:

   52.30% lost as spectrum distribution by cold mirror, 47.70% left.

   47.70% undergoes cold mirror of 92.9% transmission rate, 44.31% left.

   20% transmitted to poly-Si, the overall spectrum distribution is 64.31%

   For small poly-Si case, 64.31% reduces to the final results of 30.38%, hence lost due to internal resistance is expected around 33.93%.

   For big poly-Si, 64.31% reduces to 7.23%, internal resistance is about 61.36%

Table 5.20: Factors of losses in efficiency

	Losses (Big Poly-Si)	Losses (Small Poly-Si)
Cold Mirror Spectrum Distribution	52.30%	52.30%
Overall Spectrum Distribution	35.69%	35.69%
Internal Resistance	57.08%	33.93%
Reflection Rate of Cold Mirror	7%	7%

5.3   Discussion

1. The sequence of the power generated for different technology is:

CM Small Poly-Si › Prism Small Poly-Si › CM Big Poly-Si › Prism Big Poly-Si

2. There are three main factors that reduce the efficiency, which is internal resistance, spectrum distribution, and transmission or reflection rate of the incident light. The internal resistance account for the largest lost among these factors. From the sequence shown in above, big poly-Si give the worst results as it produce a large shaded area, highlighting the effect of internal resistance.

3. The cold mirror gives a highest efficiency of 15.76% under AM 1.5 condition. Literally main losses for both PV are caused by the overall spectrum distribution. In α-Si, the loss in overall spectrum distribution, which account for 40.18%, is caused by the restriction in reflecting full spectrum range from 290-730nm towards α-Si, leaving behind 290-400nm and 700-730nm spectrum to poly-Si. Secondly, partial of the spectrum from 400-440nm and 600-700nm is transmitted to poly-Si, instead of α-Si. The internal resistance is found even lower than the loss of reflection rate, which takes only 5.14%. This is can be explain as all the connection of arrays in cell is in parallel, so the shaded effect is thus much reduced.

Table 5.9: Factors of losses in α-Si

	Losses (α-Si)
Cold Mirror Spectrum Distribution	**15.08%**
Overall Spectrum Distribution	**40.18%**
Internal Resistance	**5.14%**
Reflection Rate of Cold Mirror	**7.1%**

4. In the case of cold mirror poly-Si PV, the highest lost is the cold mirror spectrum distribution, 52.30%. Tandem cell increase efficiency by separating spectrum towards different PV cell according to respective working range.

Hence the lost in spectrum distribution in poly-Si is necessary and expected, since spectrum lost in poly-Si is purposely distribute to α-Si to produce a higher rate of power. Yet, as the inability in distributing spectrum ideally to α-Si due to the restriction of cold mirror, the spectrum which failed to reflect toward α-Si is eventually transmitted to poly-Si, thus reducing and compensate the lost of the overall spectrum distribution, making the losses reduced to 35.69%. As the spectrum distribution is necessary in poly-Si, it shall not consider as the major lost that caused in low efficiency. In fact, internal resistance responsible for the major lost, account for 22.01%, which is unnecessary and undesired. The loss of transmission rate can hardly avoid, and it is within an acceptable loss.

Table 5.10: Factors of losses in poly-Si

	Losses (Big Poly-Si)	*Losses (Small Poly-Si)*
Cold Mirror Spectrum Distribution	52.30%	52.30%
Overall Spectrum Distribution	35.69%	35.69%
Internal Resistance	58.28%	22.01%
Transmission Rate of Cold Mirror	7%	7%

5. The lost in internal resistance are contrast especially in poly-Si case. As the results are terrible for the big poly-Si, the replacement of small poly-Si has dramatically increased the results of the poly-Si in both prism and cold mirror technology. The power produced in the fully exposed big poly-Si is 5 times of the combine power of α-Si and poly-Si that produces under cold mirror technology, and result goes even worst in the prism technology case. That means the big poly-Si itself produce a 12% efficiency, higher than both technology could produce. Hence this had completely denied the project which utilizes technology to gives a better efficiency. The replacement of the small PV help in justifying the internal resistance factor and producing higher power, thus save this project from fail in achieving the objective.

6. Noted that the power produced in the small poly-Si is 439.7mW, after account into Fill Factor (FF = 0.89 under V_{oc} = 1.1V), power reduces to 391.33mW, 1.4 times higher than the cold mirror technology 278.92mW. The light incident area for fully exposed PV is 6cm x 6cm, which absorb 36cm^2 area of sun radiation. Yet the light incident area in cold mirror is 3.54cm x 5 cm, which only absorb 17.7cm^2 area of sun radiation. The difference in area is 49.16%. Furthermore, the shaded area which further imposes internal resistance on the PV under cold mirror technology. A fair comparison should do in a same incident area for both exposed and cold mirror tech PV. This contrast the importance of the size in PV must match the area of light incident.

7. In prism technology, the main losses come from the transmission rate of prism, 72.85% have lost before the shaded area and internal resistance impose any effect on efficiency. Due to the limited budget, since lab grade prism is unaffordable, a cheap prism is the only choice. The area expose to prism is only 2cm x 5 cm, hence this gives relatively low power on PV compares to the fully exposed PV. The prism holder blocks part of the sun radiation from diffracting towards PV. The structure of the PV holder and stand has to adjust in order to avoid shaded area. It is hard to align towards sun precisely without sun tracking system, thus poses shadows on PV and reducing the performance. Together with internal resistance the efficiency is further decrease to 6.4% for big poly-Si and 9.31% for small poly-Si.

8. The results obtained through solar simulator failed badly. The efficiency goes from the highest of 0.038% to the lowest 0.014%. It shows the same sequence in terms of efficiency by different technology as in under the sun. Cold mirror technology with small poly-Si score the best, second is Prism technology with small poly-Si, while third and forth is cold mirror and prism technology both mounted with big poly-Si. The result implies that the technology performance is not affected by the light source, as the sequence maintained. Yet the performances in terms of efficiency scored badly. The light source responsible for the bad efficiency. First, the intensity of solar simulator is not even higher than the AM 1.5 intensity, but the screen showed 150W, which mean 150W is supplied to the 1.75cm of radius beam. Secondly, the area if

incident light is too small to avoid or reduce shaded area that gives rise to internal resistance. Thirdly, the beam from solar simulator apparently defective. Part of the edge is shaded, makes the circular beam seems absurd. Furthermore the light at the particular absurd edge gives bluish and violet beam. This may caused by the channel which directs the beam has worn out or run out of calibration. Hence the experiment is considered fail to demonstrate efficiency of different tandem cell technology given.

9. Comparing table 5.8 with 5.18 below, the percentage power difference of sun is always greater than solar simulator. This is due to the internal resistance effect was amplified under larger shaded area, where solar simulator have smaller area of light incident on PV. The difference between sun and solar simulator is not obvious in the case of prism technology. This may due to the help of adjustable structures which retrieve some power losses.

Table 5.8: Percentage Power Difference between tandem PV and Exposed PV

	$\Delta\%_{\alpha}$	$\Delta\%_{big\ poly}$	$\Delta\%_{small\ poly}$
Prism	28.81%	1.80%	14.76%
Cold Mirror	54.76%	6.03%	42.30%

Table 5.18: Percentage Power Difference between tandem PV and Exposed PV

	$\Delta\%_{\alpha}$	$\Delta\%_{big\ poly}$	$\Delta\%_{small\ poly}$
Prism	22.68%	1.82%	14.22%
Cold Mirror	56.43%	7.23%	30.38%

10. The timing to carry experiment under the sun is important. In dark room, solar simulator shine lights directly above prism box, and the comfortable dark room condition allows the adjustment to make precisely. When come under sun, the results are hard to obtain as precisely as in dark room. Without the aid from sun tracking system, the diffracted light on PV shift position time to time, as well as the adjustment has to accordingly.

82

11. The data sheets of PV cell are somehow inaccurate. In the α-Si case, the data sheet indicates V_{oc} is 6.8V, I_{sc} is 16.3mA, I_{ope} is 33.3mA, and power produce is 226.44mW. Yet the value carried out by experiment is V_{oc} is 6.7V, I_{sc} is 31.6mA, power produce is 211.72, 6.5% in power difference. Although they are close, but the difference cannot be neglected especially come into the calculation. For the poly-Si, there is no data sheet provided in both the big and small PV. But the power of small PV is listed when placing order from supplier. The small PV is listed 1V x 5mA to give a 5mW power, again the value carried under experiment gives 1.1V x 399.73mA, produce only 439.7mW. The difference is 12.06%, quite noticeable. Hence the data sheet can only serve as references, it shall not directly applied on calculation.

12. The Fill Factor value in calculating efficiency is an ideal FF value. Since there is no load (battery system) connected to PV, thus the operating point is unknown. Hence by introducing the ideal FF value, the efficiency is then obtained. Normally, FF value is around 80%, but the ideal FF gives from 0.883to 0.975. A handful drop down in efficiency is likely to occur when the tandem cell connected to a charging or battery system.

13. The efficiency of the Cold Mirror tandem cell is 15.76% and Prism tandem cell is 9.31%. For individual PV cell, the efficiency of the α-Si is 8.72% and poly-Si is 10.88%. The prism tandem cell has failed the objectives to give higher rate efficiency. Efficiency of prism tandem cell can be improved by changing a lab-grade prism and smaller size PV which fit to the light incident area.

14. The A.P.I (air pollution index) indicates 43 point on the day which results obtained under the sun, 11-08-2011. The API is taken from the website of Department of Environment, Malaysia [70].

CHAPTER 6

CONCLUSION AND RECOMMENDATIONS

6.1   Conclusion

1. The efficiency of the Cold Mirror tandem cell is 15.76% and Prism tandem cell is 9.31%. For individual PV cell, the efficiency of the poly-Si is 10.88% and α-Si is 8.72%. Cold mirror tandem cell has increase in efficiency by 4.88% compare to single poly-Si PV cell, while Prism tandem cell has failed to achieve higher efficiency, which has 1.57% lower than single poly-Si PV cell.

2. Internal resistance responsible for most of the losses. The area of PV in tandem cell must fully incident with convertible spectrum radiation.

3. Spectrum distribution is the second largest lost. Proper spectrum distribution can effectively increase the efficiency.

4. Cold Mirror tandem cell has proved in increase of efficiency experimentally. Despite Prism tandem cell gives lower rate than an individual functioning PV cell, yet it is expect to gives an efficiency close to Cold Mirror tandem cell after improvement done on it.

5. Both technologies can be further improved by replacing Dichroic Beam Splitter and lab-grade prism to respectively tandem cell.

6. All objectives are achieved. Design, realize and examine the efficiency of tandem cell. Cold Mirror tandem cell successfully increase the efficiency.

6.2   Recommendations in Improvement

1. The prism tandem cell has failed to achieve higher rate of efficiency, this is because of the low transmission rate in prism. To increase the transmission rate, the prism has to replace with a different material in prism, or coated with special material. Different material enhance transmission rate in different region of spectrum. The Fig.6.1 [81] lists out several of materials with spectrum enhance region respectively. UV Fused Silica served the best as it effectively enhance the poly-Si working region, 290nm – 1130nm, and give lower transmission rate after 2000nm spectrum, which spectrum radiation only contribute heat and reduce efficiency to PV cell. For low budget consideration, the option available is to do material coating on prism. Mg F_2 is the best candidate as this material coating is common and low in cost.
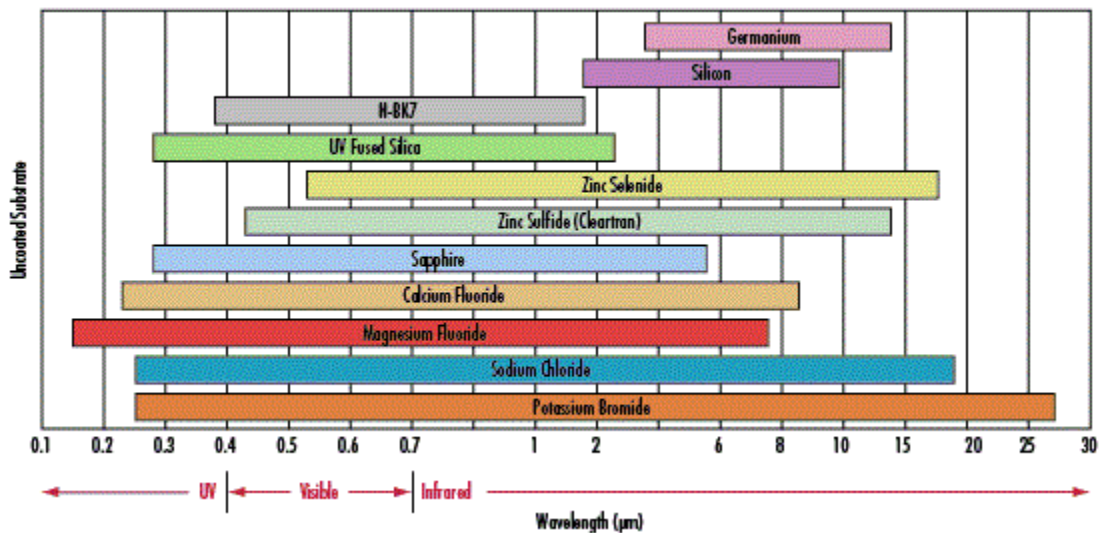
Figure 6.1: Different material with different range of optimum working spectrum.

For an example of 50cm x 50cm size Fused Silica UV grade right angle prism (Edmund Optics Company Prism, Stock A47-799) with MgF$_2$ coating and Aluminium hypotenuse to protect the edge from damage. The process of setting up prism tandem cell is provided in Appendix J. By using the Sellmeier equation, diffraction angle and all other parameter for setting up tandem cell is provided. To avoid any undesired error in calculation, a calculator is provided in a website [72] which programmed to shows the

refractive index by insert the corresponding material coefficient into the Sellmeier equation.

2. The internal resistance is the main factors causes in low efficiency. Tailor-made or purchase the PV cells with suitable sizes that work with the same area of incident radiation. Too big in size will give rise to the internal resistance yet too small fail to capture all incoming radiation. If the shaded area is unavoidable, reduce the internal resistance effect by avoiding the shadow fall on series array.

3. Redesign a prism holder without obstacle blocking the radiation from diffracted towards PV.

4. Solar tracking system is essential to avoid losses in miss-targeting toward sun. It is very sensitive to prism tandem cell, beside the reduction in incident area and the following drawback arises in internal resistance, the refractive angle changed as the incident angle on prism changed. Furthermore the solar azimuth angle varies time after time, thus the prism tandem cell may not able to obtain an optimum result without sun tracking system. This fallback will be magnified under the concentrated system, huge amount of power could lost due to the misalignment toward the sun.

5. Replace the cold mirror with a Dichroic Beam Splitter is the best way to reduce the spectrum distribution effect on efficiency. Ideally α-Si shall not receive losses from spectrum distribution before 730nm wavelength, as it gives higher rate of power than poly-Si can produce. While in another hand, the only trade off is the cost, as Dichroic Beam Splitter has to be tailor made.

6. There are only two ways to curb off the internal resistance effect in cold mirror tandem cell. First is using the PV cells which have the same area with the incident radiation. Secondly is to purchase a larger size of cold mirror so the distributed spectrum can fully incident on the PV cell.

7. Tandem cell box must be solid enough especially when mounting on solar tracking system. The prism tandem cell box which built by cardboard is not

firm to tilted and targeting towards the sun. The instrument inside the tandem cell box shifted even when the inclination is not slope. A wooden box is better than cardboard and Aluminium plate, since cardboard is not firm enough and Aluminium plate could expand under irradiation of sun.

8. After all of the losses are managed to retrieve, the next approach is to increase the efficiency by introducing concentrated system. Concentrated PV (CPV) system is to concentrate large amount of sun radiation onto a small area of PV to generate a higher rate of power. Noted that the prism tandem cell required imaging concentrating system since radiation must be uniformly incident on prism to diffract spectrum onto corresponding PV cell. While dichroic beam splitter has the flexibility to apply in both imaging or non-imaging concentrating system. Cassegrainian concentrator [66] is recommended to apply to both tandem cell technologies to examine the increase in power collecting.

9. CPV can alternately combine with thermal solar collector in a so-called CPV/T system, where part of the spectrum is distributed to PV cells and the residuals transmitted to a heat transferred fluid for thermal applications. Normally, PV cell is thermally fixed to a copper substrate containing cooling channels or thermoelectric receivers. A similar method has been used for thermoelectric devices to extract waste heat by cooling and thus maintain a high temperature gradient across the device, which results in improved conversion efficiency [24, 26]. The electric conversion efficiency for PV/T and thermoelectric receivers is constrained by the increase in temperature of the cooling medium, which is in direct thermal contact with solar conversion device. This can be improved by separating the cooling system from thermoelectric system, keeping the cooling channel relatively lower in temperature and extract heat to the thermoelectric receiver.

REFERENCES

[1] L. DeSandre, Y.D. Song, H.A. Macleod, M.R. Jacobson, D.E. Osborn, Thin-film multilayer filter designs for hybrid solar energy conversion systems, in: C.M. Lampert (Ed.), Optical Materials Technology for Energy Efficiency and Solar Energy Conversion IV, Proceedings of the SPIE, Vol. 562, 1985, 155–159.

[2] D.E. Osborn, M.A.C. Chendo, M.A. Hamdy, F. Luttmann, M.R. Jacobson, H.A. Macleod, R.Swenson, Spectral selectivity applied to hybrid concentration systems, Sol. Energy Mater. 14 (1986) pp. 299–325.

[3] M.A.C. Chendo, M.R. Jacobson, D.E. Osborn, Liquid and thin-film filters for hybrid solar energy conversion systems, Sol. Wind Technol. 4 (2) (1987) 131–138.

[4] J.C.C. Fan, F.J. Bachner, Transparent heat mirrors for solar-energy applications, Appl. Opt. 15 (4) (1976) 1012–1017.

[5] D.E. Soule,S.E. Wood, Heat-mirror spectral profile optimization for TSC hybrid solar conversion, in: C.-G. Granqvist, C.M. Lampert, J.J. Mason (Eds.), Optical Materials Technology for Energy Efficiency and Solar Energy Conversion V, Proceedings of the SPIE, Vol. 653, 1986, pp. 172–180.

[6] S.R. Clark, Spectrovoltaic solar energy conversion system, US Patent, 4,350,837, No. 1982.

[7] U. Ortabasi, A hardened solar concentrator system for space power generation: photovoltaic cavity converter (PVCC), Space Technol. 13 (5) (1993) 513–523.

[8] J.P. Penn, High concentration spectrum splitting solar collector, US Patent 6,469,241, 2002.

[9] S. McGrew, Color control in dichromated gelatin reflection holograms, in: T.C. Lee, P.N. Tamura (Eds.), Recent Advances in Holography, Proceedings of the SPIE, Vol. 215, Los Angeles, CA, 1980, pp. 24–31.

[10] W.H. Bloss, M. Griesinger, E.R. Reinhardt, Dispersive concentrating systems based on transmission phase holograms for solar applications, Appl. Opt. 21 (20) (1982) 3739–3742.

[11] J.E. Ludman, J. Riccobono, I.V. Semenova, N.O. Reinhand, W. Tai, X. Li, G. Syphers, E. Rallis, G.Sliker, J. Martin, The optimization of a holographic system for solar power generation, Sol. Energy 60 (1) (1997) 1–9.

[12] P. Gravisse,M. Prevot, Photovoltaic device with luminescent layers of differing composition, US Patent, 3,912,931, 1975.

[13] A. G.otzberger, W. Greubel, Solar energy conversion with fluorescent collectors, Appl. Phys. 14 (1977) 123–139.

[14] F. Galluzzi, E. Scafe, Spectrum shifting of sunlight by luminescent sheets: performance evaluation of photovoltaic applications, Sol. Energy 33 (6) (1984) 507–510.

[15] R.A. Powell, Solar energy conversion apparatus, US Patent 4,278,829, 1981.

[16] M. Sabry, R. Gottschalg, T.R. Betts, M.A.M. Shaltout, A.F. Hassan, M.M. El-Nicklawy, D.G.Infield, Optical filtering of solar radiation to increase performance of

concentrator systems, in: Proceedings of the 29th IEEE Photovoltaic Specialists Conference, New Orleans, LA, 2002, pp. 1588–1591.

[17] E.D. Jackson, Solar energy converter, US Patent 2,949,498, 1960.

[18] J.J. Loferski, Tandem photovoltaic solar cells and increased solar energy conversion efficiency, in: Proceedings of the 12th IEEE Photovoltaic Specialists Conference, Baton Rouge, 1976, pp. 957–961.

[19] M.F. Lamorte, D. Abbott, Two-junction cascade solar cell characteristics under 1000 concentration ratio and AM0-AM5 spectral conditions, in: Proceedings of the 13th IEEE Photovoltaic Specialists Conference, Washington DC, 1978, p. 874.

[20] M. Wolf, Limitations and possibilities for improvements of photovoltaic solar energy converters, in: Proceedings of the Institute of Radio Engineers, Vol. 48, 1960, pp. 1246–1263.

[21] G.W. Masden, C.E. Backus, Increased photovoltaic conversion efficiency through use of spectrum splitting and multiple cells, in: Proceedings of the 13th IEEE Photovoltaic Specialists Conference, New York, 1978, pp. 853–858.

[22] J.R. Onffroy, D.E. Stoltzmann, R.J.H. Lin, G.R. Knowles, High-efficiency concentration/multisolar-cell system for orbital power generation, in: Proceedings of the 15th Intersociety Energy Conversion Engineering Conference, Seattle, Washington, 1980, pp. 371–376.

[23] R.L. Bell, Solar energy converter with waste heat engine, US Patent 4,002,031, 1977.

[24] G. Rockendorf, R. Sillmann, L. Podlowski, B. Litzenburger, PV-hybrid and thermoelectric collectors, Sol. Energy 67 (4-6) (1999) 227–237.

[25] J. Padin, T.N. Veziroglu, A. Shahin, Hybrid solar high-temperature hydrogen production system, Int. J. Hydrogen Energy 25 (2000) 295–317.

[26] S.A. Omer, D.G. Infield, Design and thermal analysis ofa two stage solar concentrator for combined heat and thermoelectric power generation, Energy Convers. Manage. 41 (2000) 737–756.

[27] R.L. Bell, Concentration ratio and efficiency in thermophotovoltaics, Sol. Energy 23 (1979) 203–210.

[28] F. Demichelis, E. Minetti-Mezzetti, A solar thermophotovoltaic converter, Sol. Cells 1 (1979/80) 395–403.

[29] R.M. Swanson, A proposed thermophotovoltaic solar energy conversion system, in: Proceedings of the IEEE, Vol. 67(3), 1979, pp. 446–447.

[30] W.E. Horne, Conversion of solar to electrical energy, US Patent 4,313,024, 1982.

[31] R.E. Nelson, A brief history of thermophotovoltaic development, Semicond. Sci. Technol. 18 (5) (2003) S141–S143.

[32] D.C. White, B.D. Wedlock, J. Blair, Recent advance in thermal energy conversion, in: Proceedings of the 15th Annual Power Sources Conference, Atlantic City, NJ, 1961, pp. 125–132.

[33] B.D. Wedlock, Thermo-photo-voltaic energy conversion, in: Proceedings of the IEEE, Vol. 51, 1963, pp. 694–698.

[34] J.J. Werth, Thermo-photovoltaic converter with radiant energy reflective means, US Patent 3,331,707, 1967.

[35] E. Kittl, G. Guazzoni, Design analysis of TPV-generator system, in: Proceedings of the 25th Power Sources Symposium, Session on Thermal Energy Conversion, 1972, pp. 106–109.

[36] R.N. Bracewell, R.M. Swanson, Silicon photovoltaic cells in TPV conversion, Stanford University Interim Report ER-633, Research Project 790-1 (Stanford Electronics Laboratories, CA, 1978).

[37] L.S. Oglesby, L.E. Crackel, Spectral convertor, US Patent 4,313,425, 1982.

[38] A. Luque, Coupling light to solar cells, in: M. Prince (Ed.), Advances in Solar Energy, Proceedings of the ASES, Vol. 8, 1993, pp. 161–230.

[39] A.S. Brown, M.A. Green, Limiting efficiency of multiple band solar cells: an overview, in: Proceedings of the 17th European Photovoltaic Solar Energy Conference, Munich, Germany, 2001, pp. 246–249.

[40] L.M. Fraas, R.C. Knechtli, Design of high efficiency monolithic stacked multijunction solar cells, in: Proceedings of the 13th IEEE Photovoltaic Specialists Conference, Washington, DC, New York, 1978, p. 886.

[41] E.D. Jackson, Areas for improvement of the semiconductor solar energy converter, in: Transactions of the Conference on the Use of Solar Energy, Vol. 5, 1958, University Of Arizona Press, Tucson, 1955, pp. 122–126.

[42] N.S. Alvi, C.E. Backus, G.W. Masden, The potential for increasing the efficiency of photovoltaic systems by using multiple cell concepts, in: Proceedings of the 12th IEEE Photovoltaic Specialists Conference, Baton Rouge, 1976, pp. 948–956.

[43] A. Bennett, L.C. Olsen, Analysis of multiple-ce ll concentrator/photovoltaic systems, in: Proceedings of the 13th IEEE Photovoltaic Specialists Conference, Washington, DC, New York, 1978, pp. 868–873.

[44] S.M. Bedair, S.B. Phatak, J.R. Hauser, Material and device considerations for cascade solar cells, IEEE Trans. Electron Dev. Ed-27 (4) (1980) 822–831.

[45] H.J. Hovel, Novel materials and devices for sunlight concentrating systems, IBM J. Res. Develop. 22 (2) (1978) 112–121.

[46] J.A. Cape, J.S. Harris Jr., R. Sahai, Spectrally split tandem cell converter studies, in: Proceedings of the 13th IEEE Photovoltaic Specialists Conference, Washington DC, New York, 1978, pp. 881–885.

[47] H.A. Vander Plas, R.L. Moon, L.W. James, T.O. Yep, R.R. Fulks, Operation of multi-bandgap concentrator cells with a spectrum splitting filter, in: Proceedings of the Second European Photovoltaic Solar Energy Conference, Berlin, 1979, 507–514.

[48] R.L. Moon, L.W. James, H.A. Vander Plas, T.O. Yep, A. Antypas, Y.G. Chai, Multigap solar cell requirements and the performance of AlGaAs and Si cells in concentrated sunlight, in: Proceedings of the 13th IEEE Photovoltaic Specialists Conference, Washington, DC, New York, 1978, pp. 859–867.

[49] P.G. Borden, P.E. Gregory, O.E. Moore, L.W. James, H. Vander Plas, A s10-unit dichroic filter spectral splitter module, in: Proceedings of the 15th IEEE Photovoltaic Specialists Conference, Kissimmee, Florida, 1981, pp. 311–316.

[50] P.G. Borden, P.E. Gregory, O.E. Moore, Design and demonstration spectrum splitting photovoltaic concentration module, Sandia Report SAND 82-7120, November 1982.

[51] M.E. Ellion, High efficiency photovoltaic assembly, World Patent 8,701,512, 1987.

[52] K.H. Spring, Direct Generation of Electricity, Academic Press, New York, 1965, pp. 353–355.

[53] J.R. Dettling, High efficiency converter of solar energy to electricity, US Patent 4,021,267, 1977.

[54] A.K. Converse, Refractive spectrum splitting optics for use with photovoltaic cells: a research plan and qualitative demonstration, in: R.D. McConnell (Ed.),

Future Generation Photovoltaic Technologies: First NREL Conference, AIP Conference Proceedings, Vol. 404, Denver, CO, 1997, p. 373.

[55] D.E. Soule, Hybrid solar energy generating system, US Patent 4,700,013, 1987.

[56] L.M. Fraas, W.E. Daniels, J. Muhs, Infrared photovoltaics for combined solar lighting and electricity for buildings, in: Proceedings of the 17th European Photovoltaic Solar Energy Conference, Munich, Germany, 2001, p. 836.

[57] J.D. Muhs, D.D. Earl, Adaptive, full spectrum solar energy system, World Patent 3,038,348, 2003.

[58] N. Yehezkel, J. Appelbaum, A. Yogev, Photovoltaic conversion in a common solar concentrating and spectrally splitting system, in: Proceedings of the IEEE First World Conference on Photovoltaic Energy Conversion, Waikoloa, Hawaii, 1994, pp. 1811–1813.

[59] J.B. Lasich, A. Cleeve, N. Kaila, G. Ganakas, M. Timmons, R. Venkatasubramanian, T. Colpitts, J. Hills, Closed-packed cell arrays for dish concentrators, in: Proceedings of the IEEE First World Conference on Photovoltaic Energy Conversion, Waikoloa, Hawaii, 1994.

[60] J.D. Muhs, Hybrid lighting doubles the efficiency and affordability of solar energy in commercial buildings, in: CADDET Energy Efficiency Newsletter, Vol. 4, 2000, pp. 6–9.

[61] J.D. Muhs, Design and analysis of hybrid solar lighting and full spectrum solar energy systems, in: Proceedings of the American Solar Energy Society SOLAR 2000 Conference, Madison, WI.

[62] G.O. Schlegel, B.D. Wood, J.D. Muhs, S.A. Klein, W.A. Beckman, Full spectrum hybrid lighting for commercial buildings, in: Proceedings of the 5th International Conference on Energy-Efficient Lighting, Nice, France, 2002.

[63] L.M. Fraas, W.R. Pyle, P.R. Ryason, Concentrated and piped sunlight for indoor illumination, Appl. Opt. 22 (1983) 578.

[64] L.M. Fraas, J.E. Avery, T. Nakamura, Electricity from concentrated solar IR in solar lighting applications, in: Proceedings of the 29th IEEE Photovoltaic Specialists Conference, New Orleans, LA, 2002.

[65] A. Yogev, J. Appelbaum, M. Oron, N. Yehezkel, Concentrating and splitting of solar radiation for laser pumping and photovoltaic conversion, J. Propulsion Power 12 (2) (1996) 405–409.

[66] Laurent Cassegrain, Journal des scavans (1672).

[67] André Baranne and Françoise Launay, Cassegrain: a famous unknown of instrumental astronomy, Journal of Optics, 1997, vol. 28, no. 4, pp. 158–172(15)

[68] Alan L. Fahrenbruch, Richard H. Bube, Fundamentals of Solar Cells, Department of Materials Science and Engineering, Stanford University, Stanford, California, 1983, pp. 541-542.

[69] Encyclopaedia of Laser Physics and Technology, Sellmeier equation. Retrieved 10th August, 2011. Website: http://www.rp-photonics.com/sellmeier_formula.html.

[70] Department of Environment Malaysia, Air pollutant Index Management System. Retrieved August 11th, 2011 website:
http://www.doe.gov.my/apims/index.php?gmap=load&date=2011-08-11

[71] The correct material for infrared Application. Retrieved August 15th, 2011. Website: http://www.edmundoptics.com/technical-support/optics/the-correct-material-for-infrared-applications/?&viewall.

[72] n (Sellmeier Equation). Retrieved August 10th August, 2011. Website: http://www.calctool.org/CALC/phys/optics/sellmeier

APPENDICES

APPENDIX A: Calculation of FF Value and Efficiency

To obtain the efficiency, first have to get the Fill Factor,

The Ideal Fill Factor (assume PV cell as a ideal diode):

$$FF = \frac{I_{mpp} \cdot V_{mpp}}{I_{sc} \cdot V_{oc}} \approx \left| \frac{v_{oc} - \ln(v_{oc} + 0.72)}{v_{oc} + 1} \right| \tag{5.1}$$

and,

$$\left| v_{oc} = V_{oc} \frac{q}{m \cdot k \cdot T} \right| \tag{5.2}$$

Where,   m = 1 (diode ideality factor)

 k = 1.38 x 10^{-23} J/K (Boltzmann constant)

T = 298K (Temperature)

q = 1.6 x 10^{-19} As (charge of electron)

V_{oc} = open circuit voltage

v_{oc} = normalized open circuit voltage

For **5.1**, experiment under the sun,

1. Calculation for Prism $_{\alpha\,+\,big\,poly}$:

$V_{oc,\,\alpha}$ $= 6.5$

$v_{oc,\,\alpha}$ $= V_{oc}\dfrac{q}{m\,k\,T}$

            $= 253.118$

FF_{α} $\approx [v_{oc} - \ln(v_{oc,\alpha} + 0.72)] \,/\, [v_{oc} + 1]$

            $= 0.974$

$V_{oc,\,big\,poly}$ $= 1.7$

$v_{oc,\,big\,poly}$ $= V_{oc}\dfrac{q}{m\,k\,T}$

            $= 66.2$

$FF_{big\,poly}$ $\approx [v_{oc,\,big\,poly} - \ln(v_{oc,\,big\,poly} + 0.72)] \,/\, [v_{oc,\,big\,poly} + 1]$

            $= 0.923$

Hence, the total power,

P_{total} $= [FF_{\alpha} \times P_{oc,\,\alpha}] + [FF_{big\,poly} \times P_{oc,\,big\,poly}]$

            $= 64.23\text{mW}$

Area exposed to sun $= 2\text{cm} \times 5\text{cm} \;=\; 10\text{cm}^2$

Hence, Power density for Prism $_{\alpha+poly}$ = P_{total} / Area exposed

                                   $= 64.23\text{mW}/10\text{cm}^2$

                                   $= 6.423\ \text{mW/cm}^2$

Power density of sun under AM1.5 $= 1000\text{W} \,/\, \text{m}^2$

                                        $= 0.1\ \text{W} \,/\, \text{cm}^2$

Hence the efficiency is $= \dfrac{\text{power density for prism}}{\text{power density for AM 1.5}} \times 100\ \%$

                                   $= \underline{6.4}\ \%$

2. Calculation for Cold Mirror $_{\alpha + \text{big poly}}$:

$V_{oc,\,\alpha}$ = 6.7

$v_{oc,\,\alpha}$ = $V_{oc}\,\dfrac{q}{m\,k\,T}$

= 260.907

FF $_\alpha$ ≈ [v_{oc} − ln($v_{oc,\alpha}$ + 0.72)] / [v_{oc} + 1]

= 0.975

$V_{oc,\,\text{big poly}}$ = 3

$v_{oc,\,\text{big poly}}$ = $V_{oc}\,\dfrac{q}{m\,k\,T}$

= 116.824

FF $_{\text{big poly}}$ ≈ [$v_{oc,\,\text{big poly}}$ − ln($v_{oc,\,\text{big poly}}$ + 0.72)] / [$v_{oc,\,\text{big poly}}$ + 1]

= 0.951

Hence, the total power,

P_{total} = [FF $_\alpha$ x $P_{oc,\,\alpha}$] + [FF $_{\text{big poly}}$ x $P_{oc,\,\text{big poly}}$]

= 143.508mW

Area exposed to sun = 3.54cmx5cm = 17.7cm^2

Hence, Power density for Cold Mirror $_{\alpha+\text{poly}}$ = P_{total} / Area exposed

= 143.508 mW/17.7 cm^2

= 8.11 mW/cm^2

Power density of sun under AM1.5 = 1000W / m^2

= 0.1 W / cm^2

Hence the efficiency is = $\dfrac{\text{power density for prism}}{\text{power density for AM 1.5}}$x 100 %

= 8.11 %

3. Calculation for Prism $_{\alpha + \text{small poly}}$:

$V_{oc, \alpha}$	= 6.5	$V_{oc, \text{small poly}}$	= 1
$v_{oc, \alpha}$	= 253.118	$v_{oc, \text{small poly}}$	= 38.941
FF_{α}	= 0.974	$FF_{\text{small poly}}$	= 0.883

P_{total} = 93.100 mW

Area exposed to sun = 10 cm^2

Hence, Power density for Prism $_{\alpha+\text{poly}}$ = 9.31 mW/cm^2

Power density of sun under AM1.5 = 0.1 W / cm^2

Hence the efficiency is = <u>9.31</u> %

4. Calculation for Cold Mirror $_{\alpha + \text{small poly}}$:

$V_{oc, \alpha}$	= 6.7	$V_{oc, \text{small poly}}$	= 1.09
$v_{oc, \alpha}$	= 260.907	$v_{oc, \text{small lpoly}}$	= 42.446
FF_{α}	= 0.975	$FF_{\text{small poly}}$	= 0.890

P_{total} = 278.92 mW

Area exposed to sun = 17.7 cm^2

Hence, Power density for Cold Mirror $_{\alpha+\text{poly}}$ = 15.76 mW/cm^2

Power density of sun under AM1.5 = 0.1 W / cm^2

Hence the efficiency is = <u>15.76</u> %

For **5.2**, experiment under solar simulator:

1. Calculation for Prism $_{\alpha \, + \, big \, poly}$:

$V_{oc, \, \alpha}$	= 6.5		$V_{oc, \, big \, poly}$	= 1.7
$v_{oc, \, \alpha}$	= 253.118		$v_{oc, \, big \, poly}$	= 66.200
FF_{α}	= 0.974		$FF_{big \, poly}$	= 0.923

P_{total} = 9.948 mW

Area exposed to solar simulator = 10 cm^2

Hence, Power density for Prism $_{\alpha + poly}$ = 0.995 mW/cm^2

Power density of solar simulator = 150 W / π (r)^2

= 150 W / π (1.75cm)^2

= 15.591 W / cm^2

Hence the efficiency is = <u>0.006</u> %

2. Calculation for Cold Mirror $_{\alpha \, + \, big \, poly}$:

$V_{oc, \, \alpha}$	= 6.7		$V_{oc, \, big \, poly}$	= 3
$v_{oc, \, \alpha}$	= 260.90		$v_{oc, \, big \, poly}$	= 116.824
FF_{α}	= 0.974		$FF_{big \, poly}$	= 0.951

P_{total} = 42.788 mW

Area exposed to solar simulator = 17.7 cm^2

Hence, Power density for Cold Mirror $_{\alpha + poly}$ = 2.417 mW/cm^2

Power density of solar simulator = 15.591 W / cm^2

Hence the efficiency is = <u>0.016</u> %

3. Calculation for Prism $_{\alpha + \text{small poly}}$:

$V_{oc,\alpha}$ = 6.5 $V_{oc,\text{small poly}}$ = 0.91

$v_{oc,\alpha}$ = 253.118 $v_{oc,\text{small poly}}$ = 35.437

FF $_\alpha$ = 0.974   FF $_{\text{small poly}}$ = 0.874

P_{total} = 35.892 mW

Area exposed to solar simulator   = 10 cm^2

Hence, Power density for Prism $_{\alpha+\text{poly}}$ = 3.589 mW/cm^2

Power density of solar simulator   = 15.591 W / cm^2

Hence the efficiency is   = 0.023 %

4. Calculation for Cold Mirror $_{\alpha + \text{small poly}}$:

$V_{oc,\alpha}$ = 6.69 $V_{oc,\text{small poly}}$ = 1.09

$v_{oc,\alpha}$ = 260.517 $v_{oc,\text{small poly}}$ = 42.446

FF $_\alpha$ = 0.975   FF $_{\text{small poly}}$ = 0.890

P_{total} = 64.369 mW

Area exposed to solar simulator   = 17.7 cm^2

Hence, Power density for Cold Mirror $_{\alpha+\text{poly}}$ = 3.637 mW/cm^2

Power density of solar simulator   = 15.591 W / cm^2

Hence the efficiency is   = 0.023 %

APPENDIX B: Experiment Examine Transmission Rate of Prism

Figure 6.2: The set up for the experiment to examine transmission rate.

To examine the transmission rate of prism, an experiment is carried out in a dark room by using a 650nm red laser directed to the prism and intensity of laser is collected in the diffracted angle. The results are obtained through software called "Data Studio" which programmed to examine various optics experiments. An assumption is made: although the transmission rate for every wavelength in spectrum does not exactly same as 650nm wavelength, but they assumed to be near to 650nm.
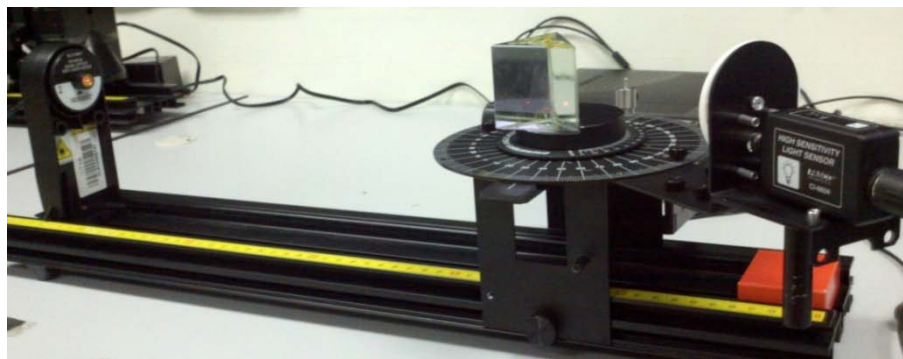
Figure 6.3: A red laser and a light sensor are located at two ends, while the prism is in between them. Transmission rate is obtained by rotate the sensor around the prism.

Results:

Calibration is done by using the integrated features that provided in the "Data Studio", hence the accuracy of the results are largely increased by eliminating background noise and dark current. The percentage error is ±1%. The results are collected 3 times separately to give an average value to reduce any possible systematic error and random error. The average of the diffracted intensity of the main beam is 37.15%, the rest is lost due the internal reflection.

Discussion:

Transmission Rate for Prism
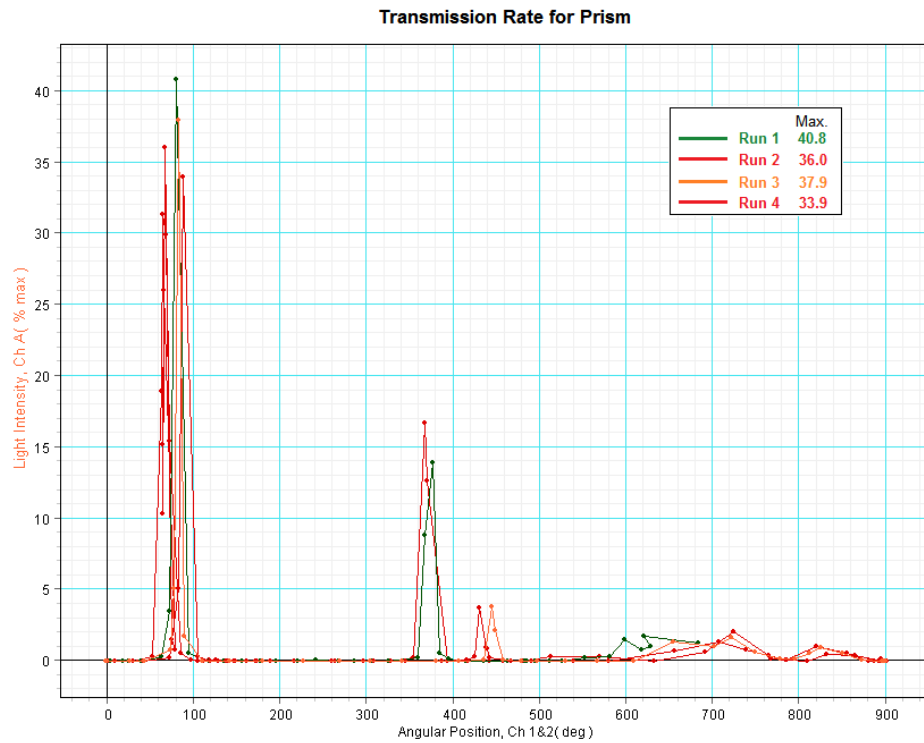
There are two major losses are separate to another two prism surface that caused by internal surface, meaning each prism surface refract one high intensity laser beam. The first peak is the main diffracted beam, and the second peak is the light that undergoes internal reflection on first refracted surface, while the third peak is unable to observe due to the light sensor has blocked the refracted beam. The intensity goes down from first, to second then third. The reason is when the first beam refracted from the prism surface, part of the beam undergoes internal reflection, incident on the second surface, and again part of the internal reflection beam from first surface undergoes refract and internal reflection towards third surface. A lot of internal reflection can be observed directly from the prism when the red laser incident on it.

The intensity shown in the last part of the graph is the background noise which contributed by monitor. Although the monitor has turned away from the sensor, as sensor rotated to particular position, the sensor is still able to detect some noises. Since the noises do not disturb the results, hence it is neglected.

Conclusion:

The average of transmission rate of the prism is 37.15%. It has a very low transmission rate and responsible for the low efficiency in the prism tandem cell.

APPENDIX C: Experiment in Examine Reflection and Transmission Rate of Cold Mirror

To examine the reflection and transmission rate of the cold mirror, a similar experiment is conducted as in Appendix B. The cold mirror is placed in between the laser and sensor to examine transmission rate while for reflection rate , the sensor is rotated to reflection angle respect to cold mirror (45˚). The laser is also 650nm wavelength, and the same software, "Data Studio", is used to obtain the results.

Figure 6.4: (Right) Examine reflection rate. (Left) Examine transmission rate.

Results:

1. Reflection Rate:
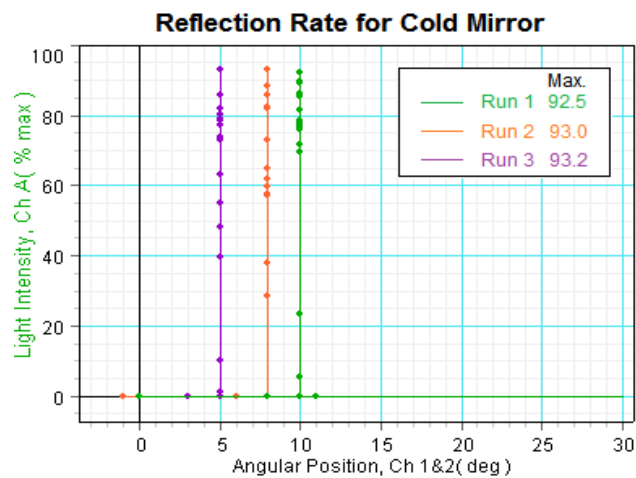
The same calibration and correction of error has been done as the previous experiment in Appendix B to reduce unnecessary losses. The percentage of error is ±1%. 3 sets of data are collected and give pretty consistent results, which yields an average 92.9% of reflection rate. Therefore the losses are estimated around 7%.

2. Transmission Rate:

Transmission Rate for Cold Mirror
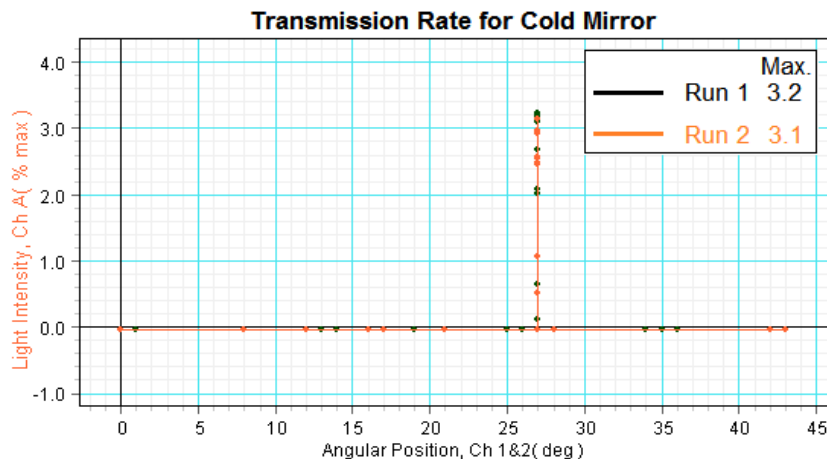
2 sets of data are collected and give an average 3.15% of transmission rate. The transmission rate is part of the losses which contribute to the lost efficiency.

Discussion:

The reflection rate directly indicates the percentage reflected toward PV cell. Normally the sum of reflection and transmission rate made up a total 100%, but it is not exactly true here since there is part of the reflected and transmitted light undergo destructive interference when incident on the cold mirror thin film. The explanation of the destructive interference on thin film is not discussed here since it is a long and pile of mathematical process. Due to the reflection and transmission rate can be fluctuated in a very minor scale from time over time, the average value has to be taken to reduce the error in graph distribution.

Conclusion:

The reflection record an average of 92.9%, in another word it lost only 7% of the total light. This is an acceptable result compare to the transmission rate of prism. Although it takes a minor effect on efficiency, it can be a huge amount of losses when come under concentrated technology. Yet this factor is not a primary concern as it gives a very satisfy result.

APPENDIX D: Rough estimation of lost efficiency in α-Si PV cell

x=[0.2950	0.6050	0.8875
0.3050	0.6150	0.9000
0.3150	0.6250	0.9075
0.3250	0.6350	0.9150
0.3350	0.6450	0.9250
0.3450	0.6550	0.9300
0.3550	0.6650	0.9400
0.3650	0.6750	0.9500
0.3750	0.6850	0.9550
0.3850	0.6950	0.9650
0.3950	0.6983	0.9750
0.4050	0.7000	0.9850
0.4150	0.7100	1.0180
0.4250	0.7200	1.0820
0.4350	0.7277	1.0940
0.4450	0.7300	1.0980
0.4550	0.7400	1.1010
0.4650	0.7500	1.1280
0.4750	0.7621	1.1310;
0.4850	0.7700	1.1311];
0.4950	0.7800	
0.5050	0.7900	
0.5150	0.8000	
0.5250	0.8059	
0.5350	0.8250	
0.5450	0.8300	
0.5550	0.8350	
0.5650	0.8465	
0.5750	0.8600	
0.5850	0.8700	
0.5950	0.8750	

y=[0.00	1255.43	793.87
1.32	1240.19	778.97
20.96	1243.79	217.12
113.48	1233.96	163.72
182.23	1188.32	249.12
234.43	1228.40	231.30
286.01	1210.08	255.61
355.88	1200.72	279.69
386.80	1181.24	529.64
381.78	973.53	496.64
492.18	1173.31	585.03
751.72	1152.70	486.20
822.45	1133.83	448.74
842.26	974.30	486.72
890.55	1110.93	500.57
1077.07	1086.44	100.89
1162.43	1070.44	116.87
1180.61	733.08	0.00
1212.72	1036.01	];
1180.43	1018.42	
1253.83	1003.58	
1242.28	988.11	
1211.01	860.28	
1244.87	932.74	
1299.51	923.87	
1273.47	914.95	
1276.14	407.11	
1277.74	857.46	
1292.51	843.02	
1284.55	835.10	
1262.61	817.12	
1261.79	807.83	

plot(x,y);hold on

fill([x(1);x(1:47);x(47)],[0;y(1:47);0],'b'); hold on

fill([x(12);x(12:43);x(43)],[0;y(12:43);0],'r'); hold on

Area1=trapz(x(1:47),y(1:47));

Area2=trapz(x(12:43),y(12:43));
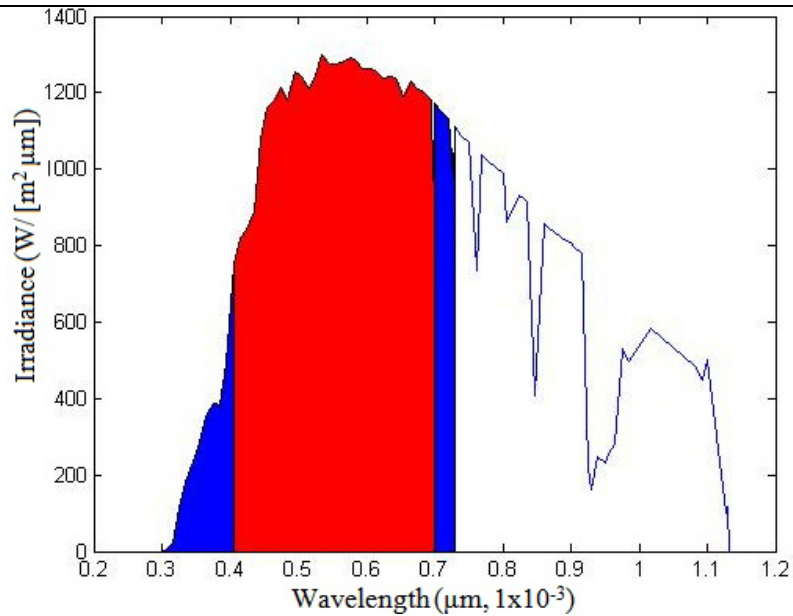
percentage=Area2/Area1

Graph 10: Absorbing range for α-Si is 290nm – 730nm (blue + red colour area).

Absorbing range for α-Si under cold mirror is 400nm – 700nm (red colour area).

$$\frac{\text{power produced } \alpha-\text{Si under cold mirror}}{\text{power produced } \alpha-\text{Si direct exposed under sun}} \text{ x } 100\% = \underline{\mathbf{84.92\%}}$$

Power lost due to wavelength distribute by cold mirror   = **15.08%**
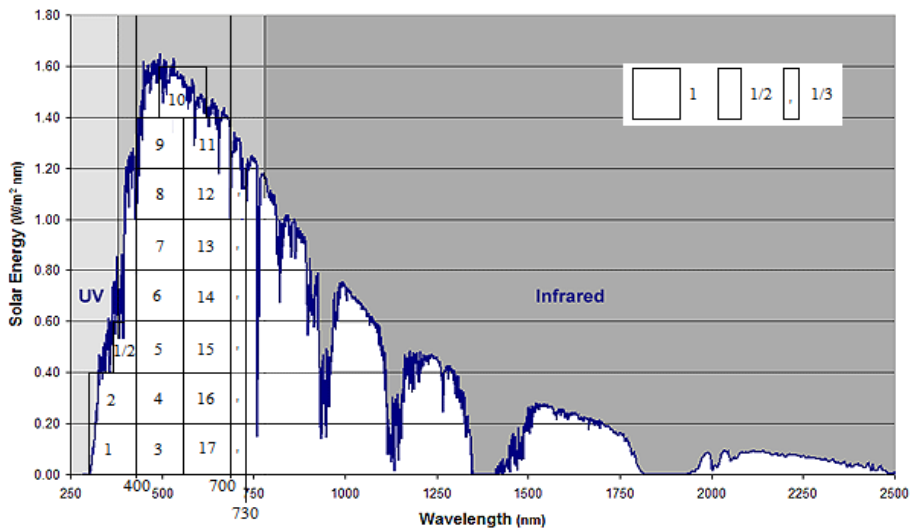
Graph 12: A rough estimation without data. Power lost is 23.08%

APPENDIX E: Rough estimation of lost efficiency in Poly-Si PV cell

Same data with Appendix D

plot(x,y);hold on

fill([x(1);x(1:81);x(81)],[0;y(1:81);0],'b'); hold on

fill([x(12);x(12:43);x(43)],[0;y(12:43);0],'r')

Area1=trapz(x(1:81),y(1:81));

Area2=trapz(x(12:43),y(12:43));
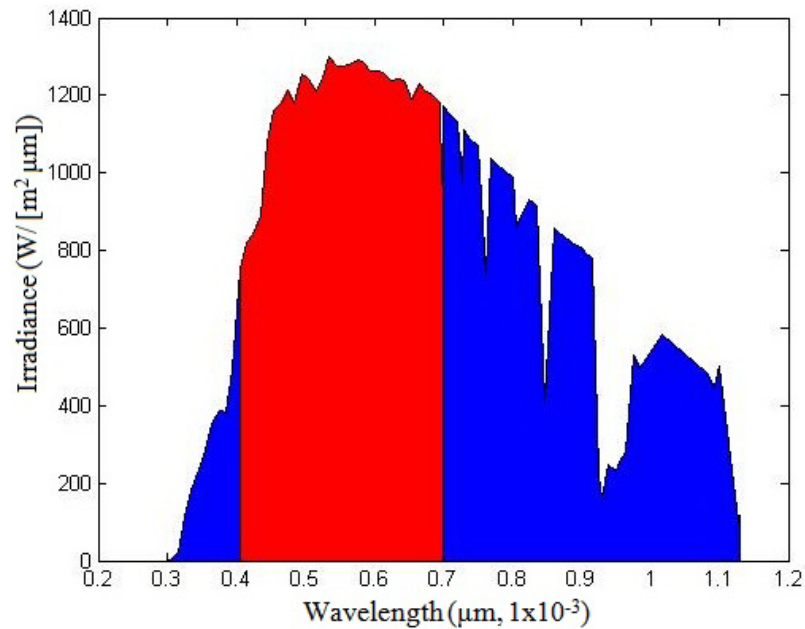
percentage=Area2/Area1

Graph 11: Absorbing range for Poly-Si is 290nm – 1130nm (Blue + red region).
Absorbing range for Poly-Si under cold mirror is 290nm – 400nm and 700nm -
1130nm (blue region).

$$\frac{power\ produced\ poly-Si\ under\ cold\ mirror}{power\ produced\ poly-Si\ direct\ exposed\ under\ sun} \times 100\% = \mathbf{\underline{52.30\%}}$$

Power lost due to wavelength distribute by cold mirror   = **47.70%**
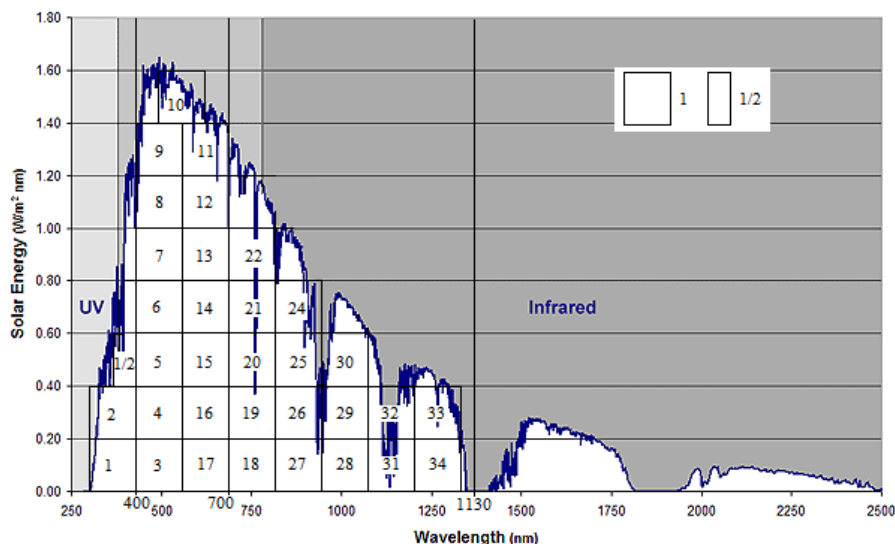
Graph 13: A rough estimation without data. Power lost is 41.10%

APPENDIX F: Experiment Examining Internal Resistance of PV cell

To examine the connection of PV array inside the cell, a few area of the PV cell has been covered up to analyse by different value obtained. Note that the internal and series resistance mention here is not the effective series resistance which arise due to photo-generated electron travel via semiconductor region to reach electrode.

It was accidentally discovered by compare the power produced between the same areas of the hole in box and area exposed on PV. By cover quarter of the total area, the power value obtained is not quarter of the total power. Although data sheet does not mention about internal resistance and the connection underneath PV cell, but it noted that if part of the area is covered by obstacle, the power may be reduced and the product may cease to function. The effective area must not be shaded.

In the Fig.41, the exposed area is 3.54cm x 5cm. Initially this is for the comparison between area of the hole in box and PV exposed area, but the power was found not correspond to the ratio of exposed area. In Fig.41, the top left give a lowest value, then come to the top right and bottom left, the highest value is the bottom right. It is an unexpected result, as same area gives different open circuit voltage in different region, that means the part of the PV arrays operate while some are not. The power value can show up to 10 times differences between lowest and highest region.
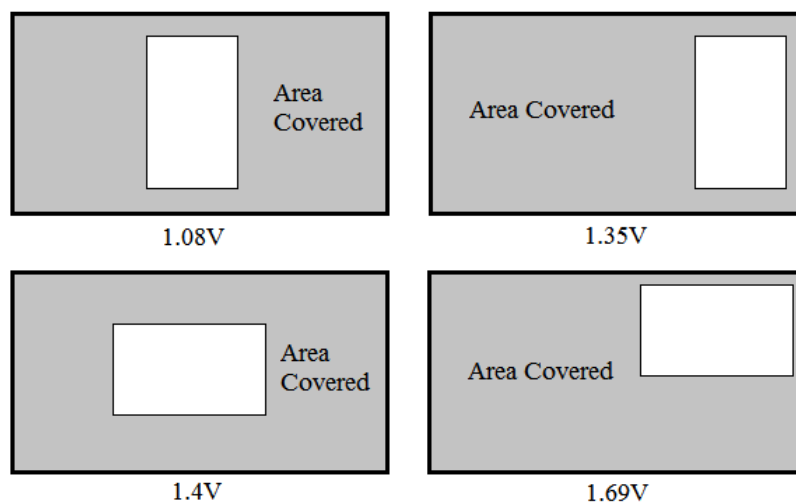
Figure 6.5: Same total area gives different V_{oc} and power in different region. Hypothesis is different exposed region activate different amount of array within PV cell, and resistance can arise due to different connection.

Follow then, the experiment carry on by cover half of the area on PV. The results give a different value in different region as previously. In Fig.6.5, by covering half of the side, the V_{oc} is almost half of the total value. But by covering the lower half, the V_{oc} drop lower than half of the total value. The power value is around 10% of the half side covered.
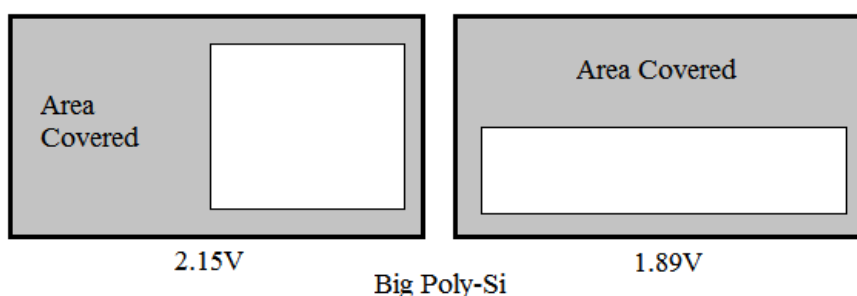
Figure 6.6: By cover the half of the side, the V_{oc} become half of the total V_{oc}. But when cover the lower half, the V_{oc} decrease further. The hypothesis may be correct as the V_{oc} is seems influenced by series or parallel connection within PV cell.

An illustration (Fig.43) of the big Poly-Si PV is drawn to match the hypothesis that different exposed region gives different V_{oc} and power value.
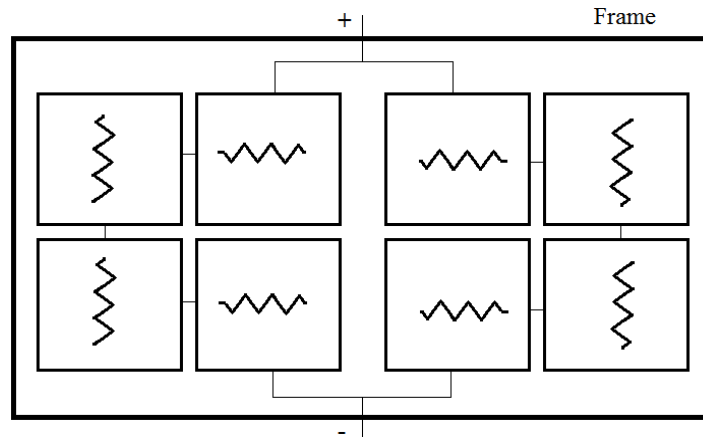
Figure 6.7: The connection of arrays in big poly-Si: 2 series of arrays connected in parallel. This match the hypothesis that different region give different power value.

First case: By cover up the half of bottom, it gives series resistance at each side as the upper part of the arrays act as high resistivity open circuit, and high resistance influence the power production.

Second case: By cover up half of the side, the shaded side act as a high resistivity open circuit. While on the exposed side, array in series connection fully functions under sun. The V_{oc} and power gives merely the half of the total value.

To further confirm the hypothesis, as well as improve results, a small Poly-Si is replaced. The same method is applied to experiment, and agrees to the hypothesis as well.
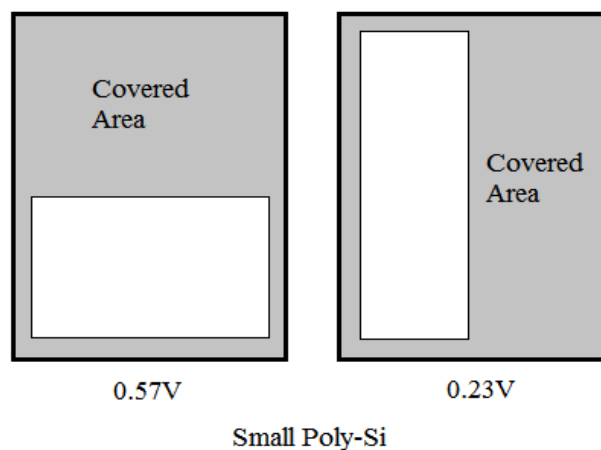
Figure 6.8: The small poly-Si agrees to the hypothesis as well.
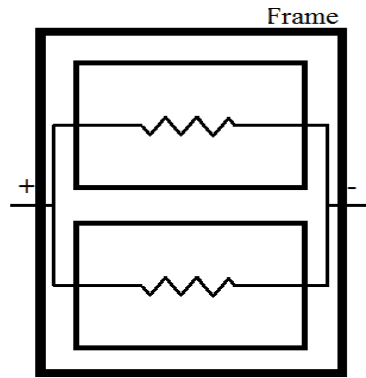
Figure 6.9: (Left) Illustration of the connection of arrays inside small Poly-Si PV cell.

Figure 6.10: (Right) Small Poly-Si PV cell

The illustration of the small poly-Si is shown in Fig.45, the picture next to the illustration is the small poly-Si PV cell. To avoid the internal resistance, the incident light have to fully fall on the series array, while part of the side can left shaded. As long as the series connection is fully operating, the series resistance is than avoid, while the parallel resistance does not influence the result as much as series resistance, the lost can be reduce over half of the fully incident power. In another word, the internal resistance can be controlled at most losses for half of the total power value, 50%.

In conclusion, internal resistance exist when the area is not fully incident with light. Secondly, to avoid major lost, light must incident on the series connection region in order to control the losses within 50%. The best way to avoid any internal resistance is to use a size that fit perfectly to the incident light.

APPENDIX G: Data Sheet of α-Si PV cell

Ordering number : ENA1308

SANYO

DATA SHEET
SANYO Amorphous Solar Cell

Amorton

AM-8804

Package Dimensions (unit : mm)

Overcoat Side

Light Receiving Side

Glass Juts(4 Corners)
Width : 0.6MAX, Length : 6.0MAX

(+) (−)

Lead Wires

Wire Overcoat

(2.5)

$105.0^{\pm 5.0}$ A

15.0MAX

$55.1^{\pm 0.3}$

$105.0^{\pm 5.0}$ B

12.0MAX

$48.1^{\pm 0.3}$

(1.05)

Effective Area

$53.0^{\pm 0.2}$

(1.05)

(1.05) $44.7^{\pm 0.2}$ (2.35)

Effective Area
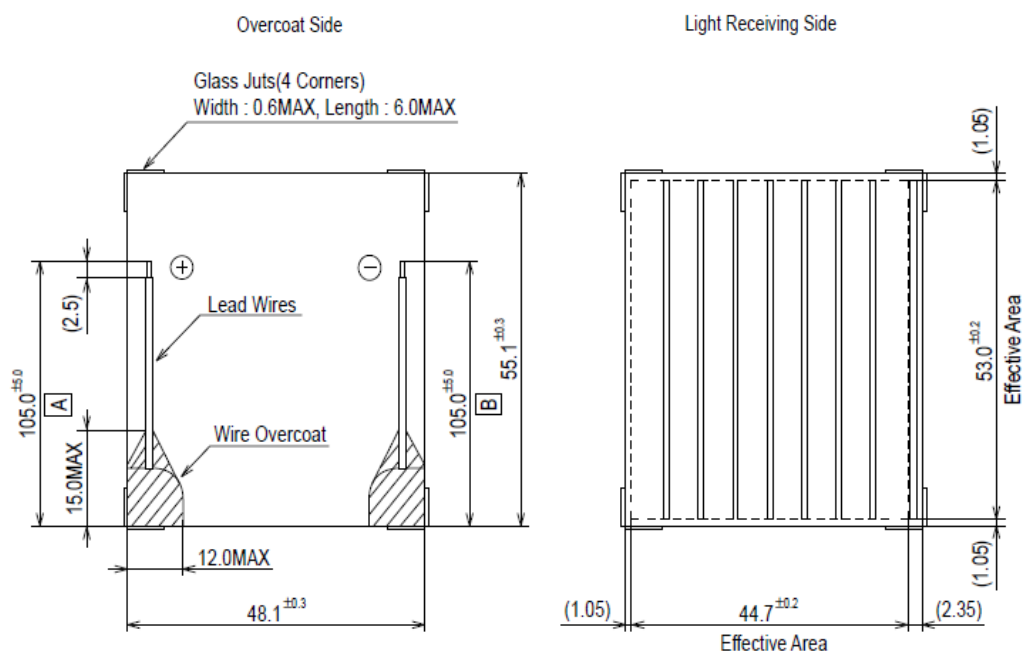
Note: Glass Substrate Thickness   : 1.1mm
Module Thickness   : 1.3mm max
Wire-Overcoat Thickness   : 2.5mm max (Including Module)
Standard lead wires length   : 105mm Marking (A & B)

AM-8804

Ratings at Ta = 25°C

Parameter	Symbol	Conditions	Ratings			Unit
			min	typ	max	
Open Circuit Voltage	Voc	SS 50kLx		6.8		V
Short Circuit Current	Isc	SS 50kLx		16.3		mA
Operating Voltage & Operating Current	Iope	SS 50kLx, Vope=4.5V	12	15.1		mA
		AM-1.5, 100mW/cm², Vope=4.5V		33.3		mA
Maximum Output	Pmax	SS 50kLx, Vop=5.2V, Iop=14.2mA		74		mW
(Reference Value)		AM-1.5, 100mW/cm², Vop=5.2V, Iop=30mA		156		mW
Operating Temperature	Topr				-10 to +60	°C
Storage Temperature	Tstg				-20 to +70	°C

SS: Solar Simulator

APPENDIX H: Data Sheet for Poly-Si

Solarex MEGA™ Series Module Products

Type	Description	Wire Length	Vld	Ild(min.)	Ild(typ.)	Length*	Width*	Thickness*
MSX-005	MEGA module with wires	6.0"(152.4mm)	3.3V	135mA	150mA	4.50"(114.3mm)	2.63"(66.8mm)	.125"(3.0mm)
MSX-01	MEGA module with wires	6.0"(152.4mm)	7.5V	135mA	150mA	5.00"(127.0mm)	5.00"(127.0mm)	.125"(3.0mm)

Solarex SA-Series Plate Products (multiple components on 12" by 13" plates)

Type	Description	Components/Plate	Vld	Ild(min.)	Ild(typ.)	Length*	Width*	Thickness*
SA-03300P	Finished 4X Plate	4	3.6V	300mA	320mA	13.00"(330.2mm)	3.00"(76.2mm)	.090"(2.3mm)
SA-06110P	Standard 4X Plated	4	7.5V	110mA	125mA	6.00"(152.4mm)	6.00"(152.4mm)	.090"(2.3mm)
SA-06110P	Coated 4X Plate	4	7.5V	110mA	125mA	6.00"(152.4mm)	6.00"(152.4mm)	.090"(2.3mm)

SA-Series Components (individual components ready to use)

Type	Description	Vld	Ild(min.)	Ild(typ.)	Length*	Width*	Thickness*
SA-03300	Finished Component	3.6V	300mA	320mA	13.00"(330.2mm)	3.00"(76.2mm)	.090"(2.3mm)
SA-0640	Standard Component	7.5V	40mA	45mA	6.00"(152.4mm)	2.17"(55.1mm)	.090"(2.3mm)
SA-0680	Standard Component	7.5V	80mA	90mA	6.00"(152.4mm)	4.33"(110.0mm)	.090"(2.3mm)
SA-06110	Standard Component	7.5V	110mA	125mA	6.00"(152.4mm)	6.00"(152.4mm)	.090"(2.3mm)
SA-1	Wired Component	17.5V	80mA	100mA	12.00"(304.8mm)	4.33"(110.0mm)	.090"(2.3mm)
SA-2	Wired Component	7.5V	290mA	325mA	13.00"(330.2mm)	6.00"(152.4mm)	.090"(2.3mm)
SA-5	Wired Component	17.5V	290mA	325mA	13.00"(330.2mm)	12.00"(304.8mm)	.090"(2.3mm)

Notes: • Vld - Voltage under load
• Ild (min.) - Minimum initial current output measured at Vld under STC (Standard Test Conditions).
• Ild (typ.) - Typical initial current output measured at Vld under STC.
• "Standard" SA-Series plates and components are provided without a protective back coating and solder pads.
• "Coated" SA-Series plates and components are provided with a protective back coating.
• "Finished" SA-Series plates and components are provided with a protective coating and solder pads.
• STC - Standard Test Conditions are illumination of 1kW/m2 (1 sun) at spectral distribution 1.5 and a solar cell temperature of 25°C.

*All plate products are 12" x 13" x .09" (304.8 mm x 330.2 mm x 2.3 mm)

Data Sheet

Electrical Specifications

Model #	MSX-005	MSX-01	SA-03300	SA-0640	SA-0680	SA-06110
Specified Load Voltage (Vld)	3.3V	7.5V	3.6V	7.5V	7.5V	7.5V
Typical Current at Vld (Ild)	150mA	150mA	320mA	45mA	90mA	125mA
Open Circuit Voltage (Ioc)	4.6V	10.3V	5.0V	12.0V	12.0V	12.0V
Short Circuit Current (Ioc)	160mA	160mA	380mA	35mA	110mA	150mA
Temperature Coefficient of Voltage per °C	-16mV	-37mV	-15mV	-30mV	-30mV	-30mV
Temperature Coefficient of Current per °C	0.15 mA	0.15mA	0.30mA	0.05mA	0.10mA	0.15mA

Notes: Data based on measurement at STC. For full electrical data on the SA-1, SA-2, and SA-5, please consult the Solarex Data Sheets for these products.

High Temperature Performance

High operating temperature reduces voltage output while slightly improving current. As a result, high temperatures may in certain conditions reduce voltage below the minimum necessary to charge a battery. Solarex OEM modules are among the only commercially available PV devices to minimize this problem. Solarex specifies high Vlds at STC for all its OEM products.

Mechanical Characteristics and Design Considerations

Active Area

A Module's Active Area—the frontal area that generates electrical power—is a critical design consideration in using any photovoltaic product. If this area is covered by a mounting bezel or hold-down, power may be reduced and the product may cease to function. For optimal performance, the Active Area must never be shaded.
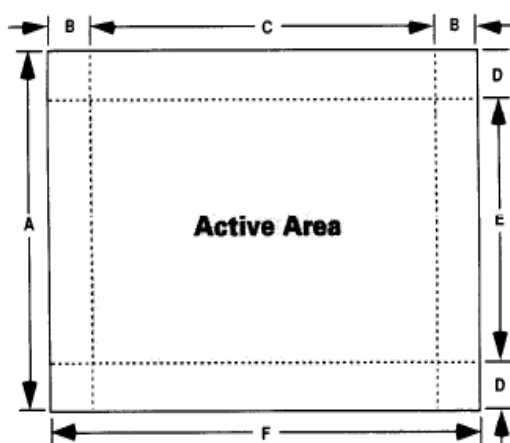
Front Face of Module

Active Area Dimensions

Type	A	B	C	D	E	F
MSX-005	4.5"	.295"	2.244"	.388"	3.772"	2.830"
MSX-01	5.0"	.230"	4.540"	.409"	4.182"	5.000"
SA-03300	13.0"	.250"	2.50"	.125"	12.75"	3.000"
SA-0640	2.16"	.250"	5.50"	.125"	1.91"	6.000"
SA-0680	4.33"	.250"	5.50"	.125"	4.08"	6.000"
SA-06110	6.00"	.250"	5.50"	.125"	5.75"	6.000"

APPENDIX I: Data Sheet of Transmission and Reflection rate for Cold Mirror [71]
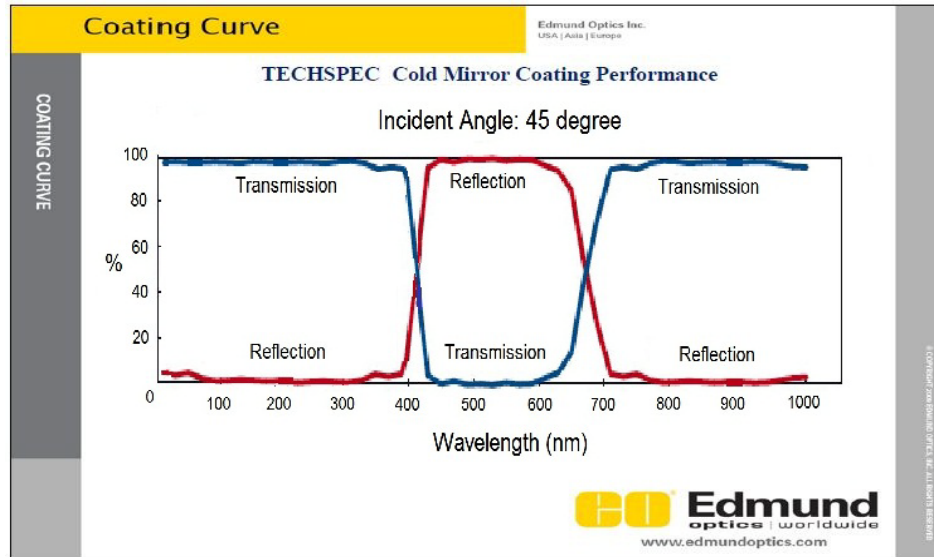
APPENDIX J: Setting up of Prism Tandem Cell using Sellmeier Equation.

By inserting the fuse silica material coefficient into Sellmeier Equation, refractive index for 730nm and 1130nm wavelength is then obtained.

Sellmeier Equation:

$$n^2(\lambda) = 1 + \frac{B_1\lambda^2}{\lambda^2 - C_1} + \frac{B_2\lambda^2}{\lambda^2 - C_2} + \frac{B_3\lambda^2}{\lambda^2 - C_3} \tag{J1}$$

Where,

B1 = 0.696166300   , B2 = 0.407942600   , B3 = 0.897479400
C1 = $4.67914826 \times 10^{-3} \mu m^2$, C2 = $1.35120631 \times 10^{-2} \mu m^2$, C3 = $97.9340025 \ \mu m^2$

Refractive index for 280nm wavelength is: <u>1.49416</u>

Refractive index for 730nm wavelength is: <u>1.45464</u>

Refractive index for 1130nm wavelength is: <u>1.44885</u>

Finding critical angle is essential in order to avoid total internal reflection:

$$\theta_c = \arcsin\left(\frac{n'}{n}\right) \tag{J2}$$

where θ_c is critical angle, n' is refractive index of air, n is refractive index of prism.

$n' = 1,$ $n_{280nm} = 1.49416,$ $n_{730nm} = 1.45464,$ $n_{1130nm} = 1.44885$

$\theta_{c,280nm} = 42.011°$ $\theta_{c,7300nm} = 43.429°$ $\theta_{c,1130nm} = 43.646°$

Angle below critical angle: $42° - 20°$ (internal reflection will not occur below θ_c)

Hence incident angle without the occurrence of internal reflection:
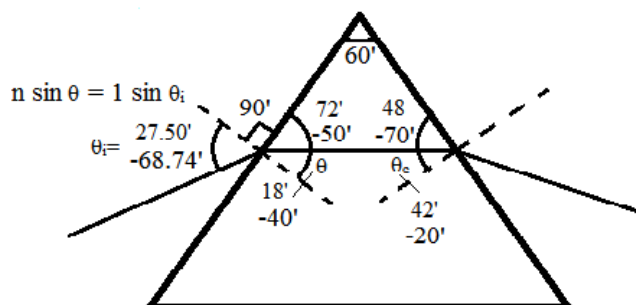
Figure 6.11: Incident angle can obtained by using the angle below critical angle.

The range of incident angle for prism to diffract spectrum: $27.50°$-$68.74°$.

Assume the incident angle, $\theta_a = 30°$,

The diffracted angle for 280nm, 730nm, 1130nm angle is:
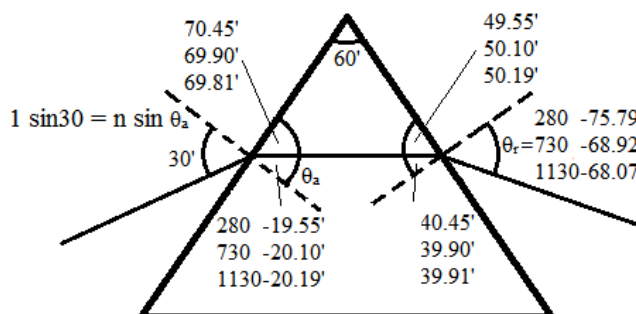
Figure 6.12: Diffracted angle for each wavelength
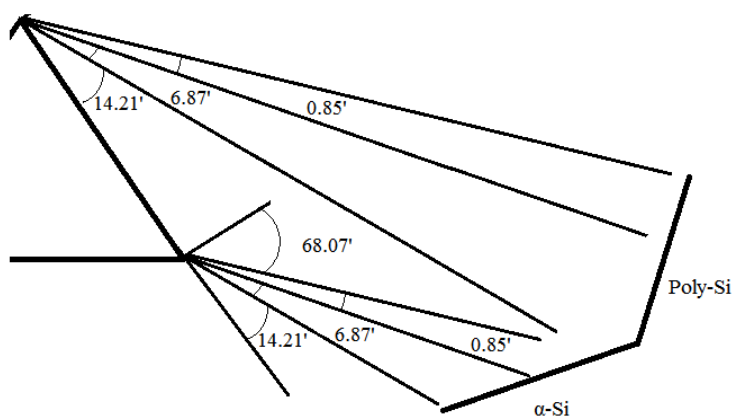
Figure 6.13: Parameter of position and size of PV can be customizing accordingly.